Towards a systematic design approach of D-regions in reinforced concrete
Optimization-based generation of Strut-and-Tie models

Xia, Y.

DOI
10.4233/uuid:6be49718-24c9-4bd4-94cc-f3968662385e

Publication date
2021

Document Version
Final published version

Citation (APA)
Xia, Y. (2021). *Towards a systematic design approach of D-regions in reinforced concrete: Optimization-based generation of Strut-and-Tie models*. [Dissertation (TU Delft), Delft University of Technology]. https://doi.org/10.4233/uuid:6be49718-24c9-4bd4-94cc-f3968662385e

TOWARDS A SYSTEMATIC DESIGN APPROACH OF D-REGIONS IN REINFORCED CONCRETE

OPTIMIZATION-BASED GENERATION OF STRUT-AND-TIE MODELS

TOWARDS A SYSTEMATIC DESIGN APPROACH OF D-REGIONS IN REINFORCED CONCRETE

OPTIMIZATION-BASED GENERATION OF STRUT-AND-TIE MODELS

Proefschrift

ter verkrijging van de graad van doctor
aan de Technische Universiteit Delft,
op gezag van de Rector Magnificus prof.dr.ir. T.H.J.J.van der Hagen,
voorzitter van het College voor Promoties,
in het openbaar te verdedigen op maandag 22 February 2021 om 10:00 uur

Yi XIA

Master of Engineering in Structural Engineering,
Harbin Institute of Technology, Heilongjiang, China,
geboren te Zunyi, China.

Dit proefschrift is goedgekeurd door de

promotor: Prof. dr. ir. M.A.N. Hendriks
promotor: Dr. ir. M. Langelaar

Samenstelling promotiecommissie:

Rector Magnificus,	voorzitter
Prof. dr. ir. M.A.N. Hendriks,	Technische Universiteit Delft, Norwegian University of science and technology
Dr. ir. M. Langelaar,	Technische Universiteit Delft
Onafhankelijke leden:	
Prof. dr. ir. J.G. Rots,	Technische Universiteit Delft
Prof. dr. ir. A. van Keulen,	Technische Universiteit Delft
Dr. M. Bruggi,	Politecnico di Milano
Prof. dr. ir. M. Schevenels,	Katholieke Universiteit Leuven
Prof. dr. ir. A.S.J. Suiker,	Technische Universiteit Eindhoven

Keywords: Reinforced concrete, Strut-and-Tie, Topology optimization, Integrated optimization, Nonlinear finite element analysis

Printed by: Ipskamp Printing, The Netherlands

ISBN 000-00-0000-000-0

An electronic version of this dissertation is available at
http://repository.tudelft.nl/.

To my grandparents

谨以此书献给我的爷爷奶奶

CONTENTS

SUMMARY

Reinforced Concrete (RC) structures are widely used in our society for more than a century. In order to design safe and economical RC structures, various methods have been proposed by engineers and researchers. Remarkably, it still is a challenging task for engineers to design D-regions of RC structures, regions with nonlinear strain distributions. Strut-and-Tie Modelling (STM) is a well-known method for designing such regions. The STM method uses a truss-analogy model to represent the force flow within the D-region, thereby providing insight to engineers for reinforcement design. The relative simplicity of the method and the fact that STM leads to a safe design are beneficial to engineering practice. However, in investigations of the STM method, the creation of suitable truss-analogy models has been identified as the key problem for a systematic application of STM.

During the past three decades researchers have conducted intensive efforts to find systematic approaches for obtaining truss-analogy models for the STM method. Adopting topology optimization (TO) methods to assist the making of Strut-and-Tie (ST) models appears the most promising direction. For this reason, various TO methods have been proposed, however which method leads to the most suitable ST models is still unknown. Very few investigations have been carried out regarding the systematic evaluation of TO results from the perspective of the STM method. In this thesis, a procedure to evaluate the TO result for STM is presented. Using this procedure, an evaluation of TO methods revealed an urgent and challenging problem of generating a suitable ST model in the TO process. Currently, TO methods only provide optimized material layouts as inspiration for creating ST models. Manual and subjective adjustments are required to convert TO results into adequate ST models. These additional processes not only affect the performance of the desired design, but also hinder the application of TO methods for STM.

In this thesis, first a 2D generation method that integrates TO, topology extraction and shape optimization is proposed to solve this problem. The proposed method successfully generates valid ST models for D-regions automatically and without manual adjustments. In addition, an evaluation procedure adopting nonlinear finite element analysis (NLFEA) is proposed to evaluate the performance of the generated ST models. Based on the evaluation results, the generated ST models show a high stiffness and sufficient, yet not overly conservative load capacity. By comparing the generated ST models with various previously manually-created ST models, the generated ST models lead to the most economical steel usage relative to load capacity. Through two case studies and three parameter investigations, the effectiveness of the proposed generation method is validated.

For 3D D-regions, generating suitable ST models is an even more challenging task. Therefore, subsequently, the proposed generation method was extended to 3D conditions. In the 3D generation method, three additional measures are adopted to improve the computational efficiency of the TO process, and a new robust procedure is proposed to extract

3D truss-like structures from the TO results. Three 3D D-regions are investigated, and the corresponding ST models are generated based on the proposed method. Again, the generated ST models lead to economically superior designs compared to the manually created ST models. In addition, the proposed generation method is used to investigate three other aspects of the STM method: 1) a parametric study of four-pile caps; 2) STM generation considering complex load conditions; 3) the influence of load discretization. The robustness and effectiveness of the 3D generation method are validated through these investigations.

In spite of these improvements, challenges remain for engineers in application of the STM method. The standard STM method involves human choices, which depend on the engineer's experience and preferences. These subjective factors hinder the application of the STM method and bring uncertainties and variations to the STM design. Developing a systematic STM method that reduces the subjective choices and uncertainties is identified as an important future research direction. In order to explore this problem, in this thesis, the main choices and uncertainties are identified and discussed. In addition, the proposed generation method can be used to investigate these subjective aspects. Therefore, next to being of value for engineers already in the design of D-regions, the proposed generation method is expected to also form a fruitful basis for future refinements in this research direction.

SAMENVATTING

Al meer dan een eeuw wordt in onze samenleving veelvuldig gebruik gemaakt van constructies van gewapend beton. Om veilige en economische te ontwerpen, zijn verschillende methoden voorgesteld door ingenieurs en onderzoekers. Opmerkelijk genoeg is het nog steeds een uitdagende taak voor ingenieurs om D-gebieden (D van *disturbed*) van betonconstructies te ontwerpen; D-gebieden zijn gebieden met niet-lineaire spanningsverdelingen. Het gebruik van staafwerkmodellen is een bekende methode voor het ontwerpen van dergelijke gebieden. De methode gebruikt een staafwerkanalogie om de krachtsafdracht binnen het D-gebied weer te geven, waardoor ingenieurs inzicht krijgen in het ontwerp van de wapening. De relatieve eenvoud van de methode en het feit dat staafwerkmodellen leiden tot een veilig ontwerp zijn gunstig voor de technische praktijk. Echter, bij het onderzoek naar de staafwerkmethode is het bepalen van geschikte staafwerkanalogieën geïdentificeerd als het belangrijkste probleem voor een systematische toepassing van staafwerkmodellen.

In de afgelopen drie decennia hebben onderzoekers veel inspanningen geleverd om systematische benaderingen te vinden voor het verkrijgen van staafwerkanalogieën. Het toepassen van topologie-optimalisatiemethoden (TO-methoden) om te helpen bij het maken van staafwerkanalogieën lijkt de meest veelbelovende richting. Om deze reden zijn verschillende TO-methoden voorgesteld, maar welke methode leidt tot de meest geschikte staafwerkanalogieën is nog onbekend. Er is zeer weinig onderzoek gedaan naar de systematische evaluatie van TO-resultaten vanuit het perspectief van de staafwerkmethode. In dit proefschrift wordt een procedure beschreven om het TO-resultaat voor staafwerkmodellen te evalueren. Deze procedure bracht een urgent en uitdagend probleem aan het licht bij het genereren van een geschikt staafwerkmodel met een TO-methode. Momenteel bieden TO-methoden alleen geoptimaliseerde materiaalverdelingen als uitvoer die slechts als inspiratie voor het maken van staafwerkmodellen kunnen dienen. Handmatige en subjectieve aanpassingen zijn nodig om TO-resultaten om te zetten in adequate staafwerkanalogieën. Deze aanvullende processen hebben niet alleen invloed op de prestaties van het ontwerp, maar belemmeren ook de toepassing van TO-methoden voor staafwerkmodellen.

In dit proefschrift wordt eerst een 2D-generatiemethode voorgesteld die TO, topologie-extractie en vormoptimalisatie integreert om dit probleem op te lossen. De voorgestelde methode genereert automatisch adequate staafwerkanalogieën voor D-gebieden, zonder dat handmatige aanpassingen nodig zijn. Tevens wordt een evaluatieprocedure voorgesteld die gebruikmaakt van niet-lineaire eindige-elementenanalyses om de prestaties van de gegenereerde staafwerkanalogieën te evalueren. Op basis van de evaluatieresultaten vertonen de gegenereerde modellen een hoge stijfheid en voldoende, maar niet al te conservatieve, draagvermogens. Een vergelijking van de gegenereerde staafwerkanalo-

gieën met verschillende eerdere handmatig gemaakte staafwerkanalogieën, laat zien dat de gegenereerde modellen het meest economisch zijn wat betreft staalgebruik in verhouding tot het draagvermogen. Door middel van twee casestudies en drie parameteronderzoeken wordt de effectiviteit van de voorgestelde generatiemethode gevalideerd.

Voor 3D D-gebieden is het genereren van geschikte staafwerkanalogieën een nog uitdagendere taak. Daarom werd de voorgestelde generatiemethode vervolgens uitgebreid naar 3D. In de 3D-generatiemethode worden drie aanvullende maatregelen genomen om de rekenefficiëntie van het TO-proces te verbeteren, en wordt een nieuwe robuuste procedure voorgesteld om 3D staafwerken uit de TO-resultaten te extraheren. Drie 3D D-gebieden worden onderzocht en de bijbehorende staafwerkmodellen worden gegenereerd op basis van de voorgestelde methode. Ook hier blijkt dat de gegenereerde staafwerkmodellen leiden tot, economisch gezien, superieure ontwerpen in vergelijking met de handmatig gemaakte modellen. De voorgestelde generatiemethode wordt ook gebruikt om drie andere aspecten van de staafwerkmethode te onderzoeken: 1) een parametrische studie van poeren met vier palen; 2) staafwerkgeneratie rekening houdend met complexe belastingsomstandigheden; 3) de invloed van discretisatie van de belasting. De robuustheid en effectiviteit van de 3D-generatiemethode worden gevalideerd door deze onderzoeken.

Ondanks deze verbeteringen blijven er uitdagingen voor ingenieurs bij het toepassen van de staafwerkmodellen. De standaard staafwerkmethode omvat menselijke keuzes, die afhangen van de ervaring en voorkeuren van de ingenieur. Deze subjectieve factoren belemmeren de toepassing van de methode en brengen onzekerheden en variaties in het ontwerp met zich mee. Het ontwikkelen van een systematische staafwerkmethode die de subjectieve keuzes en onzekerheden vermindert, wordt geïdentificeerd als een belangrijke toekomstige onderzoeksrichting. Om dit probleem te onderzoeken, worden in dit proefschrift de belangrijkste keuzes en onzekerheden geïdentificeerd en besproken. Bovendien kan de voorgestelde generatiemethode worden gebruikt om deze subjectieve aspecten te onderzoeken. Daarom wordt verwacht dat de voorgestelde generatiemethode niet alleen nu al van waarde is voor ingenieurs met het ontwerpen van D-gebieden, maar ook een vruchtbare basis zal vormen voor toekomstige verfijningen in deze onderzoeksrichting.

1

INTRODUCTION

From past to now, engineers continuously develop effective and convenient tools to design structures and satisfy increasing requirements from our modern society. With the development of computer algorithms and the assistance of computer-aided tools, the developed techniques enable the structural design in a more effective and convenient manner. The goal of engineers is always on conceiving safe and economical buildings and infrastructure, and this thesis aims to bring that vision a few steps closer.

1.1. RESEARCH CONTEXT

In this section, the background of the related research topics of this thesis is introduced. A brief introduction of the Strut-and-Tie Modelling (STM) method is first introduced in Section 1.1.1. Next, the traditional methods to determine Strut-and-Tie (ST) models are discussed in Section 1.1.2. The basis of TO methods and the application of TO methods for STM are presented in Section 1.1.3 and 1.1.4, respectively.

1.1.1. STRUT-AND-TIE MODELLING IN REINFORCED CONCRETE DESIGN

Reinforced Concrete (RC) structures are widely used in our society for more than a century. In order to design safe and economical RC structures, researchers have proposed various design methods. Some of these methods have been implemented as design codes, which facilitate engineers to design safe and economical RC structures.

Noting the St. Venant's Principle, concrete structures can be divided into B (Bernoulli) regions and D (Disturbed) regions based on the linearity of strain distribution. For B-regions, the Bernoulli's hypothesis that the plane sections of the structures remain plane after deformation, is assumed to be valid. Slender beams without geometrical discontinuities are typical B-regions. Based on Bernoulli's assumption, the stress distribution along a cross section can be calculated, taking into account concrete cracking and crushing and steel yielding and rupturing. The calculated stress distribution is sufficiently accurate for engineers to determine the required reinforcement and design slender structural

elements. In contrast, for D-regions, the assumption of a plane section that remains plane after deformation is invalid, and the strain distribution is nonlinear. There are two main discontinuities that result in the nonlinear strain distribution in D-regions. They comprise load discontinuity and geometrical discontinuity. An example of a beam structure including B-regions and D-regions is shown in Figure 1.1. In practice, deep beams, corbels, pile caps, etc. are typical D-region members, where the complete structural element is considered as one single D-region.

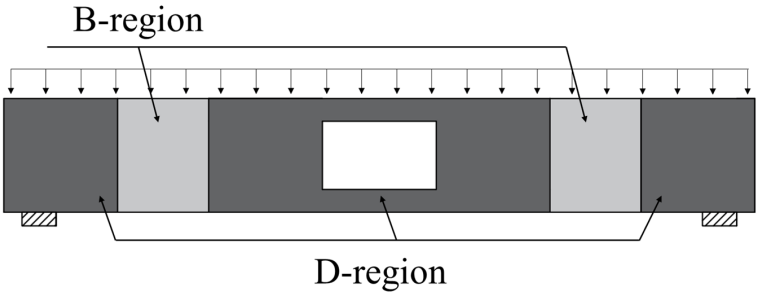

Figure 1.1: B-regions and D-regions of a beam with a rectangular opening. According to St. Venant's principle, the extent of D-regions spans approximately one section depth.

STM is a well-known method for designing D-regions. It uses truss analogy models to simulate load transfer mechanisms within D-regions. The idea of using truss analogy models to design RC structures originates from 1900 [100, 115]. Later on, this concept was refined and many truss analogy models were proposed by Rausch [113], Leondardt [82] and Lampert and Thurlimann [80]. Based on the concept of truss analogy, the Compression Field Method (CFM) [98] and the Modified Compression Field Method (MCFM) [145] were proposed to design RC structures under shear and torsion. Hsu et al. [66] and Hsu [65] proposed a softened truss model method which combines the equilibrium, compatibility and softened stress-strain relationships for the shear and torsion design of RC structures. As for the STM method, the investigations in the early stage can be found in [41, 93, 116]. The STM method was further generalized as a consistent method for designing all parts of concrete structures by Schlaich and Schafer [121], Schlaich et al. [122] around 1990. Since then, the STM method has been gradually implemented in design codes and used by engineers in practice.

The STM method uses a discrete truss system to represent the stress flow of RC structures that transfers the load from load points to supports. The adopted truss system is an idealization and simplification of the actual complex stress distribution. In the discrete truss members, axial forces are used to represent the surrounding stresses. The STM method is based on the lower-bound limit analysis of plasticity theory, and assumes that the structure has adequate ductility for the assumed truss system to develop. In the STM method, the model is created by considering the force equilibrium and the stress yield criterion while ignoring compatibility conditions. Based on the lower-bound

theorem, "*if an equilibrium distribution of stress can be found which balances the applied loads, and is everywhere below yield or at yield, the structure will not collapse or will be just at the point of collapse*"[47]. The adopted ST models based on the lower-bound theorem thus always lead to conservative predictions of the structural resistance. Therefore, safe RC structures can be designed based on the created ST models.

In the ST model, there are three types of elements: struts, ties and nodes. Struts are compression members representing the concrete stress field. The basic type is the prismatic strut in which the compressive stress is confined in the neutral axis, shown in Figure 1.2. In practice, struts are usually idealized as prismatic members. In reality, compressive stresses cannot be restricted in this way, which leads to the bottle-shaped struts. Note that internal lateral spread of compressive stresses could result in splitting of the bottle-shaped struts. Web reinforcement is always implemented to resist this.

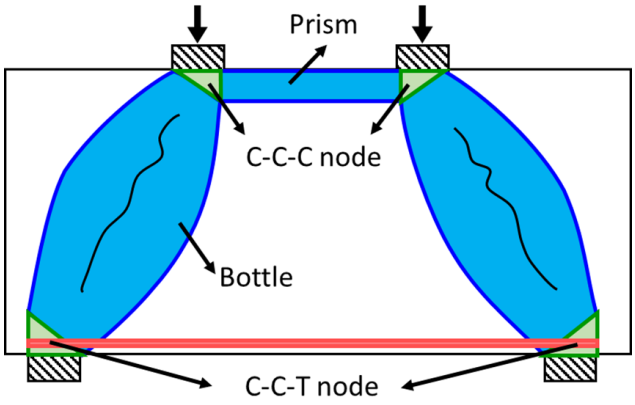

Figure 1.2: Schematic ST model of a deep beam with two strut types, prismatic and bottle-shaped. Blue and red members indicate struts and ties respectively. Green areas indicate node regions.

Ties are tension members to resist tensile forces. A tie represents one or more layers of reinforcements in RC structures, such as standard steel and pre-stressed steel. Reinforcement detailing aspects need to be considered in designing practical steel layouts from ties, for example, the necessary anchorage length of reinforcement needs to be considered to develop full tensile strength.

Nodes where the struts and ties intersect correspond to the joints in the truss model. Nodes are always in a multidimensional stress state which allows the stress transfer between struts and ties. Based on the combination of struts and ties joining at a node, nodes are classified into different types. Typically, there are four standard types in 2D ST models, as shown in Figure 1.3. In the figure, the dashed line marked with C indicates a compressive strut, whereas the solid line with T indicates a tensile tie. The performance of these nodal zones is different and this affects the stress checking procedure of the STM method. For a C-C-C node, the bi-axial compressive stress state allows the full utilization of concrete strength, thus there is no reduction applied in the strength checking. For the

other nodes, lateral tensile stress will reduce the concrete compressive strength.

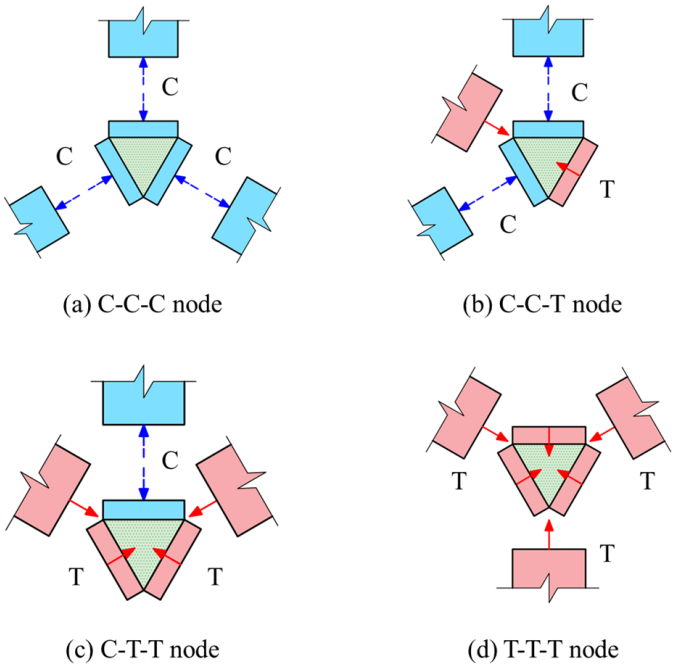

Figure 1.3: Four types of nodal zones in 2D ST models. Blue regions and red regions indicate struts and ties respectively. Green regions indicates nodal zones. T indicates forces in tensile ties, whereas C indicates force in compressive struts. All the nodes are in the compressive stress state and they are categorized based on the original forces.

In the standard STM method, there are four main steps. Here, a beam structure from Schlaich and Schafer [121] is taken as an example to introduce these steps, as shown in Figure 1.4. The detailed steps are as follows:

1. Determining the discrete loads and reactions of the given D-region. In the illustrative example, the uniform distributed load is discretized into two concentrated loads.

2. Creating a truss system to represent the force transfer mechanism of this D-region, and calculating the equilibrium forces based on the created truss system.

3. Based on the created truss system and the obtained equilibrium forces, determining the usage of steel and preceding with the strength checking for struts and nodes.

4. Based on the developed ST model, detailing the steel layout considering various practical requirements, such as anchorage length and constructability.

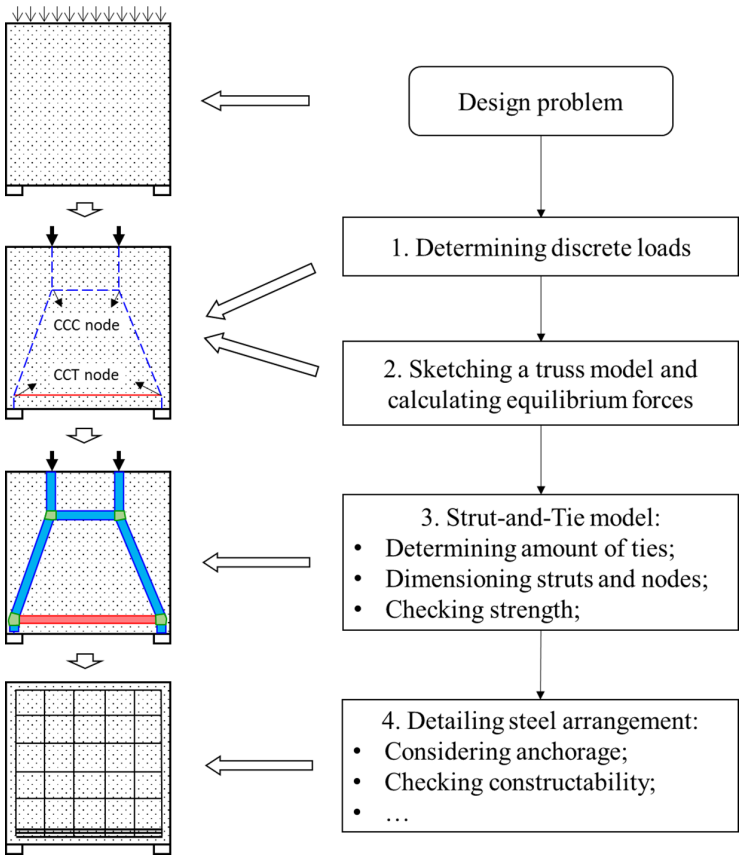

Figure 1.4: Flowchart of implementing the standard STM method. The illustrative example is adapted from Schlaich and Schafer [121].

1.1.2. TRADITIONAL METHODS TO DETERMINE STRUT-AND-TIE MODELS

The simplicity of the process of implementing the STM method and the resulting safe lower-bound designs are preferred qualities for engineers. However, the STM method requires engineers to take initiative in creating suitable models for D-regions (Step 2). Note that numerous ST models can be created for one single D-region. In the STM method, finding a suitable ST model is a priority which determines the accuracy and effectiveness of the designed structure. Currently, the creation of a suitable ST model is highly dependent on the experience of engineers. They may lack the required creativity or experience in designing more complex D-regions. In order to create ST models for complex D-regions, Schlaich and Schafer [121] proposed two standard methods.

The first method is the load path method. In the method, non-overlapped curves are created to connect discrete loads and their equilibrium reaction forces. These curves indicate the flow of forces in a given structure under the prescribed loads, geometry and boundary conditions. A truss system is developed by tracing these curves, and several

struts and ties are also added for equilibrium. An example by Schlaich and Schafer [121] of using the load path method to create ST models for a deep beam is shown in Figure 1.5.

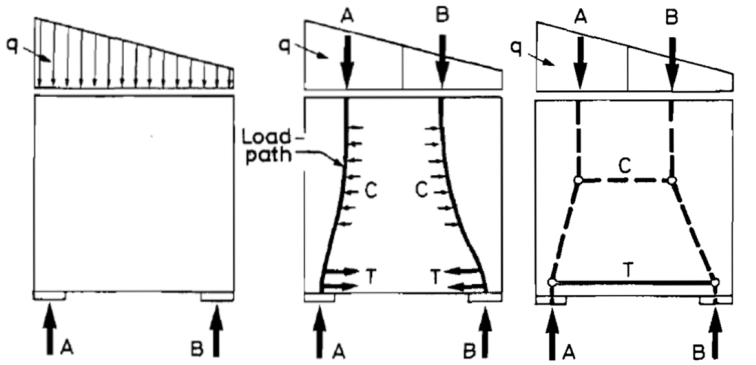

Figure 1.5: Example of applying the load path method for a deep beam [121]

The second method makes use of the linear finite element analysis. The obtained stress fields provide information, such that struts and ties can be positioned at the centers of the compressive and tensile stress diagrams respectively. The generated truss system is usually adjusted to obtain axial equilibrium forces. An example by Schlaich and Schafer [121] of using the calculated stress field is shown in Figure 1.6.

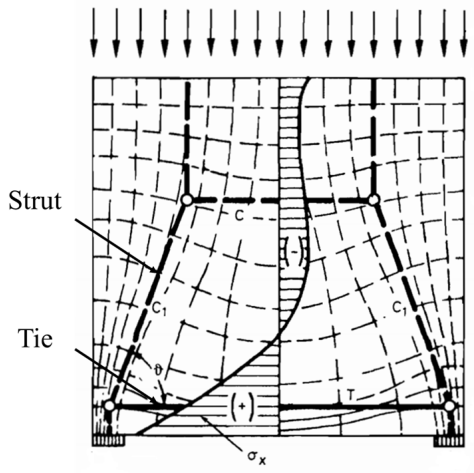

Figure 1.6: Example of using a stress field to create an ST model for a deep beam [121]

These two methods provide some guidance for engineers to design complex D-regions. However, they cannot directly generate suitable ST models and manual adjustments are required. Engineers still need to spend efforts to create effective and accurate

ST models. In addition, when the conditions of the D-region change, these efforts need to be conducted again.

1.1.3. TOPOLOGY OPTIMIZATION

Optimization techniques have been applied to find optimized structures in various fields. Among the different variants of structural optimization, topology optimization is the most versatile.

Structural topology optimization (TO) aims to find the optimum material distribution in a certain region to obtain the best structural performance [126]. In this process, the topology (i.e. number of holes and connectivity of the structure) can change, which provides more design freedom than classical shape and size optimization. Continuum TO methods have been investigated broadly since the landmark work by Bendsøe and Kikuchi [21]. Among the various proposed TO methods, there are several main branches:

- Density-based methods. In these methods, finite element models are created for analysis, and element-wise design variables are used to represent structural topology, for example, the SIMP (solid isotropic material with penalization) method [22]. The flowchart of a TO procedure of a density-based method is shown in Figure 1.7.
- Level-set methods. In a level-set TO method, the structural topology is described implicitly by iso-contours. Compared to the density-based TO method, the level-set TO method ensures crisp boundaries of optimized structures. For discussions on various level-set methods, see van Dijk et al. [143].
- Evolutionary structural optimization (ESO) methods. The basic idea of ESO methods is to gradually optimize an initially fully solid structure by removing elements with lowest performance [154].
- Other types, for example, the phase field methods [136] and the moving morphable components methods [59].

TO methods have been successfully applied in various fields for different purposes. In aeronautics and aerospace engineering, TO has been demonstrated as an effective tool for least-weight and performance design [172], for example, designing the aircraft wing box ribs [77] and designing wing internal structures [1]. In designing compliant mechanism structures, optimized topologies for displacement performance were proposed in Sigmund [125]. TO methods have been used to generate conductive structures that are efficient in heat dissipation, for example based on the SIMP method [167] and level-set method [173]. In the field of civil engineering, Baandrup et al. [17] used the SIMP TO method to design a super-long suspension bridge. The weight of the optimized bridge was reduced significantly. Stromberg et al. [131] used a TO method to design frame bracing structures. Xia et al. [149] proposed an integrated method to optimize shape and topology of free-form shell structures. In Liu and Qiao [91], optimized bridge layouts were obtained through the TO process. Bogomolny and Amir [28] and Amir [12] used TO methods to design steel arrangements for reinforced concrete structures. Numerous

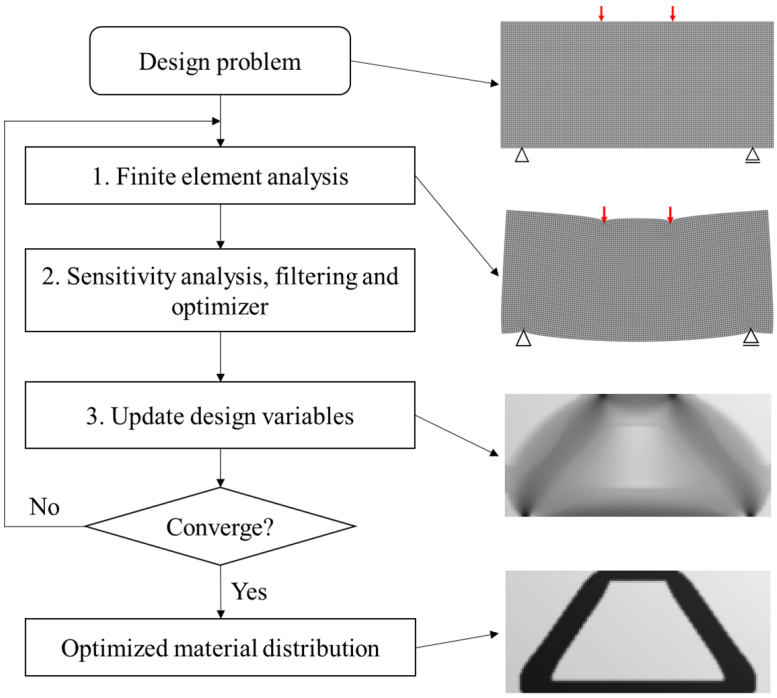

Figure 1.7: Flowchart of the procedures involved in a density-based TO method

applications in various fields have proved the effectiveness of using TO methods in the design process, especially in the conceptual design stage.

1.1.4. TOPOLOGY OPTIMIZATION TO DETERMINE STRUT-AND-TIE MODELS

In the field of STM, TO methods have been adopted to help find suitable truss-analogy models for two decades. At an early stage, Biondini et al. [25] and Ali and White [8] used the ground structure based TO methods to find optimized truss layouts for STM. Later on, using the continuum-based TO methods became the main research direction. Liang et al. [87] firstly applied an ESO method to obtain optimized material distributions to create ST models. Later on, more ESO methods have been proposed to create ST models under different configurations [10, 56, 79, 169]. Alternatively, SIMP TO methods [31], the isoline method [147] and the full-homogenization method [63] have been applied for the same purpose. Apart from using different methods, more sophisticated material models were adopted in the TO process. Victoria et al. [147] and Du et al. [46] used bi-modulus material properties in the optimization process for STM. Bruggi [33] considered no-tension concrete in the SIMP TO method to obtain the optimized material layout for the STM method. Similarly, Gaynor et al. [54] and Jewett and Carstensen [70] considered bi-modulus material properties within a hybrid truss-continuum element formulation in the SIMP TO methods.

To date, most investigations of using TO for the STM method focused on 2D D-regions. Compared to these, there are fewer studies on the 3D ST models. Leu et al. [83] applied a refined ESO TO method to obtain optimized material layouts for creating 3D ST models. Similarly, based on the ESO TO methods, He and Liu [62] generated ST models for anchorage diaphragms, Shobeiri and Ahmadi-Nedushan [124] applied a bi-directional ESO method to obtain optimized material distributions for several 3D D-regions, and Zhong et al. [168] used a micro-truss based ESO method for 3D ST models.

1.2. RESEARCH QUESTIONS

Despite intensive efforts of using various TO methods for the STM method, there are some problems that have not been solved yet. These are reflected in the research questions of the current study:

- *How to evaluate published STM-TO results to identify the best TO method for the STM method?*

  Although various TO methods and sophisticated models have been used, the question which method yields the most suitable ST models is unanswered. No research has been conducted to quantitatively evaluate various TO results and objectively compare different TO methods. For this purpose, establishing an evaluation method is an important prerequisite.

- *How to automatically generate suitable and effective ST models to facilitate the design process?*

  The use of TO methods for STM has not been widely adopted in engineering practice. A main reason is that the generated TO results cannot directly be used as ST models. Currently, TO results merely serve as inspiration for the creation of ST models. A manual process is required to transfer TO results to suitable ST models. This manual adjustment becomes particularly difficult for 3D ST models.

- *How to evaluate the performance of the generated ST model and quantify its effectiveness?*

  Although various ST models have been proposed for some D-regions, the performance and effectiveness of these ST models has not been discussed, and which ST model provides the best performance is still unknown. In order to validate the effectiveness and performance of generated ST models, an evaluation procedure needs to be proposed. In the evaluation, the practical performance of STM designs is the main focus.

- *What aspects need to be considered and implemented in the STM method to achieve a systematic design approach for D-regions?*

  There is an urgent need for a systematic approach for designing D-regions. The STM method provides a promising direction, however, there still exist some subjective aspects in its implementation. For example, the STM design needs to be

adjusted by engineers considering practical requirements. In order to develop a consistent and systematic design method, these aspects need to be investigated.

1.3. RESEARCH OBJECTIVES

In this thesis, we aim to address the outlined challenges to enable a systematic approach for designing D-regions. In order to achieve this goal, four objectives with respect to four research questions are planned, as follows:

- Proposing an approach to objectively evaluate the previously proposed TO methods and TO results for STM. Through the proposed evaluation method, the suitable TO methods can be identified.
- Based on the identified TO method, developing a method which avoids manual and subjective adjustments to automatically generate effective ST models.
- Proposing a procedure to evaluate the generated ST models. The effectiveness of the generated ST models can be validated by comparing with manually created ST models.
- Identifying the important subjective aspects in the STM method which hinder the development for a systematic approach for D-regions and investigating the identified issues based on the proposed generation method. In this way, it paves the path for investigating a systematic and widely applicable STM method in the future.

1.4. OUTLINE OF THIS THESIS

The thesis contains six chapters. The details of each chapter are introduced as follows:

Chapter 1 introduces the background, research questions and research objectives of this thesis.

Chapter 2 reviews the previous studies of using TO methods for STM. An objective evaluation procedure is proposed to evaluate the performance of these TO results from the perspective of STM. Based on the evaluation results, the advantages and disadvantages of various TO methods are discussed. In addition, some important aspects of using TO methods for STM are identified.

Chapter 3 develops a method to automatically generate 2D ST models. The proposed method is an integrated procedure that includes the TO method, a topology extraction method and a shape optimization step. Several suitable ST models are generated, and the effectiveness of the proposed method is validated. In addition, in order to demonstrate the effectiveness of the generated ST models, an evaluation procedure based on Nonlinear Finite Element Analysis (NLFEA) is proposed. The evaluation results of the generated ST models are compared with the traditional manually created ST models for the same D-regions.

Chapter 4 extends the proposed 2D ST model generation method to the 3D setting, and studies various 3D D-region design problems. The generated 3D ST models validate

the effectiveness of the proposed generation method. In addition, three important aspects (a geometrical parameter investigation, the generation considering complex loads and the influence of load discretizations) in the STM method are investigated based on the proposed generation method.

Chapter 5 discusses the main remaining subjective aspects in the STM method. These subjective aspects result in variations of the STM design and hinder the application of the STM method for complex D-regions. Two identified aspects are further investigated based on the proposed ST model generation method.

Chapter 6 presents the conclusions of this thesis, and provides directions for future research.

Note that this is a paper-based thesis. Due to this, some duplication is inevitable. The contents of the chapters 2 to 4 have been published in peer-reviewed journals. Apart from changes to the layout, there are no other differences compared to these papers.

2

A CRITICAL EVALUATION OF TOPOLOGY OPTIMIZATION RESULTS FOR STRUT-AND-TIE MODELLING OF REINFORCED CONCRETE

Defining a suitable truss model is one of the most important steps of applying the Strut-and-Tie modelling (STM) method to design D-regions in reinforced concrete (RC) structures. The truss model is a discrete representation of the stress field developed within a region of a concrete element. Topology optimization (TO) methods have been investigated by researchers for about two decades to generate suitable models for the STM method. Several truss models and numerous continuum TO results that could serve as an inspiration for suitable truss models have been proposed. However, limited attention has been paid to the evaluation of various TO results in the perspective of the STM method. As a result, it is at present unclear to what extent TO results offer a benefit for STM, and which method should be preferred. In order to address this gap, an automatic and objective evaluation procedure is proposed in this chapter. First, a TO result extraction method is proposed to systematically convert optimized topologies to truss-like structures. Next, based on the extracted structures, three evaluation measures are formulated to evaluate TO results. These measures indicate whether an analyzable truss model could be extracted, to which extent tensile stress regions are covered by tensile ties and how economical the design will be. The effectiveness of the proposed evaluation procedure is validated using known STM solutions. Subsequently, the evaluation procedure is applied to 23 TO results from literature, covering three different design problems. Most TO results show a good performance in covering tensile regions and would result in economical designs, and some undesired topologies are

The contents of this chapter have been published in Computer-Aided Civil and Infrastructure Engineering (2020) [152].

also identified by the evaluation method. Nevertheless, the use of continuum TO is most hampered by difficulties in identifying a suitable truss from the TO results.

2.1. INTRODUCTION

Strut-and-Tie modelling (STM), a truss analogy method, is a design approach for reinforced concrete structures. The use of truss analogy models originates from 1900 [100, 115]. In order to select a suitable model to design concrete structures, concrete structures are subdivided into B-regions and D-regions. B-regions are the parts of a structure with linear strain distribution, where Bernoulli beam theory applies. D-regions are the remaining parts with highly nonlinear strain distribution. Due to complex structural behaviour, design codes give limited guidance to civil engineers for designing D-regions. Consequently, finding a suitable truss analogy to design D-regions is an important topic in concrete structure designs.

The STM method was further generalized as a consistent design method for different problems of reinforced concrete structures by Schlaich et al. [122] and Schlaich and Schafer [121]. Nowadays, it is accepted that the STM method is a practical and convenient method for designing D-regions [73, 138, 141]. A Strut-and-Tie model is created to represent the flow of stress within a concrete structure carrying loads from loading regions to supports. The STM method is based on the plasticity theory and is the result of the lower bound limit analysis [16, 93, 104, 159]. Based on the lower bound limit analysis, the STM method requires force equilibrium and satisfaction of stress constraints, while compatibility conditions are neglected. Suitable analogy models play a key role in the performance and the resulting designs are conservative. The internal forces in the truss elements are used for design or verification of concrete and (steel) reinforcements. The STM approach has been implemented in various design codes (CEB-FIB, 1993; CEN, 2017; CSA, 2004; ACI-318, 2008; AASHTO, 2014).

In various studies of STM methods, finding a suitable truss system to represent a force transfer mechanism is the first priority. In order to generate a suitable truss system for STM, the use of load path methods was suggested by Schlaich and Schafer [121] and Mezzina et al. [97]. Muttoni et al. [101] suggested to generate Strut-and-Tie (ST) models based on the principal stress fields obtained by continuum finite element analysis. However, these methods have difficulties to generate suitable ST models for complex geometrical discontinuities and load conditions [87].

Optimization techniques play a more and more important role in the structural design and industry applications. In the optimization investigations, heuristic optimization methods are powerful design tools. Adeli and Balasubramanyam [6] applied a Man-Machine approach for solving the structural shape optimization. Paya et al. [109] used the simulated annealing optimization method with multiple objectives to find an overall-well RC frame. Yepes et al. [155] used a hybrid glowworm swarm algorithm to optimize precast-prestressed RC beams. The effectiveness of using genetic algorithms for structural optimizations has been investigated in a large number of studies (e.g. Aldwaik and Adeli [7], Kociecki and Adeli [75, 76], Perera and Vique [110].

Topology optimization (TO) methods have been applied in designing RC structures. Bogomolny and Amir [28] and Amir [12] considered non-linear material relations of concrete material in the TO process to design the steel of RC structures. TO methods have been applied by researchers to find suitable ST models as well. It is one of the most

popular research directions in this field. Categorized by TO approaches, these include (i) Ground structure based TO methods, (ii) ESO (Evolutionary Structural Optimization) TO methods, (iii) Density based TO methods, for example, the SIMP (Solid Isotropic Material with Penalization for intermediate densities) TO method. The relevant contributions will be discussed below. Other TO methods exist (e.g. level set methods [143], phase field methods [136] and Moving Morphable Components methods [59]), however they have not been applied for STM design yet.

Ali and White [8, 9], Biondini, Bontempi, and Malerba [25] used the ground structure based TO method to find optimized truss systems for use as Strut-and-Tie models. Also numerous continuum TO approaches have been explored in the past two decades. Liang et al. [87, 88] firstly used the ESO method to develop an optimized material layout for creating Strut-and-Tie models. Guan [56] and Guan and Doh [57] investigated suitable models of a deep beam under various numbers of holes and size configurations. Kwak and Noh [79], Almeida et al. [10] and Zhong et al. [169] considered micro-truss elements in the ESO optimization instead of continuum elements for generating optimized models. Bruggi [31, 32, 33] used the SIMP TO method to generate optimized material layouts that serve as inspiration for Strut-and-Tie models. The result of the SIMP TO method revealed a load path representing a force transfer mechanism of the structure. Moreover, in Victoria et al. [147] and Bruggi [33], considering the effect of different mechanical properties of steel and concrete regions, material models with different tensile and compressive moduli were used in the optimization to generate optimized models. Most researchers generated optimized topologies for the use as ST models by solving the compliance optimization problem. By generating various optimized topologies for different design problems, TO methods have shown a potential to develop suitable Strut-and-Tie models. However, limited attention has been paid to evaluate these results in the perspective of the STM method. In order to fill this gap, the evaluation of continuum TO results for STM methods is our main focus.

Thus, in spite of all these studies, the question which method yields the most suitable ST model is still unanswered, and the use of TO for STM has not been widely adopted in the engineering practice. To our best knowledge, very few investigations have been carried out regarding the systematic evaluation of TO results in the perspective of the STM method. Zhou et al. [171] found that the current TO process was not able to directly generate desired ST models. Recently, Zhong et al. [169] proposed a procedure to evaluate different TO results for ST models. In their method, they selected the most suitable result by visually comparing the location of ties with the tensile elastic stress field and the suspected locations of cracks, followed by an estimate of the ultimate capacity based on nonlinear finite element analysis. Their evaluation procedure marks a first attempt to quantify the suitability of TO results for STM, but contains some manual processes and subjective choices. For example, starting with the TO result, a manual interpretation and simplification is required to obtain a truss-like structure for the STM method. Similarly, many manually adjusted ST models were found in different studies. However, variation in the manual interpretation of a TO result can considerably change the suitability and quality of the optimized result. This arbitrary topology interpretation process prevents

a fair and objective evaluation of various optimized results of different TO methods. Besides, the manual interventions are impractical and inefficient for large-scale evaluations, thus an automatic method is desired.

In order to investigate to what extent TO results benefit from STM and which method should be preferred, in this chapter, an evaluation method is proposed to quantitatively and objectively compare the optimized topologies from different TO methods for the STM method. Note that, our aim is to perform a comparative evaluation and not to propose a new TO method. In the proposed evaluation method, manual steps to identify truss-like structures are replaced by a fully automatic truss extraction process. This process prevents and replaces ad-hoc topological changes of TO results, and may also simplify the process of using TO results for ST models by civil engineers in practice. Subsequently, an evaluation procedure including three measures is proposed to evaluate the suitability of obtained truss-like structures in the STM method. These measures indicate whether a truss model can be extracted from the TO results, to which extent tensile stress regions are covered by tensile ties and how economical the design will be. Together, these indices quantify the suitability of a geometry as an ST model regarding these three different aspects. In the evaluation, the proposed indices are primarily intended for comparative evaluations. Reinforcement detailing aspects, application of minimal reinforcement ratios as required by design codes and issues related to the constructibility were not addressed explicitly in the TO studies, we are evaluating. Although relevant for practical applications, these issues were consequently considered as outside the scope of our study.

In order to conduct a comparative study of various TO approaches for ST modelling, we focus on cases that have been considered in multiple studies. As these concern cases in a planar setting, our evaluation method is also defined and formulated in 2D. Nevertheless, the fundamental concepts also extend to the 3D case.

The evaluation method is implemented as an integrated and automatic procedure. Using this objective evaluation procedure, 23 TO-based results for ST modeling and 5 traditional ST models (manually generated without TO process) for three design problems are analyzed and compared based on three measures (introduced in Section 3.2). This is the first study, to our knowledge, that systematically and objectively evaluates the quality and suitability of topology optimization results for the STM method. This finally leads to recommendations for future TO research to improve its performance for generating Strut-and-Tie models.

This chapter is organized in five parts. After this introduction section, in Section 1.2 our method to interpret TO results as a truss-like structure is introduced. In Section 1.3 the three evaluation measures are introduced and the evaluation procedure is exemplified for a simple case. Section 1.4 applies the truss-like structure generation algorithm and the evaluation method to three design problems which were broadly investigated in literature. The conclusions of this chapter are presented in the last section.

2.2. INTERPRETING TOPOLOGY OPTIMIZATION RESULTS AS TRUSS-LIKE STRUCTURES

Strut-and-tie models are based on imaginary truss structures within the domain of the concrete volume. Strut-and-Tie models based on continuum TO face the problem of interpreting TO results as a truss structure. A method that converts TO results as truss-like structures is proposed in this section.

Continuum TO results typically consist of a material distribution given by a density field, with densities ranging from 0 (void) to 1 (solid). The results are data in a matrix and do not directly provide the structural information needed for STM analysis. How to interpret TO results for further applications is another broad research field. In Hsu and Hsu [64], TO results were interpreted by B-splines to obtain a parameterized geometry. Lin and Chao [89] set several shape configurations to match holes of topology optimization results and then proceeded with shape optimization based on interpreted configurations. Yi et al. [157] and Chou and Lin [39] proposed methods to identify geometrical features of TO results, followed by the shape and section optimization. A similar concept was found in Yi and Kim [156]. Nana et al. [102] proposed an automatic method to create skeletons based on TO results, and beam analysis models were created based on the pixels of the skeleton. However, none of these methods was dedicated to the extraction of ST models from continuum TO results. How to effectively extract truss-like structures based on TO results is the focus in this section.

2.2.1. PROCESS OF THE EXTRACTION METHOD FOR OPTIMIZED TOPOLOGIES

In the process of the extraction method for TO results, preserving a similar topology is the most important point. Mendoza-San-Agustin et al. [96] used a skeletonization method to simplify TO results without losing their topology. A similar skeletonization method is used here to provide simplified TO skeletons. Subsequently, these TO skeletons are used for identifying truss-like structures. In this chapter, a truss-like structure denotes a network of straight structural members that carries forces from load points to supports. The term truss-like is coined to indicate that the network does not necessarily need to represent a suitable truss for STM analysis, as will be discussed below. In the extraction process, the nodes and their connections are identified and thus the truss-like structures are generated.

The whole process of transforming TO results to truss-like structures is shown in Figure 2.1. The process consists of a thinning phase, which produces the skeleton curve of the TO result. From this, nodes in the truss network are determined and connectivity information is generated, resulting in a truss-like structure. The steps of the process are described in more detail in the following subsection.

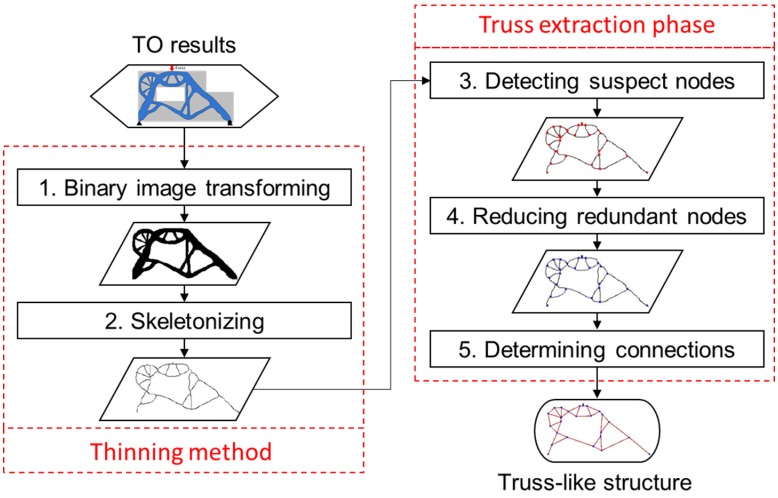

Figure 2.1: Process of the extraction method

2.2.2. THINNING PHASE

In this phase, based on image processing methods TO results are converted to simplified binary skeletons for the further truss extraction. First, TO density fields are transformed to binary designs using a threshold. For our comparative study, based on the quality of TO result images from publications, an appropriate threshold is chosen in each case to capture well optimized topologies and prevent noise. For space efficiency reasons, all resulting thresholded images are not shown here but are included in Section 4.1, Figures 17-19. Next, based on the binary design, the thinning method removes the contour until the skeleton is of one-pixel width.

1) Generating binary designs. The optimized topologies are represented by continuous density fields. For further processing, first clear solid/void (0/1) binary designs based on TO density fields are generated. A TO result by Zhong et al. [169] is used as an example. In this case, the grayscale image of the optimized topology is the source data. The binary design is obtained by setting the threshold at 0.5 to determine the 1-bit number of a pixel. The obtained binary designs of different resolutions are shown in Figure 2.2. Figure (b) is the result of a coarse mesh case, and (c) is the result of a refined mesh.

2) Thinning. Image skeletons are simplified data containing the topology information and can be extracted from the source binary data through the thinning process. Skeletonization methods have been widely investigated. Huang et al. [67] extracted the skeleton curve from a point cloud. Jiang et al. [72] used graph contraction to obtain a curve skeleton. Abu-Ain et al. [3] applied a thinning method to extract the skeleton.

In this chapter, the thinning method from Zhang and Suen [166] is used to skeletonize TO results. Its basic working principle is an iterative removal of boundary pixels, until the skeleton curve remains and no further pixels can be removed without changing the topology. In this method, pixel-wise elimination rules are firstly set. Next the method de-

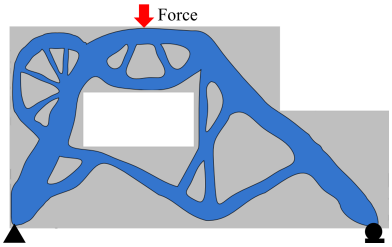

(a) Optimized topology from Zhong et al. [169]

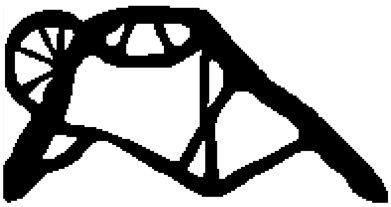

(b) Coarse mesh binary image (mesh size 50, 254 × 120 pixels)

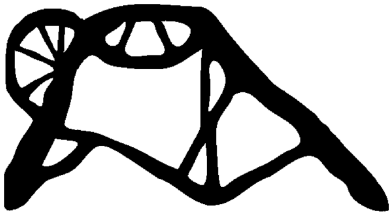

(c) Refined mesh binary image (mesh size 25, 508 × 240 pixels)

Figure 2.2: Generating binary designs based on a TO result

tects the local binary images with pixel dimension 3 × 3 and the binary image is thinned iteratively. For further details, the reader is referred to Zhang and Suen [166]. The generated skeletons are shown in Figure 2.3. The load and boundary points are taken as fixed black pixels which remain present during the thinning process. As long as the topology can be maintained, the computational time of the topology interpretation process is reduced by reducing pixels. For efficiency, a relatively coarse mesh size is used in this research. The obtained skeletons provide the essential information to identify truss-like structures.

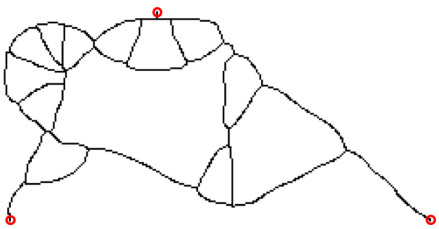

(a) Coarse mesh skeleton (mesh size 50, 254 × 120 pixels)

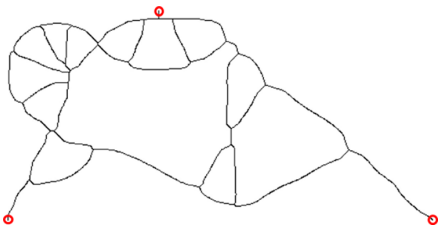

(b) Refined mesh skeleton (mesh size 25, 508 × 240 pixels)

Figure 2.3: Skeletons after the thinning process. The fixed load and boundary points are shown with red circles.

2.2.3. TRUSS EXTRACTION PHASE

In order to create truss-like structures, based on the topology skeleton the procedure of identifying nodes and bars is proposed in this section. The detailed steps of the truss extraction method in Figure 2.1 are presented below:

3) Detecting candidate nodes. The obtained skeleton is stored as a binary image. Whether a pixel in the skeleton is denoted as a candidate node is based on its value and the values of the eight neighbouring pixels. Figure 2.4 shows all five cases where a pixel is identified as a node. Note that the cases 1 to 4 include four rotationally equivalent cases, as is shown for case 1 only. If the pixel pattern of the skeleton matches one of these cases, it is selected as a candidate node. The candidate nodes of the skeleton from Figure 2.3 (b) are marked in Figure 2.5.

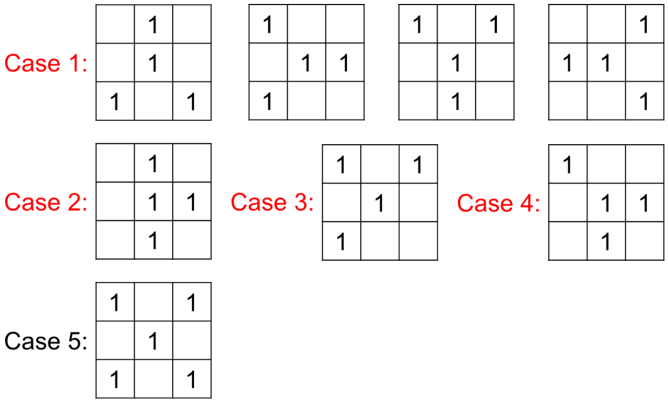

Figure 2.4: Set of patterns used for determining candidate nodes

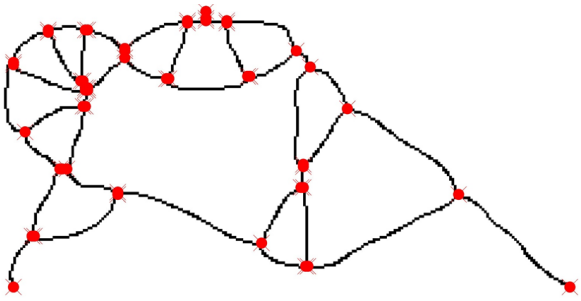

Figure 2.5: The skeleton after identifying candidate nodes, indicated in red

4) Reducing redundant nodes. Several candidate nodes may cluster in a small region. A reduction method is used to reduce redundant candidate nodes. If the mutual distance of candidate nodes is smaller than a preset tolerance (5 % of the length of the shortest edge of the original domain), then this set of nodes is replaced by a single node at the averaged location. The reduced nodes of the example are shown in Figure 2.6.

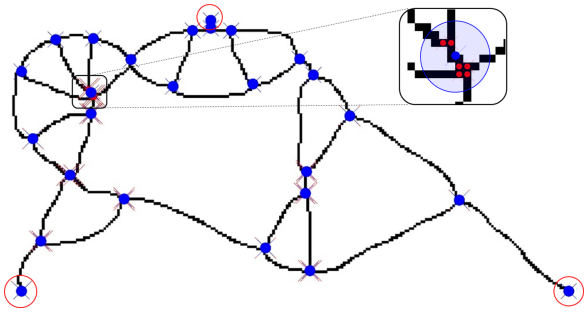

Figure 2.6: The example with reduced nodes, indicated in blue. The tolerance area to reduce redundant nodes is presented with blue regions in the enlarged inset. The nodes marked by a red circle are not connected to any hole.

5) Determining connections. After determining the nodes, their connections are required to obtain truss-like structures. First, the holes of the skeleton are identified. The identification process is similar to the process in Lin and Chao [89]. All non-skeleton pixels are detected sequentially and pixels adjacent to each other and surrounded by skeleton pixels are marked as a hole, shown in Figure 2.7. The hole information of nearby nodes is stored as topology information. For each node, it is determined which holes the node is adjacent to. Based on the center point of each hole and the vertical direction, the nodes are ordered clock-wise around the hole and connected by lines, shown in Figure 2.8. Some nodes may not be connected to any hole, such as load points and support points (Figure 2.6). These nodes are connected to a nearby node, starting from connecting to the closest node and checking the match of the connected line to the skeleton. Although this method may potentially fail with certain pathological shapes, it has proven effective for all TO results tested in this study. The resulting truss-like structure of this case is shown in Figure 2.9.

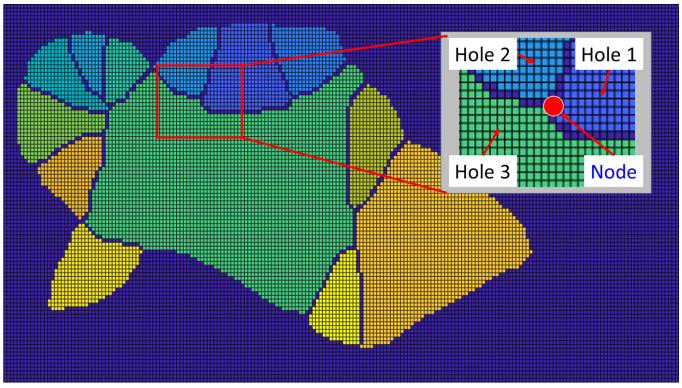

Figure 2.7: Identification of holes and topology relation of a node

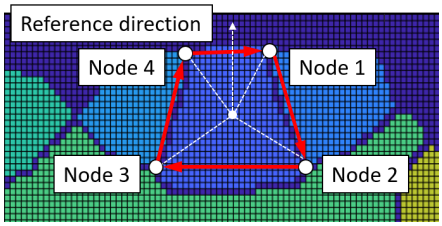

Figure 2.8: Determining connections for a hole. The connections are indicated by red arrows.

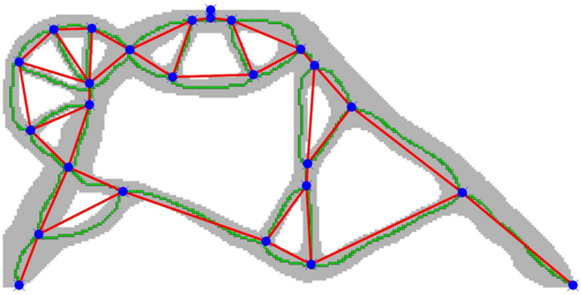

Figure 2.9: Obtained truss-like structure. The grey part is the binary TO result, the green pixels form the thinned skeleton, blue points and red lines are the identified nodes and members respectively.

2.3. EVALUATION PROCESS OF TOPOLOGY OPTIMIZATION RESULTS

In this section, three main measures are defined to evaluate the obtained truss-like structures for their suitability in the STM method. The first measure is the STS (Suitable Truss Structure) index. It measures the degree to which the obtained truss-like structure, as identified from the TO result, can be analyzed and forms an axial-force equilibrium system that is suited for the STM method. Note that ST models are often kinematic; however, any slight change of the model geometry would induce diagonal compression forces in the concrete to stabilize the structure [47]. The second measure is the TRS (Tensile Region Similarity) index. It measures whether the tension regions in optimized topologies spatially correspond to the regions of tensile stress in the original full domain. Covering tensile stress regions in original concrete domain is considered as an advantageous property of the truss analogy as the resulting steel layout will limit severe concrete cracking before reaching the ultimate loading capacity of the D-region [50]. The third measure is the SR (Steel Reinforcement) ratio. It provides an estimate how much reinforcement steel will be required for the proposed truss analogy and it thus indicates how economical the design will be.

2.3.1. FRAMEWORK OF THE EVALUATION METHOD

An automatic evaluation method is proposed. The framework is shown in Figure 2.10. At the beginning of the evaluation process, images of TO results are used as input files. In this chapter, we use 21 different TO results and 5 traditional ST models for three design problems from literature. Two more TO results are created using SIMP TO method to provide a more complete comparison and discussion. These results will be introduced in Section 4.1. Based on using the TO result extracting method from the previous section, a set of truss-like structures can be extracted for a certain design problem. The process provides a uniform platform to compare various TO results from literature for the same design problem. Next, Finite Element Analysis (FEA) is used to obtain the structural response. The 4 node bilinear quadrilateral element under the plane stress assumption is used for the continuum full concrete domain and the classical beam element is used for the truss-like structure. Use of beam elements is necessitated because the truss-like structures generated by the truss extraction process are usually statically and kinematically unstable trusses. The equilibrium forces of unstable structures cannot be calculated through truss analysis. Based on the obtained structural response, the STS index and SR ratio are calculated. However, determining the TRS index needs two more steps introduced in the following section. After calculating these three measures, the advantages and disadvantages of various TO results for STM can be evaluated.

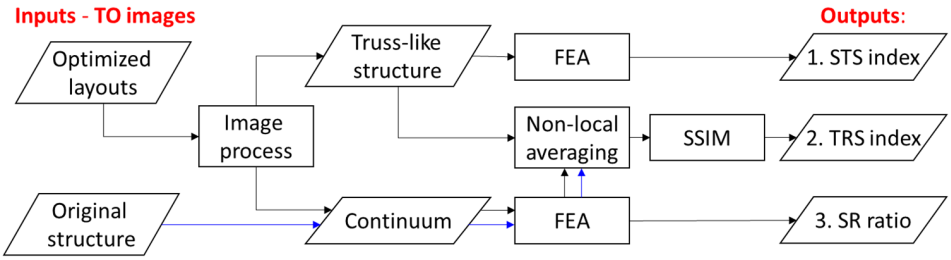

Figure 2.10: Framework of the evaluation method

2.3.2. EVALUATION MEASURE DEFINITION

SUITABLE TRUSS STRUCTURE (STS) INDEX

In the STM method, a basic requirement is that all members are subjected to an axial-force equilibrium state. However, we find that the truss-like structures generated by the truss extraction process often do not meet this requirement. For our comparative evaluation, it is relevant to quantify the closeness of the structure to an analyzable truss. In order to discuss this point, slender beam elements are used to analyze the interpreted truss-like structures. The slender beam model has members with a low bending stiffness. The axial forces are obtained for conventional kinematic ST models. The shear forces indicate (unwanted) moments in the elements. In the slender beam element analysis, the cross section is assumed as rectangular in which the width equals to the out-of-plane

thickness of the original continuum and the height is 1 % of its width. The distribution of axial and shear forces stabilizes as slenderness is increased, hence this thickness is chosen as an adequate value. The resulting axial forces and shear forces are used to formulate the STS index, defined in Equation (2.1):

$$\text{STS} = \frac{1}{n}\sum \frac{|N_e|}{|N_e|+|V_e|}, \tag{2.1}$$

where, N_e is the element axial force, V_e is the element shear force, and n is the number of elements. The STS index has the range [0,1]. When STS = 1, all members in the truss-like structure are subjected to axial forces only and it can be used as-is in the STM method. For lower values, adjustments would be necessary before use in the STM method, however these modifications are outside our scope. In this study, our focus is on comparing suitability of the results provided by TO methods. Results with a lower STS index are further from true truss structures, and therefore less desired.

TENSILE REGION SIMILARITY (TRS) INDEX

Tensile stress is critical to concrete structures. Following recommendations by Schlaich et al. [122], Schlaich and Schafer [121] and Bergmeister et al. [24], the position and orientation of ties and struts should ideally reflect the stress field of a linear analysis of the complete domain. This will prevent excessive cracking at the service load level (whereas the STM method is a capacity check at the higher ultimate load level). Considering that steel reinforcements are located and aligned at the places where they contribute most to the bearing capacity of the structure (for the ultimate limit state) and avoid excessive concrete cracking (for the serviceability limit state), it is especially relevant that the tensile regions of the stress fields are well covered by ties of the truss. Therefore, tensile stress fields of the original structure and TO results are compared to formulate the TRS index. Based on linear FEA, the principal stress vectors $\boldsymbol{\sigma}^{\text{ori}}$ and $\boldsymbol{\sigma}^{\text{TO}}$ of the original structure and optimized results are obtained, where σ_{I} and σ_{II} are first and second principal stress respectively ($\sigma_{\text{I}} > \sigma_{\text{II}}$). In this research, the critical tensile regions are defined as those, where the first principal stress is much larger than the second principal stress, $\sigma_{\text{I}} > 0$ and $\sigma_{\text{I}} > -5\sigma_{\text{II}}$. Based on the tensile stress, the TRS index is formulated after a non-local averaging operation and image comparison, as defined below.

Two important aspects must be included in formulating the TRS index. First, a larger volume fraction in the TO process leads to topologies with wider structural members. Regardless of the volume fraction, TRS indices should be similar as long as the main topology is comparable. Second, the reinforcement would improve the crack-resisting capacity of the nearby concrete. So, the criterion has been formulated such, that it is relatively insensitive to changes in volume fraction and to minor differences in positioning of tensile regions/members. The non-local averaging operation is used to determine the influenced tensile region. This operation has been applied in the investigation of fracture behaviour analysis [see 18], the sensitivity filtering in TO methods to solve mesh-independence and checker-board problems [see 127], and achieving the minimum length scale in the TO process[see 58]. In this research, the stress of tensile regions is spread through non-local

averaging. The non-local averaging is implemented through the filter, defined as:

$$\bar{\boldsymbol{\sigma}}_i = \frac{\sum_{j=1}^{n} h(i,j)\cdot \boldsymbol{\sigma}_j}{\sum_{j=1}^{n} h(i,j)}, \tag{2.2}$$

where $h(i,j)$ is a convolution filter, $\boldsymbol{\sigma}_j$ is the stress of element j whereas $\boldsymbol{\sigma}_j = \mathbf{0}$ outside the tensile region, $\bar{\boldsymbol{\sigma}}_i$ is the averaged stress of element i which is affected by surrounded elements. The stress vectors $\boldsymbol{\sigma} = \{\sigma_x, \sigma_y, \tau_{xy}\}$ of all elements in the tensile region are filtered. Next, the averaged principal stresses are calculated based on the averaged stress $\bar{\boldsymbol{\sigma}}$. The convolution filter $h(i,j)$ is defined as:

$$h(i,j) = \max(0, r_0 - r(i,j)), \tag{2.3}$$

where $r(i,j)$ indicates the centroid distance between elements i and j, and r_0 is the averaging radius, defined as:

$$r_0 = \frac{1}{2}\frac{V}{L\cdot t}. \tag{2.4}$$

Here, V is the volume of the original structure, L is the total length of the extracted truss-like structure calculated by summing lengths of all its members, and t is the thickness of the original structure. Based on this formulation, as long as the main topologies of different optimized results are the same, the extracted truss-like structures are the same and their total length L is also equal. Therefore the radius is the same for these results regardless of the volume fraction and minor topology differences.

After obtaining the averaged tensile stress fields, the TRS index quantifies the similarity of two stress fields with the help of an image analysis method. The image analysis method quantifies the difference of images compared to a reference image. The SSIM (Structural Similarity) index for image comparison was proposed in Wang et al. [148]. It quantifies the similarity between two samples based on 3 metrics: luminance, contrast and structure [85, 148]. The calculation of the SSIM index is defined as:

$$\mathrm{SSIM}(\boldsymbol{a},\boldsymbol{b}) = \frac{[2\mu(\boldsymbol{a})\mu(\boldsymbol{b}) + C_1][2\tau(\boldsymbol{a},\boldsymbol{b}) + C_2]}{[\mu^2(\boldsymbol{a}) + \mu^2(\boldsymbol{b}) + C_1][\lambda^2(\boldsymbol{a}) + \lambda^2(\boldsymbol{b}) + C_2]}, \tag{2.5}$$

where $\boldsymbol{a}$ and $\boldsymbol{b}$ are two sample data, μ is the sample mean, λ is sample standard deviation and τ is the sample correlation coefficient. C_1 and C_2 are chosen as 10^{-6} to avoid a zero in the denominator. The SSIM index has the range [0,1], where 0 means extremely poor similarity and 1 means perfect similarity.

In this research, the SSIM analysis is used to compare stress fields. First, the averaged tensile principal stress of the original structure and optimized results are scaled as $\hat{\boldsymbol{\sigma}}^{\mathrm{ori}}$ and $\hat{\boldsymbol{\sigma}}^{\mathrm{TO}}$ respectively, where $\hat{\boldsymbol{\sigma}} = \bar{\boldsymbol{\sigma}}_1 / \max(\bar{\boldsymbol{\sigma}}_1)$ is the averaged first principal stress in the tensile region. Next, the SSIM index is used to quantify the similarity between the tensile principal stress field in the topology optimized structure and the original structure, which defines the Tensile Region Similarity or TRS index, defined as:

$$\mathrm{TRS} = \mathrm{SSIM}(\hat{\boldsymbol{\sigma}}^{\mathrm{ori}}, \hat{\boldsymbol{\sigma}}^{\mathrm{TO}}). \tag{2.6}$$

A large TRS index indicates that the topology optimization result is effective in representing the tensile regions of the original structure.

STEEL REINFORCEMENT (SR) RATIO

The amount of steel usage is an important aspect in designing RC structures. Efficient steel utilization results in a less costly design. In this research, the steel reinforcement ratio is taken as the third metric to compare various TO results. Based on the FEA structural response of the TO results, the SR ratio is calculated as the volume fraction of steel with respect to the concrete volume, defined as:

$$\mathrm{SR} = \frac{1}{V_{\mathrm{ori}}} \int \frac{\max(\sigma_1, 0)}{f_y} \mathrm{d}\Omega_e. \tag{2.7}$$

In the equation, f_y is the yield strength, Ω_e denotes the elements in the tensile region, and V_{ori} is the total volume of the original structure. The proportions of the positive first principal stress to the yield strength indicate the usage of steel in designing RC structures. Throughout the chapter $f_y = 450$ MPa has been assumed.

2.3.3. A SIMPLE CASE FOR ILLUSTRATION

A classical case study is used to illustrate the evaluation method. The basic information of the case is shown in Figure 2.11. In the figure, (a) shows load and boundary conditions of the deep beam of equal length and height (2 m). The thickness of the structure is 0.1 m, the concentrated forces are 1000 kN, Young's modulus is 30 GPa, Poisson's ratio is 0.2, and the yield strength is 450 MPa. Figure 2.11(b) and (c) are the relatively good and bad Strut-and-Tie models provided by [121], where all members have been given a thickness of 0.1 m, and the designs are represented by images that can be processed by our evaluation method in the same way as TO results, and (d) is our example TO result based on compliance minimization using the SIMP method [14]. The optimized topology is obtained with 50 % volume fraction of the original structure and using the sensitivity filtering technique [127].

Following the proposed evaluation method from Figure 2.10, Figure 2.12 depicts the result of truss extraction applied to each of the topologies. After FEA of the continuum, the principal stress plots are shown in Figure 2.13.

Based on the obtained truss-like structure, the total lengths of all members of three truss-like structures are 6.92 m, 9.92 m and 6.85 m respectively, and the radius r_0 in the non-local averaging analysis is 0.29 m, 0.2 m and 0.29 m. The averaging domains are shown in Figure 2.12. Figure 2.14 shows the scaled averaged tensile principal stress after non-local averaging, using a grayscale colour scheme. The TRS indices are subsequently calculated through SSIM analysis. The evaluation results are shown in Table 2.1. Comparing results of two ST models by Schlaich and Schafer [121], a bad model in the STM method results in a higher SR ratio and a lower TRS index. The evaluation result based on the optimized topology has a higher TRS index and a lower SR ratio than the two Strut-and-Tie models. However, the extracted truss-like structure has a lower STS index, i.e. more shear force than the other two cases, which indicates it is not a pure truss structure. This is primarily due to the orientation of the bars near the load and support points. An adaptation towards a proper truss structure is possible, but the lower STS index is indicative of the fact that some modification is needed.

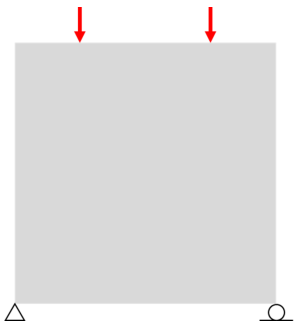

(a) Original structure

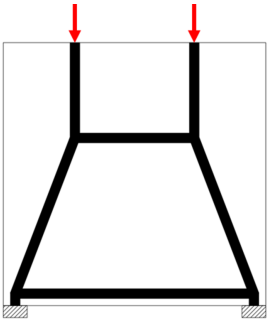

(b) Good ST model

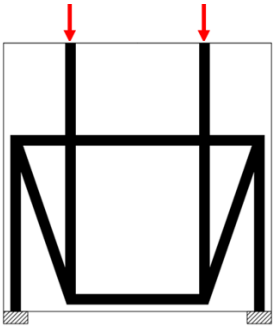

(c) Bad ST model

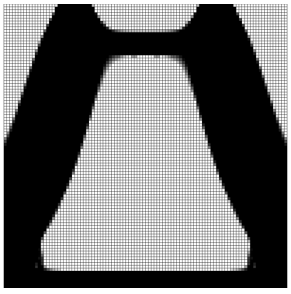

(d) TO result

Figure 2.11: Geometries considered to illustrate the evaluation method. (a) shows the deep beam design problem; (b) and (c) show manually generated ST models; (d) shows the TO result.

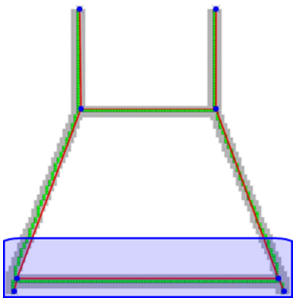

(a) Good ST model

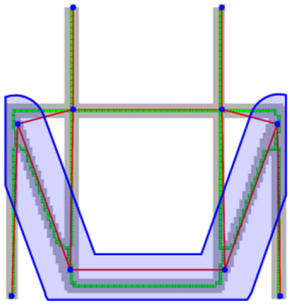

(b) Bad ST model

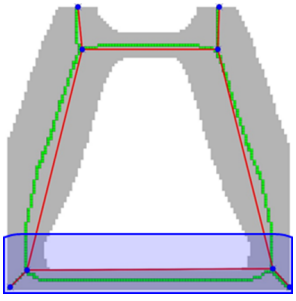

(c) TO result

Figure 2.12: Results after image processing and truss extraction. The blue regions indicate the averaging domains in the non-local averaging operation.

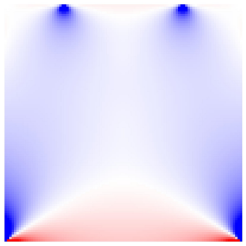

(a) Original structure

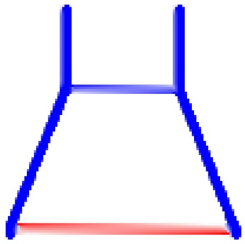

(b) Good ST model

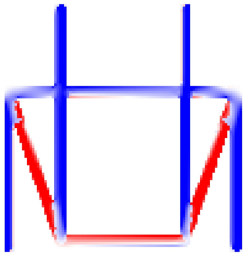

(c) Bad ST model

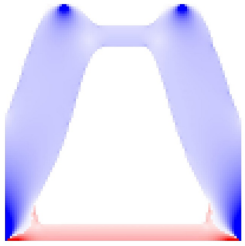

(d) TO result

Figure 2.13: Principal stress plots. Red and blue parts indicate the tensile and compressive regions respectively.

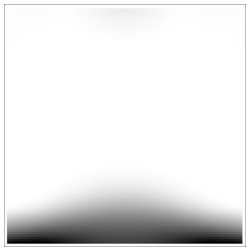

(a) Original structure

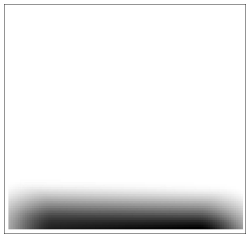

(b) Good ST model

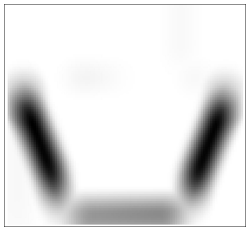

(c) Bad ST model

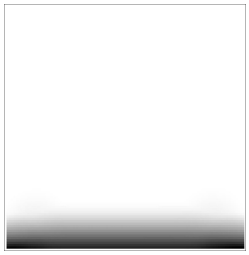

(d) TO result

Figure 2.14: Scaled tensile principal stress after non-local averaging

Table 2.1: Evaluation results of the illustrative case study (%)

Cases	STS index	TRS index	SR ratio
Good ST model	98.8	83.7	1.59
Bad ST model	99.3	**46.4**	**4.82**
Optimized result	**93.6**	84.1	1.42

2.4. STM CASE STUDIES FROM LITERATURE

2.4.1. PROBLEM INTRODUCTION

Based on different considerations and requirements in the perspective of the STM method, researchers have proposed different TO methods to generate a large variety of optimized layouts, as reviewed in the first section. The majority of papers have explored multiple 2D problems and proposed several optimization results. A limited number of papers (Guan and Doh [57], Almeida et al. [10], Zhou et al. [171] and Zhong et al. [169]) contained also Strut-and-Tie models, however these models were not directly determined from the optimized topology and usually manual changes were made. Regardless of various applications of different TO methods, efforts were proposed to improve the TO method, for example, smoothing the constitutive relation in the optimization process, considering different tensile and compressive moduli and using micro-structure based elements instead of continuum elements. We found three cases which were investigated relatively frequently: a deep beam with square opening, a corbel, and a dapped-end beam with rectangular opening (Figure 2.15). These cases form the basis for our comparison of TO-based ST models. Various published results are evaluated, compared and discussed in this section.

In the evaluation process, the thickness of the structures is 300 mm, the Young's modulus and Poisson's ratio are 20 GPa and 0.2 respectively. The principal stress plots of the full concrete domains are plotted in Figure 2.16, where red and blue regions show the tensile and compressive regions respectively.

Table 2.2 gives an overview of the considered topology results from literature that are used in this section. The detailed settings of all these results are shown in Table 2.3. For the different mesh settings, the number indicates the ratio of coarse mesh size and refined mesh size.

The study includes 28 different results from 11 individual papers. The TO results of the three cases, as extracted from the publications at identical resolution, are shown in Figure 2.17, Figure 2.18 and Figure 2.19. The test set contains a variety of models that allow comparisons of different aspects. Result I-10 and I-11 are generated by a conventional SIMP optimization method with a 40 % volume fraction and sensitivity filtering. The traditional ST models which were proposed without using TO methods are recreated as continua in our study (Result I-1, I-2, II-1, III-1 and III-2). Result I-3 and II-2 are generated based on a conventional ESO method by Liang et al. [87]. The mesh size is an aspect affecting TO results. Optimized results with coarse mesh sizes are shown

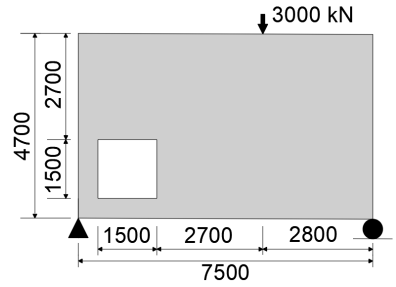

(a) Case I: Deep beam with opening

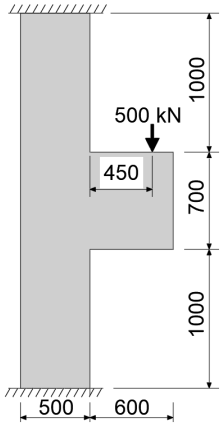

(b) Case II: Corbel

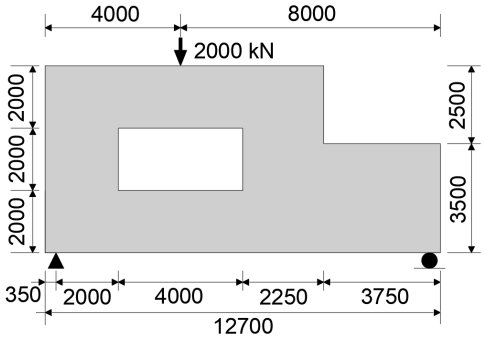

(c) Case III: Dapped-end beam with opening

Figure 2.15: Basic information of three cases (mm)

as Result I-4, I-10, II-3, II-5 and II-9. In contrast, Result I-5, I-11, II-4, II-6 and II-10 are optimized topologies for corresponding cases using a refined mesh size. Victoria et al. [147] considered different tensile and compressive moduli in the optimization process: Result I-7 and II-8 are optimized topologies with a larger tensile modulus, while Result I-6 and II-7 are commonly optimized topologies with the same method. Moreover, the topology using a small volume fraction is shown as Result I-8. Similarly, Du et al. [46] proposed an orthotropic material model considering different tensile/compressive modulus in the SIMP TO process. Result II-11 is the optimized result obtained by using a large tensile modulus. A truss-continuum hybrid topology optimization method was proposed in Gaynor et al. [54], the optimized result and a reference result based on conventional TO are included as Result III-5 and III-4 respectively. Result III-3 is generated by using the full-homogeneous optimization method. Result III-6 is generated by using the ESO

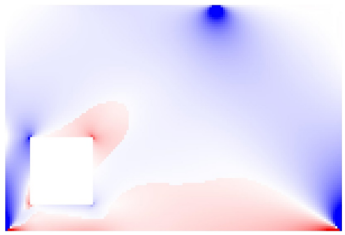

(a) Case I: Deep beam with opening (mesh size: 50 mm)

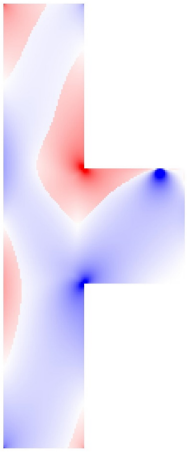

(b) Case II: Corbel (mesh size: 10 mm)

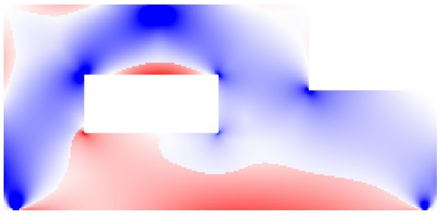

(c) Case III: Dapped-end beam with opening (mesh size: 50 mm)

Figure 2.16: Principal stress plots of three cases. Red and blue parts indicate the tensile and compressive regions respectively.

method with the removal criterion of the first principal stress.

Using the 3-measure evaluation process defined in Section 3, all considered models have been evaluated. Section 4.2 presents the results, followed by further discussion in Section 4.3.

Table 2.2: Categorization of TO results of three cases

Literature	Result I	Result II	Result III
Schlaich et al. [122]	I-1,2	II-1	-
Liang et al. [87]	I-3	II-2	-
Kwak and Noh [79]	I-4,5	II-3,4	-
Bruggi [31]	-	II-5,6	-
Reineck [114]	-	-	III-1,2
Victoria et al. [147]	I-6,7,8	II-7,8	-
Herranz et al. [63]	-	-	III-3
Gaynor et al. [54]	-	-	III-4,5
Almeida et al. [10]	I-9	II-9,10	-
Zhou et al. [171]	-	-	III-6
Du et al. [46]	-	II-11	-
This research	I-10,11	-	-

2.4.2. EVALUATION RESULTS OF THREE CASES

Here, the results of the three cases are discussed individually. Overall result analysis and discussion are provided in Section 4.3. The evaluation result of Case I is shown in Table 2.4, the principal stress plots for this case are shown in Figure 2.20, the extracted truss-like structures are shown in Figure 2.21. The considered traditional Strut-and-Tie models (that are not based on TO), have a relatively high STS index. Indeed, they are designed as trusses. They have a relatively low TRS index since they miss a tensile tie bottom-left, below the opening. The models based on TO score higher on average for representing the tensile region, with exceptions (Result I-4,7,8). Among the different TO results, Result I-9 has the highest TRS index. Also on average, optimized models have small SR ratios, which indicates less steel utilization. The lowest SR ratios are obtained in Result I-9, I-10 and I-11, while again Results I-4, I-7 and I-8 score comparatively worse. Traditional ST models result in larger SR ratios than TO based models. Overall, the TO based models of Result I-5, I-10 and I-11 show good performance. On contrary, Result I-4, I-7 and I-8 show a relatively poor performance.

The principal stress plots for the Case II and Case III are shown in Figure 2.22 and Figure 2.23, and their extracted truss-like structures are shown in Figure 2.24 and Figure 2.25.

The evaluation result for Case II is shown in Table 2.5. From the standard deviation of indices, it is seen that this case has an overall stable result, except for Result II-8 and Result II-11 which have considerably larger SR ratios than the other results. All results

Table 2.3: Detailed information of selected TO results

Results	Literature	Method	Optimization setting	Special measure	Details
I-1 I-2	Schlaich et al. [122]	STM (not based on TO)	-	-	-
I-3	Liang et al. [87]	ESO	Strain energy removal criterion	-	-
I-4 I-5	Kwak and Noh [79]	ESO	Strain energy removal criterion	Micro-truss elements	Coarse mesh Refined mesh 1.5x
I-6 I-7 I-8	Victoria et al. [147]	Isoline approach	Mises stress removal criterion	- Different tensile and compressive modulus -	Volume fraction 17% Volume fraction 17% Volume fraction 8 %
I-9	Almeida et al. [10]	Smooth ESO	Mises stress removal criterion	Smoothing constitutive relation	-
I-10 I-11	This research	SIMP	Minimizing compliance	-	Coarse mesh Refined mesh 2x
II-1	Schlaich et al. [122]	STM (not based on TO)	-	-	-
II-2	Liang et al. [87]	ESO	Strain energy removal criterion	-	-
II-3 II-4	Kwak and Noh [79]	ESO	Strain energy removal criterion	Micro-truss elements	Coarse mesh Refined mesh 1.5x
II-5 II-6	Bruggi [31]	SIMP	Minimizing compliance	-	Coarse mesh Refined mesh 4x
II-7 II-8	Victoria et al. [147]	Isoline approach	Mises stress removal criterion	- Different tensile and compressive modulus	-
II-9 II-10	Almeida et al. [10]	Smooth ESO	Mises stress removal criterion	Smoothing constitutive relation	Coarse mesh Refined mesh 4x
II-11	Du et al. [46]	SIMP	Orthotropic constitutive relation	Different tensile and compressive modulus	-
III-1 III-2	Reineck [114]	STM (not based on TO)	-	-	-
III-3	Herranz et al. [63]	Full-homogenous method	Minimizing compliance	-	-
III-4 III-5	Gaynor et al. [54]	Hybrid truss-continuum	Minimizing compliance	- Different tensile and compressive modulus	-
III-6	Zhou et al. [171]	ESO	Axial stress removal criterion	Micro-truss elements	-

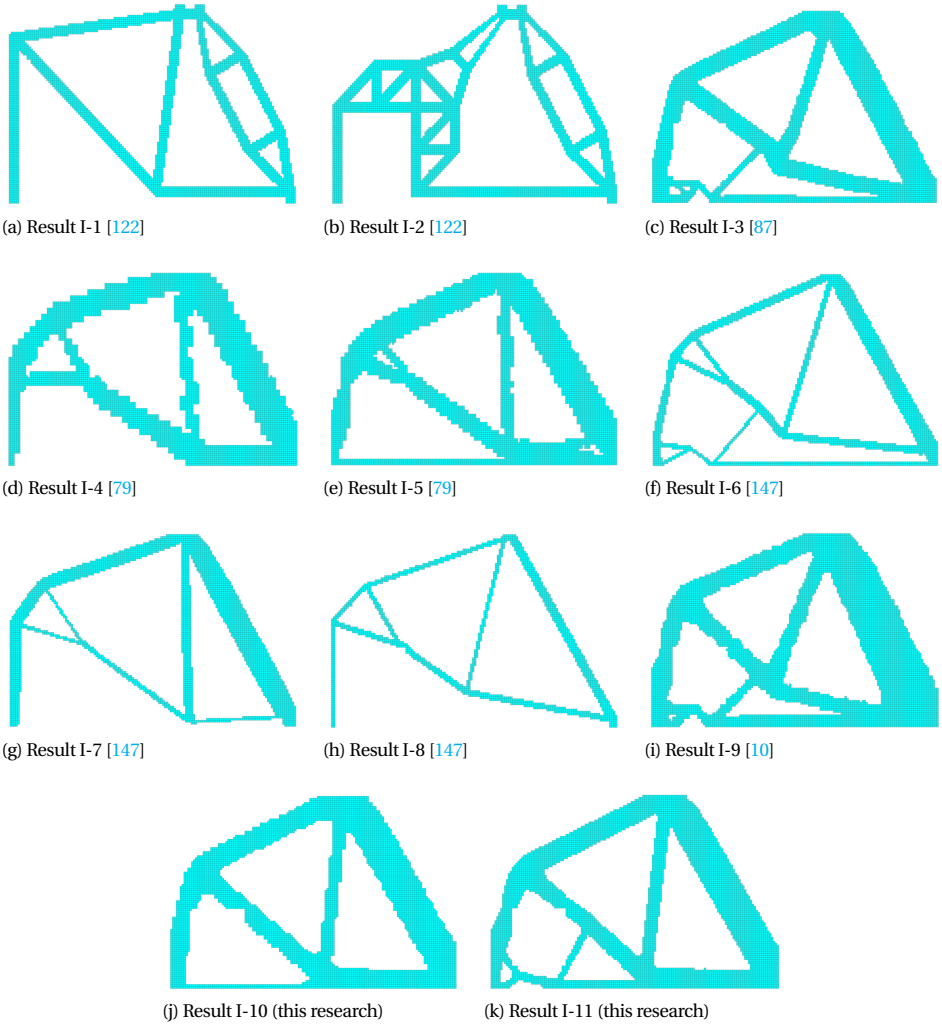

(a) Result I-1 [122] (b) Result I-2 [122] (c) Result I-3 [87]

(d) Result I-4 [79] (e) Result I-5 [79] (f) Result I-6 [147]

(g) Result I-7 [147] (h) Result I-8 [147] (i) Result I-9 [10]

(j) Result I-10 (this research) (k) Result I-11 (this research)

Figure 2.17: Case I: Topology optimized results of the deep beam with an opening

have an overall high STS index. In general, the traditional ST model again has a slightly smaller TRS index and larger SR ratio than topology optimized results. In this case, Result II-8 and II-11 would require more than twice the amount of steel compared to the most economical design.

The evaluation results of Case III are shown in Table 2.6. Similar to the previous two cases, traditional ST models show smaller TRS indices and larger SR ratios. The topology optimized results show similar performance with the exception of Result III-6, which performs poorly on all three aspects.

Based on the evaluation results of three cases, Case II is less sensitive to TO meth-

(a) Result II-1 [122]

(b) Result II-2 [87]

(c) Result II-3 [79]

(d) Result II-4 [79]

(e) Result II-5 [31]

(f) Result II-6 [31]

(g) Result II-7 [147]

(h) Result II-8 [147]

(i) Result II-9 [10]

(j) Result II-10 [10]

(k) Result II-11 [46]

Figure 2.18: Case II: Corbel

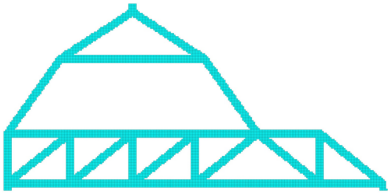

(a) Result III-1 [114]

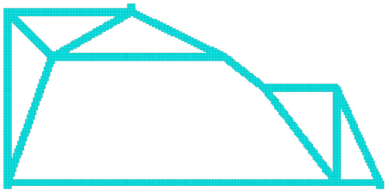

(b) Result III-2 [114]

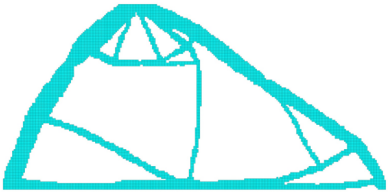

(c) Result III-3 [63]

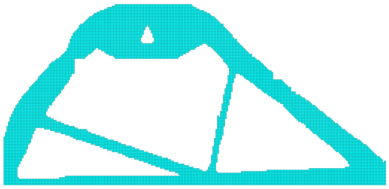

(d) Result III-4 [54]

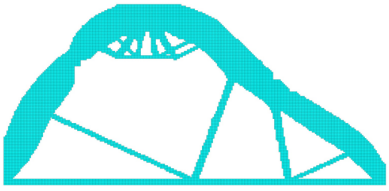

(e) Result III-5 [54]

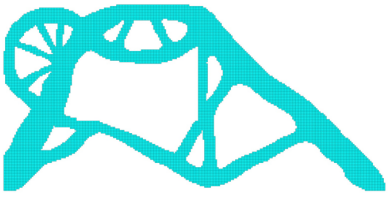

(f) Result III-6 [171]

Figure 2.19: Case III: Dapped-end beam with opening

Table 2.4: Evaluation results for Case I: Deep beam with an opening (%)

Results	STS index	TRS index	SR ratio
I-1	94.8	**61.5**	0.861
I-2	**96.8**	66.3	**1.111**
I-3	**77.0**	81.0	0.761
I-4	94.1	64.9	0.894
I-5	93.9	78.0	0.744
I-6	95.7	72.1	0.80
I-7	94.4	65.2	0.978
I-8	95.1	64.1	0.928
I-9	77.5	**83.0**	**0.717**
I-10	92.8	77.8	**0.717**
I-11	88.9	81.4	**0.717**
Avg	91.0	72.3	0.839
Std	7.09	8.13	0.129

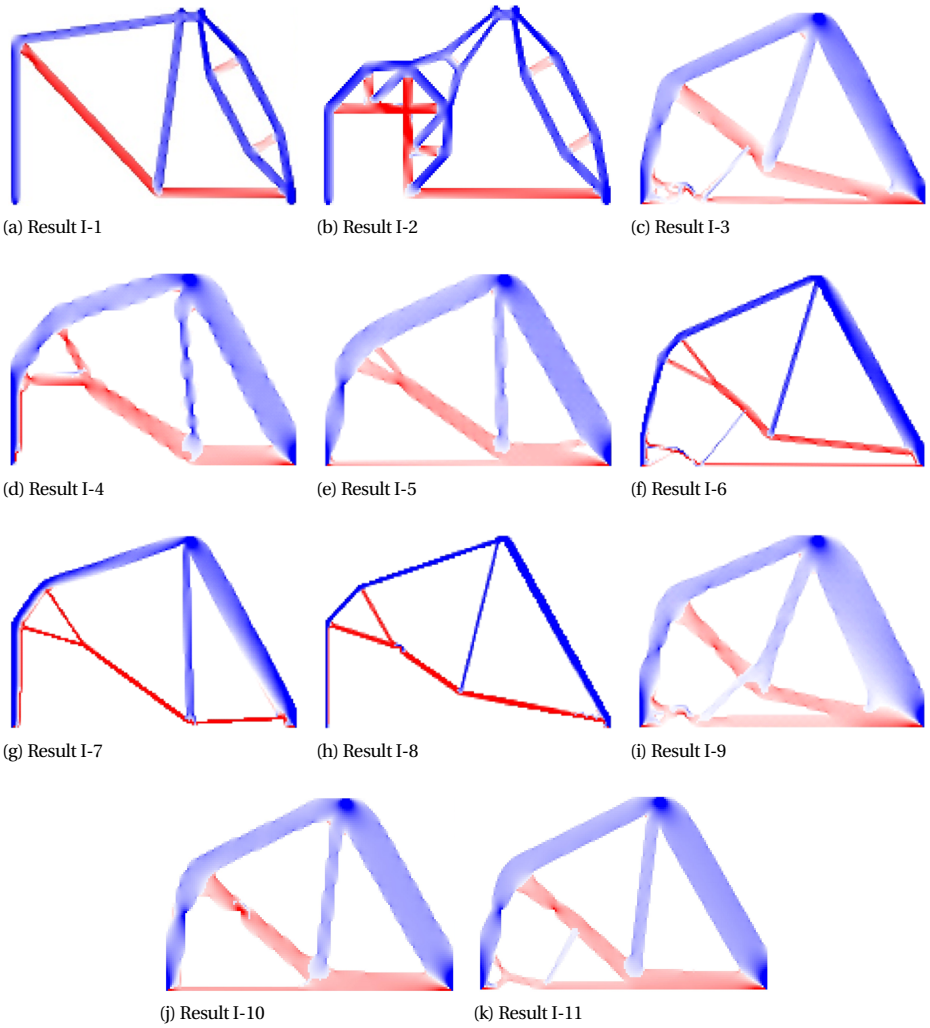

(a) Result I-1 (b) Result I-2 (c) Result I-3

(d) Result I-4 (e) Result I-5 (f) Result I-6

(g) Result I-7 (h) Result I-8 (i) Result I-9

(j) Result I-10 (k) Result I-11

Figure 2.20: Principal stress plots of Case I: Deep beam with an opening. Red and blue parts indicate the tensile and compressive regions respectively

ods than the other cases. Most of the TO results lead to similar results even when the optimized topologies are different visually. No matter what type of TO approach (ESO, SIMP, full-homogeneous method etc.) is used, in general, topology optimized results have better scores in representing the tensile region of the original structure and will result in less steel utilization than traditional ST models. However, the recognized truss-like structures of the TO results have less than ideal STS indices, which indicates that the results cannot be directly applied in the STM method.

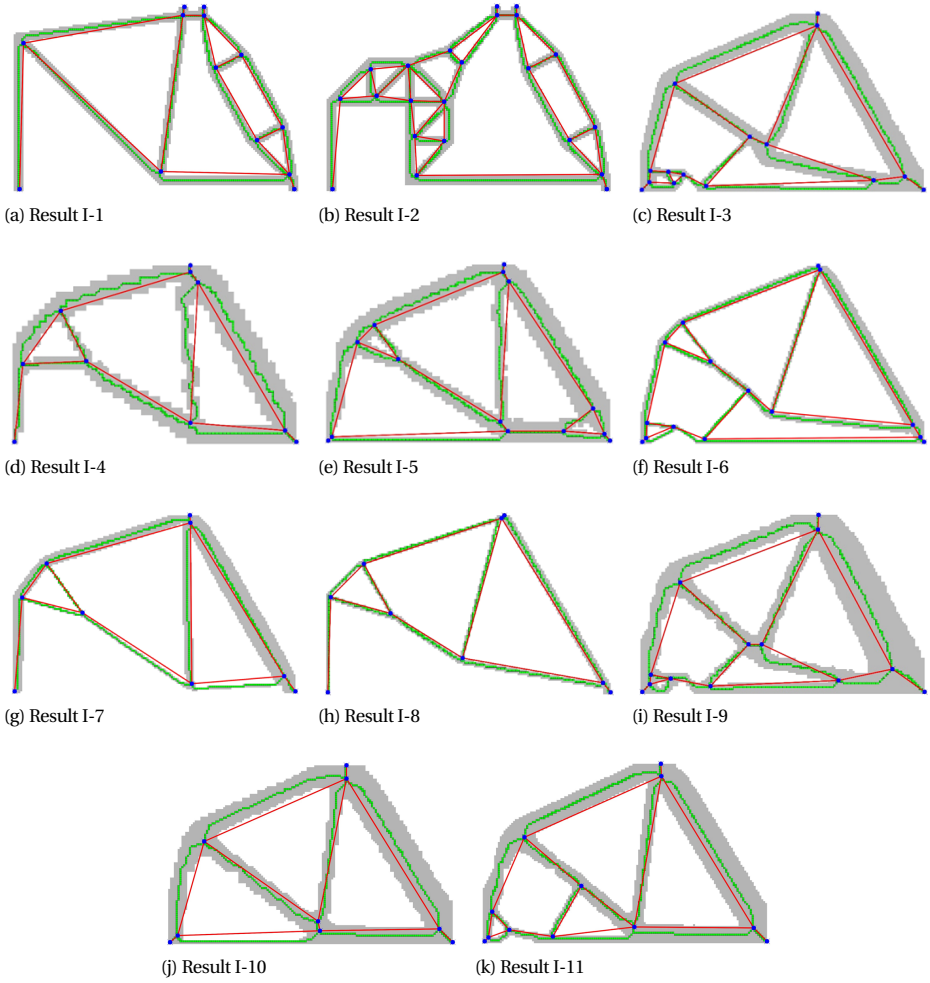

(a) Result I-1 (b) Result I-2 (c) Result I-3

(d) Result I-4 (e) Result I-5 (f) Result I-6

(g) Result I-7 (h) Result I-8 (i) Result I-9

(j) Result I-10 (k) Result I-11

Figure 2.21: Extraction results of Case I: Deep beam with an opening

2.4.3. RESULT DISCUSSIONS

In this section, based on the evaluation results of three cases, four main aspects are analyzed and discussed. Firstly, the influence of using different material models in the TO process on the three suitability measures is discussed. Secondly, the optimization result is usually a local minimum based on a certain set of parameters in the TO process. Similarly, the influence of different optimization parameters is discussed. Thirdly, the advantages of using TO methods is discussed by comparing to conventional ST models. Lastly, regarding to the axial-force equilibrium requirement for the STM, the suitability of the generated truss-like structures based on the proposed extraction method is discussed.

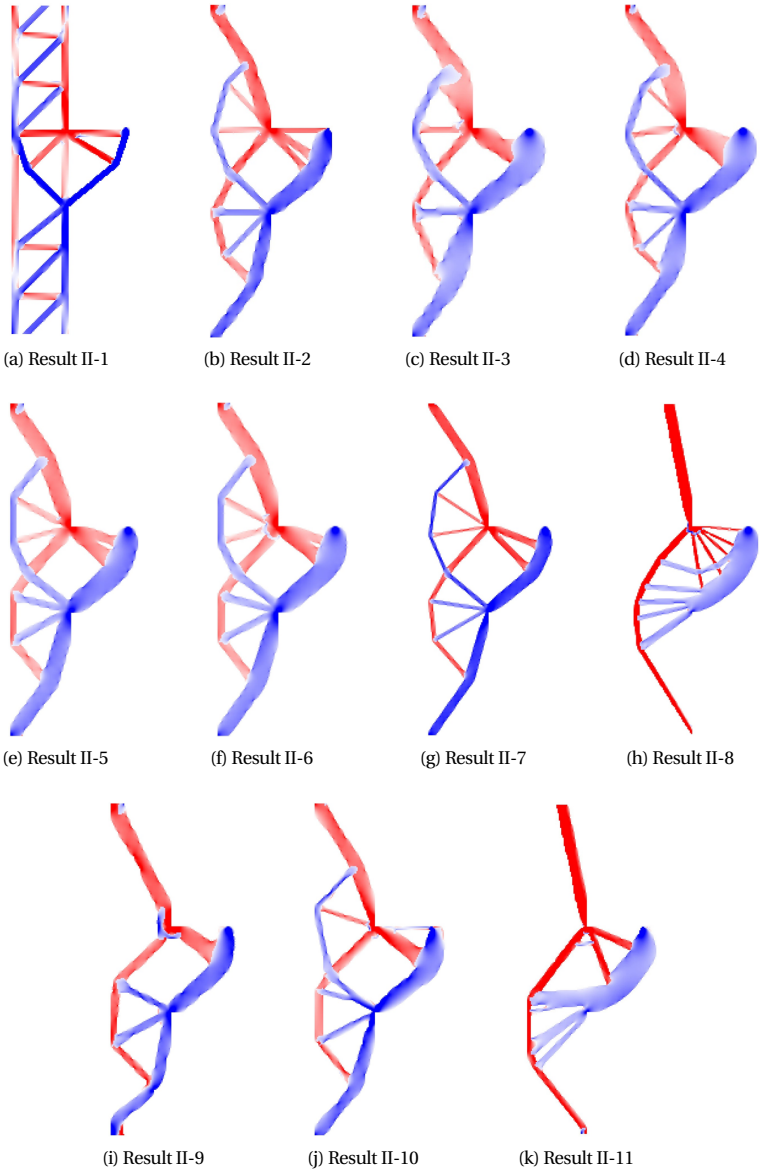

(a) Result II-1 (b) Result II-2 (c) Result II-3 (d) Result II-4

(e) Result II-5 (f) Result II-6 (g) Result II-7 (h) Result II-8

(i) Result II-9 (j) Result II-10 (k) Result II-11

Figure 2.22: Principal stress plots of Case II: Corbel

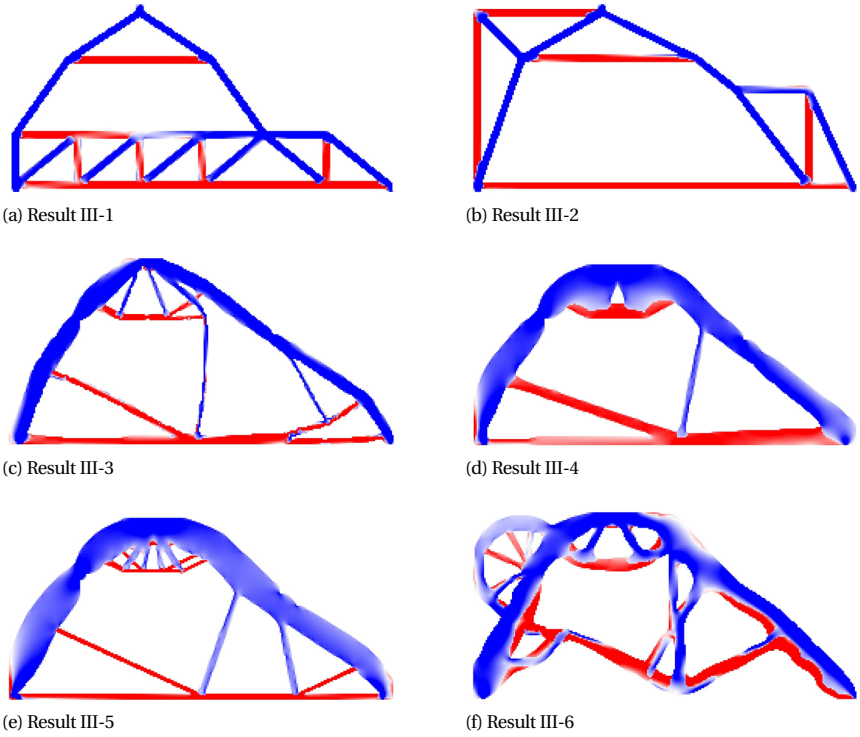

(a) Result III-1 (b) Result III-2

(c) Result III-3 (d) Result III-4

(e) Result III-5 (f) Result III-6

Figure 2.23: Principal stress plots of Case III: Dapped-end beam with opening

Table 2.5: Evaluation results for Case II: Corbel (%)

Results	STS index	TRS index	SR ratio
II-1	**98.5**	**72.7**	1.53
II-2	92.1	75.3	1.36
II-3	93.9	76.9	**1.26**
II-4	**91.1**	**77.5**	1.28
II-5	93.4	76.3	1.30
II-6	93.8	76.4	1.28
II-7	98.4	75.4	1.36
II-8	94.6	74.6	**2.69**
II-9	92.0	73.1	1.54
II-10	93.5	76.0	1.39
II-11	93.6	73.1	2.54
Avg	94.1	75.2	1.59
Std	2.38	1.64	0.515

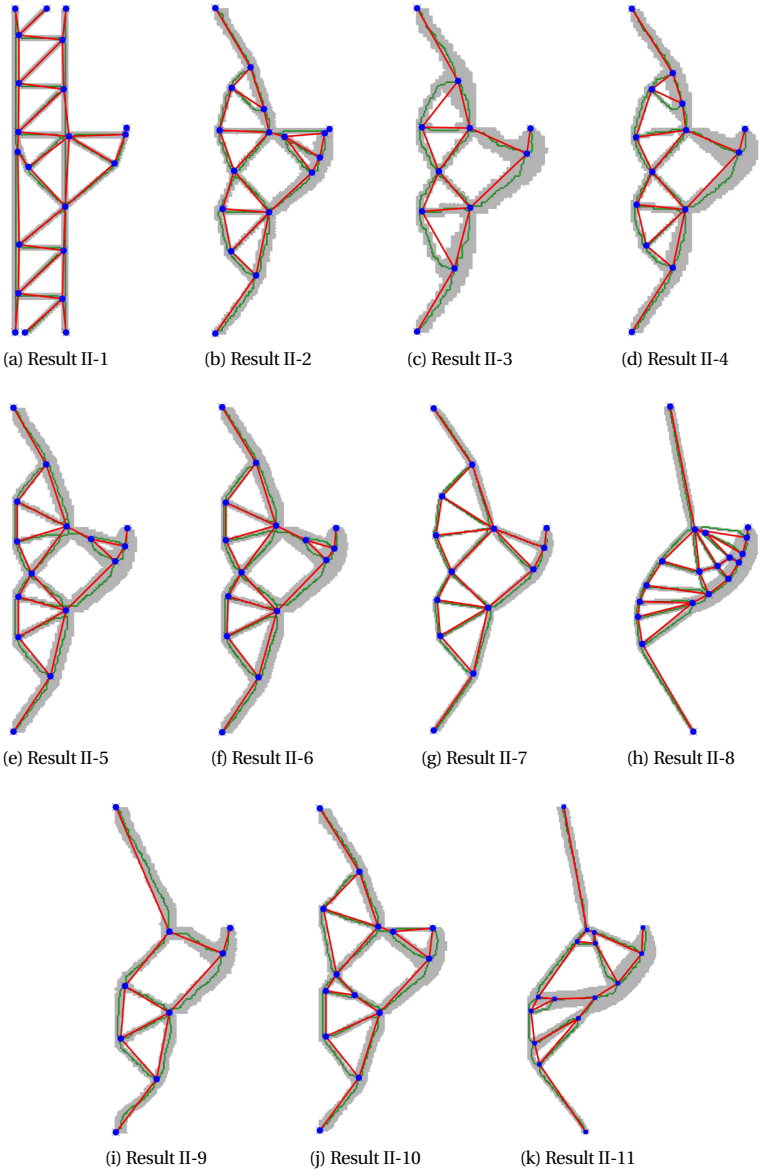

(a) Result II-1 (b) Result II-2 (c) Result II-3 (d) Result II-4

(e) Result II-5 (f) Result II-6 (g) Result II-7 (h) Result II-8

(i) Result II-9 (j) Result II-10 (k) Result II-11

Figure 2.24: Extraction results of Case II: Corbel

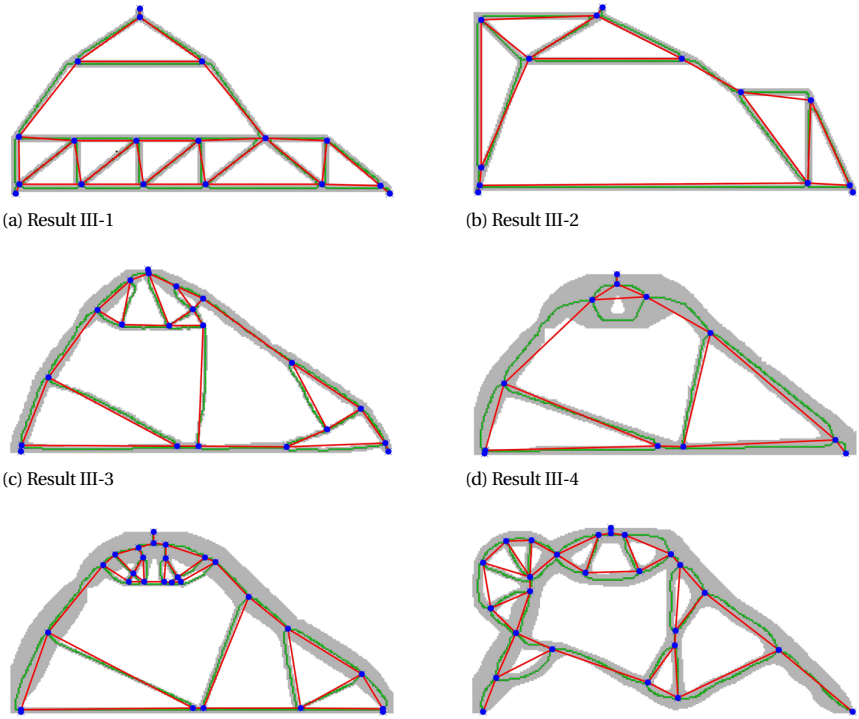

(a) Result III-1 (b) Result III-2

(c) Result III-3 (d) Result III-4

(e) Result III-5 (f) Result III-6

Figure 2.25: Extraction results of Case III: Dapped-end beam with opening

Table 2.6: Evaluation results for Case III: Dapped-end beam with an opening (%)

Results	STS index	TRS index	SR ratio
III-1	**97.8**	69.7	0.917
III-2	95.3	55.9	**1.01**
III-3	91.6	70.7	**0.539**
III-4	89.5	**71.3**	0.550
III-5	96.2	69.4	0.561
III-6	**71.1**	**50.7**	0.928
Avg	90.3	64.6	0.751
Std	9.87	8.94	0.222

INFLUENCE OF DIFFERENT MATERIAL MODELS IN THE TOPOLOGY OPTIMIZATION

In the literature related to the use of TO for STM, methods have been proposed to obtain better results. Instead of using isotropic continua, different material models (in broad sense) in the TO method have been proposed in the literature. Based on the evaluated cases, three aspects are discussed in this section: (1) using micro-truss elements instead of continuum elements, (2) considering different tensile/compressive moduli, (3) using truss-continuum hybrid elements.

Firstly, instead of plane stress elements, micro-truss elements were used in the optimization procedure. The results are included as Result I-4 & 5, Result II-3 & 4 and Result III-6. Kwak and Noh [79] demonstrated that the optimization results using micro-truss elements was less sensitive to mesh size and more efficient in finding Strut-and-Tie models than classical ESO methods. The absence of the tensile members at the bottom of Result I-4 is the key reason for the observed performance reduction. Comparing the evaluation of Result I-3 with Result I-5 and Result II-2 with Result II-4 regarding the TRS index and the SR ratio (see Tables 2.4, 2.5), no obvious improvements are observed using micro-truss elements. However, in Case I the force equilibrium system is significantly closer to an axial-force equilibrium using micro-truss elements.

Secondly, optimization procedures involving different tensile and compressive moduli were considered in Victoria et al. [147] and Du et al. [46]. These studies aimed to include the effect of the different mechanical properties of steel and concrete regions, in order to obtain better STM layouts. The optimized results of these cases are clearly different from the results using the isotropic material model. The optimized results considering the orthotropic tensile/compressive material model are shown in Result I-7, II-8 and II-11. Based on the evaluation results, these optimized results lead to high SR ratios and low TRS indices in both Case I and Case II, and are surpassed by cases using standard linear elastic material models.

Thirdly, Gaynor et al. [54] used a truss-continuum hybrid element and considered orthotropic material model during the optimization procedure, as shown in Result III-5. In this way, the truss elements in the hybrid model provide orthotropic mechanical behaviour in the tensile regions, which has a similar effect as using different tensile and compressive moduli in a continuum model. The optimized result in this case leads to a high SR ratio and a low TRS index, which is similar with the obtained results from the orthotropic material model.

Generally, we have not observed a case where more sophisticated material models or discretizations resulted in a clear benefit in terms of quality of the resulting ST models. In the evaluated cases considering bi-modulus material properties, due to tensile material having a larger stiffness, the topology optimization process results in designs that contain more tensile material. In the studied examples, better results were obtained using standard linear elastic material models. This is a counter-intuitive result, as generally more sophisticated modelling should lead to more efficient designs. As an example, nonlinear finite element analysis to study crack patterns provides much more detailed design information than a linear elastostatic analysis. An investigation towards more effective ways to include refined material behaviour in the TO process for ST models,

actually leading to noticeable improvements, is recommended as future research.

INFLUENCE OF DIFFERENT SETTINGS IN THE TOPOLOGY OPTIMIZATION METHOD

The optimized result in the TO process is a local minimum of different solutions to the same design problem when choosing different parameters in the TO method [127]. In this section, the parameters affecting TO results in different TO methods thus affecting the suitability of results to be used as ST models are discussed based on the evaluated cases. These parameters include: (1) removal criteria in ESO methods, (2) mesh sizes of the analysis model, (3) TO volume fraction and (4) different TO methods.

Firstly, the influence of the removal criteria in ESO methods is discussed. Liang et al. [87] and Kwak and Noh [79] used the strain energy removal criterion in the ESO method, whereas Almeida et al. [10] took the Von Mises stress removal criterion and smoothed the material constitutive relation in the optimization process. Similarly, the Von Mises stress removal criterion was used in Victoria et al. [147]. Comparing their result (I-6) with Result I-3 of the ESO method based on the strain energy criterion, the topology optimized layouts are similar. Consequently, the evaluation results of these cases are similar as well. This observation is confirmed by the earlier study by Li et al. [86], who demonstrated the equivalence of using the Von Mises stress criterion and the strain energy criterion in the ESO method.

In the study by Zhou et al. [171], the first principal stress was taken as the removal criterion in the ESO method. Result III-6 is the optimized layout which is determined as a suitable optimization result based on their evaluation procedure. However, by comparing the evaluation result with others (see Table 2.6), Result III-6 results in the lowest TRS index and a relative large SR ratio, thus it may be not a good choice to create ST models. In order to analyze the lower performance of this case, its principal stress plot is shown in Figure 2.26. In the figure, severe bending behaviour is observed in the region within black circles, which leads to the low TRS index and indicates that this layout is far from a truss model, and thus leading to a low STS index as well. The region within the blue circle was introduced by the authors to cover the tension in the original structure, shown in Figure 2.16 (c). However, from our analyses the indicated arch is in compression (Figure 2.26), and does not contribute to a better TRS index.

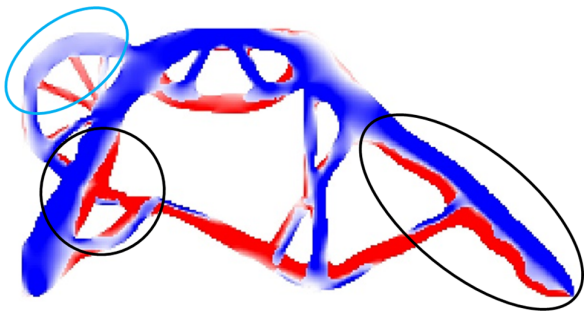

Figure 2.26: Principal stress plot of Result III-6. Red and blue parts indicate the tensile and compressive regions respectively

Secondly, the influence of mesh size of the analysis model is discussed. In Case I, regarding the TRS index and SR ratio, Result I-5 based on the ESO method with the refined mesh size performs better than Result I-4 with the coarse mesh size. However, based on TO results generated by the SIMP method, by comparing the evaluation results of coarse mesh size results (I-10 and II-5) with refined mesh size results (I-11 and II-6), only small differences are observed. In fact the filter technique in the SIMP method prevents the mesh dependency problem. Similarly this filter technique can be applied in ESO methods to improve results [68].

Thirdly, the volume fraction affects the numbers of members and their width in the optimized results. In Result I-6 and Result I-8, different volume fractions for one TO method are used. With a much lower volume fraction in the optimization, Result I-8 has a lower TRS index and a larger SR ratio than Result I-6. A similar observation applies to Result II-9 and Result II-10. Regarding to the three measures Result II-10 with a relatively large volume fraction performs better than Result II-9. However, with a small volume fraction in the optimization, generally a relatively simple optimized topology is obtained. This is beneficial for extracting truss-like structures resulting in a high STS index.

Fourthly, we compare different types of TO methods for STM. In the SIMP TO method, the optimized results are generated by solving the compliance optimization problem.They are very comparable to results of ESO methods with the strain energy or Von Mises stress removal criterion. This can be observed by comparing evaluation results of classical ESO methods with the SIMP method in Case I and Case II. They have similar TRS indices and SR ratios. Similar conclusions are observed by comparing the Isoline method and the Full-homogeneous method with the ESO method (SIMP method). Generally, regarding to the TRS index and the SR ratio, these methods have similar performance although their optimized results show some differences. All of these results perform well in representing tensile regions and leading to economical designs.

COMPARING TO RESULTS TO CONVENTIONAL STRUT-AND-TIE MODELS

Finding an unique and suitable model for the STM is one of the most important reasons to use objective-oriented TO methods. Based on the evaluation results of the considered cases, this aspect is discussed in this section.

Result I-1,2, II-1 and III-1,2 are the conventional ST models. In Case I, regarding to the TRS index, Result I-1 performs better than Result I-2, however the comparison of SR ratios leads to the opposite result. In Case III, Result III-2 performs better than Result III-1 for both the TRS index and the SR ratio. It is difficult to manually improve the conventional ST models. Based on the previous discussion on different TO methods in the fourth part in Section 4.3.2, the evaluation of TO results only shows slight differences for the same problem. Moreover, TO results have better performance in the TRS indices and the SR ratios comparing to conventional ST models in all three cases. Although it should be noted that an evaluation of compression struts was outside the scope of our measures, these observations confirm the prospects of using TO methods to find suitable ST models.

THE AXIAL-FORCE EQUILIBRIUM REQUIREMENT

Most of the studied TO methods could provide helpful layouts as an inspiration for generating suitable ST models. However, none of them can be applied in the STM method directly without further manual post-processing. The STM method requires an axial-force equilibrium system. As long as the generated truss-like structures have STS indices less than 1, shear force is present. The shear forces can be resisted by the surrounding concrete, however in this way, this model cannot fully represent the stress mechanism for the structure, thus they cannot be used as an ST model. This problem can originate from the provided topology, and the truss extraction process in Section 2 also affects the suitability of truss-like structures. The node positions can be shifted due to the thinning and node clustering in the extraction process. An example is shown in Figure 2.27. In the figure, the model with dashed lines shows the truss-like structures generated through the extraction process. The solid-line model indicates the adjusted truss model in which the positions of nodes are manually adjusted to a geometry similar to the conventional ST model, aligning members with applied loads and reaction forces. The three indices (STS, TRS, SR) of the two truss-like structures are (96.8%,66.3%,1.11%) and (99.8%,66.5%,1.11%) respectively. An improvement of the STS index is noted, as expected. Little change is seen in the other indices of the two truss-like structures. The truss-like structure based on the traditional ST model provides an axial-force equilibrium system and can be used in the STM method.

In some cases, by similar manual adjustments, the STS indices of truss-like structures based on the TO results can be improved. An example of Result I-8 is shown in Figure 2.28(a), three indices (STS, TRS, SR) are (95.1%,64.1%,0.928%) and (99.8%,64.1%,0.928%) respectively. Especially, the STS index is improved from 95.1 % to 99.8 %, which is close to a desired axial-force equilibrium state. However, this manual adjustment does not work for all cases: an example of Result I-3 shows insufficient improvement of the STS indices from 77.0 % to 92.8 % (Figure 2.28(b)), while TRS and SR indices again remain similar.

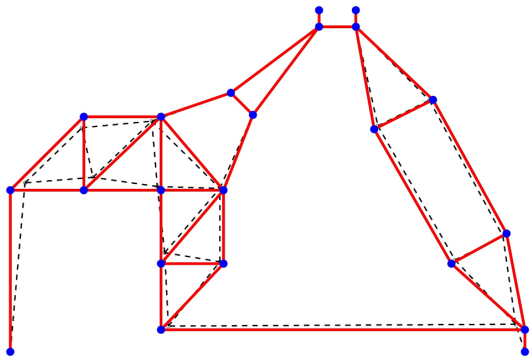

Figure 2.27: Truss-like structure of Result I-2. Dashed lines indicate the generated truss-like structures and solid lines show the adjusted structure.

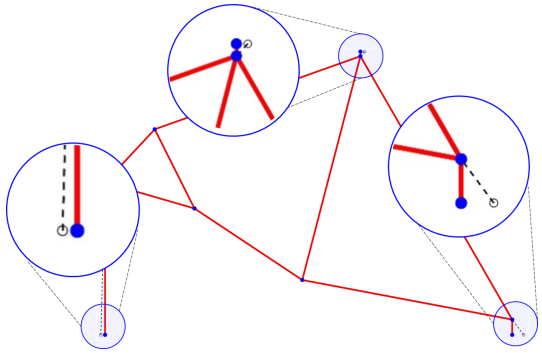

(a) Result I-8

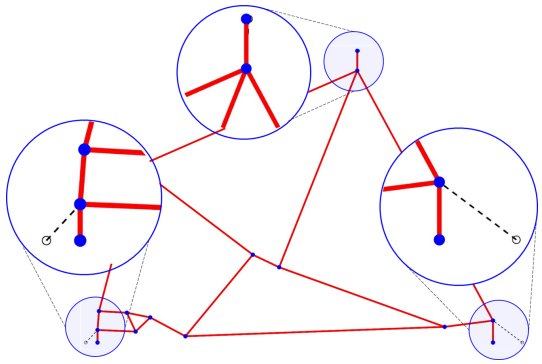

(b) Result I-3

Figure 2.28: Truss-like structure with zoomed-in details. Dashed lines indicate the generated truss-like structures and solid lines show the adjusted structure.

2.5. CONCLUSION

In this chapter, an automatic and objective evaluation method is proposed to evaluate TO results generated by various methods for use in Strut-and-Tie modelling, in order to enable a comparison between the many approaches suggested for this problem. In the evaluation procedures, a dedicated topology interpretation method is proposed to create truss-like structures from optimized layouts. In this way, the topology results can be processed and evaluated in an automatic and systematic manner. Next, based on the analyzed structural response, three measures are proposed for comparing various topology optimized layouts in the perspective of Strut-and-Tie modelling. The Suitable Truss Structure (STS) index measures the degree to which truss models based on the TO results can be analyzed and form an axial-force equilibrium system that is suited for the STM method. The Tensile Region Similarity (TRS) index measures the effectiveness of TO results in representing tensile regions of the original structures. The Steel Reinforcement (SR) ratio indicates how economic the design will be. Together, these criteria form our definition of suitability of a TO result for the purpose of STM. In total 28 results of three

design problems are evaluated and discussed. Based on the present investigation, the conclusions are summarized as follows:

1) The proposed evaluation method can reliably deal with a wide variety of cases automatically. The method provides an objective way to evaluate various optimized layouts, without manual intervention. The method has been presented here for planar cases, but the concept extends naturally to 3D. Implementation of a thinning method for voxel images and connectivity detection for 3D skeletons would be required. Moreover, in order to evaluate the practical structural performance of ST models, such as crack behaviour and failure mode, nonlinear finite element analysis can provide additional insight.

2) Many efforts were investigated by researchers to improve topology optimization methods to generate better layouts for the STM method. Based on our present evaluations, we do not observe an obvious improvement of nonstandard TO methods or more sophisticated material models over conventional approaches. These efforts may not be the most important steps towards improving the suitability of TO for the STM method. Interestingly, by considering a large tensile stiffness in the tension/compression orthotropic material model, the TO process results in more tensile regions. This clearly leads to worse STM results in the studied cases compared to simple isotropic material assumptions, and indicates potential for improved formulations in which results do benefit from refined material modelling.

3) Different parameters and settings in the TO process that affect optimized layouts have been investigated, such as the mesh size, removal criteria in ESO methods, volume fractions and different types of TO methods. Based on the analyzed cases, the filtering technique is suggested to solve the mesh dependent problem in the TO process. The strain energy and the Von Mises stress removal criteria in the ESO methods result in the similar results. However, the result based on the first principal stress criterion leads to a poor performance. All the applied TO (ESO, SIMP, Isoline and Full-homogeneous) methods have generally similar and good performance for the STM.

4) Comparing with conventional ST models, most topology optimization results perform better in representing the key tensile regions and limiting steel usage. Topology optimization methods are therefore promising and powerful tools to provide information for the STM method.

5) Currently, without manual adjustment, continuum TO procedures do typically not result in truss structures. The truss structure extraction method is proposed in this research to solve this problem. However the resulting truss-like structures may be not in a pure axial-force equilibrium state. In other words, in contrast to the expectations found in many papers on this topic, the generated TO-based layouts are not directly suitable for the STM method. Generating truss structures in the TO process that fully satisfy the STM requirements, is identified as an open problem in this field.

3

AUTOMATED OPTIMIZATION-BASED GENERATION AND QUANTITATIVE EVALUATION OF STRUT-AND-TIE MODELS

Strut-and-Tie modelling (STM) is a well-known approach to design D-regions in reinforced concrete structures. Because the STM method is based on lower-bound analysis, finding a suitable truss-analogy model is the most important aspect to guarantee good structural and economic performance of a resulting design. Continuum topology optimization (TO) methods have been studied for two decades to solve this problem. However, while these studies provide inspiration to designers, they lack the capability to automatically generate valid truss-analogy models as needed in the STM method. In order to prevent manual interpretation and automatically generate suitable Strut-and-Tie (ST) models for various D-regions, a method is proposed for the generation of optimization-based Strut-and-Tie (OPT-STM) models. The proposed method includes three phases: the TO phase, the topology extraction phase and the shape optimization phase. Next, in order to evaluate the effectiveness of the generated OPT-STM models, an evaluation using Nonlinear Finite Element Analysis (NLFEA) is performed to analyze the performance of ST models. For two D-region problems, two OPT-STM models and 11 manually constructed ST models from literature are evaluated, and their performance is compared and discussed, demonstrating the validity and effectiveness of the proposed automated generation method.

Contents of this chapter have been published in Computers & Structures (2020) [151].

3.1. INTRODUCTION

The Strut-and-Tie modelling (STM) method is an effective tool for engineers to design disturbed regions (so-called D-regions) of reinforced concrete (RC) structures. The STM method as a truss analogy method was first generalized as a consistent RC structure design method by Schlaich et al. [122] and Schlaich and Schafer [121]. It uses truss analogy models to indicate force and stress distributions in D-regions, and is based on the limit lower-bound theory of plasticity [104, 159]. The method requires axial force equilibrium while neglecting strain compatibilities [47, 93]. The design process of applying STM methods is convenient for engineers in practice, and resulting designs are conservative, assuming sufficient ductility. Various investigations of the STM method have been conducted by engineers and researchers in past decades, and results have been implemented in design codes worldwide, e.g. British Standards [34], Canadian Standards [43], code requirements from the American Concrete Institute [4], fib Model Code for Concrete Structures 2010 [51], the American Association of State Highway and Transportation Officials [2] and Eurocode [36].

In STM analysis, the load-to-support transfer mechanisms of design problems are represented using truss analogy models. Axial equilibrium forces are calculated, and model members with compressive and tensile forces are categorized as struts and ties respectively. The corresponding dimensioning process and strength checks are carried out for nodes, struts and ties. Regarding the whole process of the STM method, different aspects have been investigated by researchers: 1. In order to predict the ultimate behaviour of concrete structures, concrete cracking and compatibility conditions were implemented in the STM method [19, 38, 69, 73, 170]; 2. In order to predict accurate load capacity using the STM method, the ultimate strength and strength factors of struts and nodes under various conditions were investigated [60, 112, 132, 162]; 3. In order to validate the effectiveness and safety of STM designs, experiments of various STM designs for different D-regions were conducted [37, 55, 70, 78, 84, 99]; 4. In order to facilitate the STM design process in engineering practice, computer STM design tools were developed by researchers to generate various ST models [11, 108, 141, 160, 161, 163].

Among different investigation aspects related to the STM method, finding a suitable truss analogy model is a priority and is one of the most important problems [121]. Based on the lower-bound theory, various models are available and perform differently, however more economical (i.e. less conservative) designs are preferred and can be obtained by using suitable models [47]. Schlaich and Schafer [121] suggested using the load path method or using stress fields obtained through linear finite element analysis (FEA) as inspirations to construct truss analogy models for the STM analysis. However, difficulties of using these methods to generate ST models arise when D-regions become more complex [87]. In order to address this problem and to provide a method for a more generalized treatment of D-regions, topology optimization (TO) methods have been considered. Using TO to find suitable ST models is one of the most popular research directions in this field.

Various investigations using TO in the STM method have been conducted in the past two decades. Ali and White [8, 9], Biondini et al. [25, 26] used ground structure based TO methods to generate truss-analogy models for the STM method. Numerous approaches

using continuum TO methods have been explored for the same purpose. Liang et al. [87] firstly used the evolutionary structural optimization (ESO) method for creating ST models from the optimized material layouts. Later on, various other ESO approaches were proposed [10, 56, 79, 83]. Alternatively, for the same problem, Bruggi [31, 32] and Jewett and Carstensen [71] used SIMP (solid isotropic material with penalization) TO methods to generate optimized topologies for the STM method, whereas the isoline TO method was used in Victoria et al. [147] and the full-homogenization method was used in Herranz et al. [63]. Apart from using different TO methods, more sophisticated material models were adopted in the TO process: Victoria et al. [147] and Du et al. [46] used bi-modulus material properties for the generation of ST models, Bruggi [33] implemented an energy-based TO approach considering no-tension concrete for deriving ST models. and Gaynor et al. [54] and Jewett and Carstensen [70] considered bi-modulus material properties within a hybrid truss-continuum element formulation for generating optimized material layouts for the STM method.

Despite intensive efforts of using various TO approaches for the STM method, the generated optimized results from these approaches cannot be used as ST models without manual adjustments. Because TO results are continua and ST models are truss analogy models, most approaches can only provide optimized material layouts as inspiration for subsequent manual generation of ST models. Manual and subjective interpretations are required to transform TO results to adequate ST models. Consequently, interpreted ST models show considerable variation. Moreover, the manual interpretation process is impractical and inefficient in engineering practice. This hampers the utilization of TO methods for STM. The problem how to generate ST models directly through the optimization process has thus far not been solved. This problem is first clearly identified and discussed in more depth in our recent review on evaluating TO methods for STM [152]. To our best knowledge, no investigations have been reported that fully address this gap. Thus, automated optimization-based procedures to construct an ST model are highly desired.

In this chapter, we therefore propose an automatic generation method for optimization-based STM (OPT-STM) models. The method starts with a design problem which includes the geometry, boundaries and load conditions, and compliance minimization-based topology optimization is conducted for this problem to obtain optimized material layouts. Next, instead of manually interpreting truss-like structures based on TO results, a fully automatic topology extraction method is proposed to replace this manual process. Note that the STM method requires a truss-analogy model satisfying axial-force equilibrium, however the extracted truss-like structures are usually unstable trusses and equilibrium forces cannot be calculated through truss analysis [152]. Consequently, a subsequent shape optimization method is introduced to automatically adjust the extracted truss-like structures to valid ST models, in which axial force equilibrium is satisfied. Moreover, important practical geometrical conditions, such as minimum concrete cover for reinforcement and the member distances to outer surfaces, are included as constraints in the optimization process. The whole generation method is implemented as an integrated and automatic procedure. Thus, the generation method prevents ad-hoc topological changes of TO results commonly applied in manual ST model generations

and simplifies the process of generating ST models in engineering practice.

In order to validate the effectiveness of the generated OPT-STM models, an evaluation method is proposed by using Nonlinear Finite Element Analysis (NLFEA). The nonlinear behavior of concrete cracking and crushing and steel yielding and rupturing are considered. This provides more detailed insights to evaluate the performance of ST models. Two typical D-region design problems are investigated. By comparing the evaluation results of the generated OPT-STM models with 11 previously proposed ST models from literature, the effectiveness of the proposed automated generation method is demonstrated. As will be shown, in particular the amount of necessary reinforcement is significantly lower for the OPT-STM designs, while load capacities remain comparable between all models. Note that, in order to avoid subjective manual interventions, reinforcement detailing aspects and constructibility issues after the STM analysis are not considered in the evaluation process.

The remainder of the chapter is organized as follows: the novel generation method of optimization-based ST models is introduced in Section 3.2. The evaluation method for ST models is presented in Section 3.3. Three aspects of the generation method, including the influence of optimization parameters in the TO process, the merging length in the topology extraction process and the importance of satisfying axial equilibrium forces, are discussed in Section 3.4. Finally, a comparative evaluation based on two D-region design problems is presented in Section 3.5 and conclusions are given in Section 3.6.

3.2. AUTOMATIC GENERATION OF OPTIMIZATION-BASED STRUT-AND-TIE MODELS

An automatic and integrated generation method is introduced in this section for the generation of OPT-STM models. An example of a D-region design problem (a dapped-end beam with an opening) is used to exemplify the proposed generation method. The geometry, loads and supports of this D-region are shown in Figure 3.1. The thickness of this structure is 120 mm. The D-region has been experimentally investigated by Oviedo et al. [106]. The proposed method includes three main phases, as shown in the flowchart in Figure 3.2:

Topology optimization phase: The compliance minimization-based TO method is adopted for generating optimized material layouts of given design problems. The classical density-based SIMP TO method [22] is used in this research. The details are introduced in Section 3.2.1.

Topology extraction phase: A topology extraction method is developed to transform TO continua to truss-like structures. The extracted truss-like structure comprises a network consisting of straight, connected structural members which distributes forces from loads to supports. The detailed procedures of the extraction method are introduced in Section 3.2.2.

Shape optimization phase: The extracted truss-like structures are usually unstable trusses. Therefore, the equilibrium forces cannot be calculated by truss analysis in most cases. However, the requirement of the axial-force equilibrium state is a prerequisite for using truss analogies in ST models. In Section 3.2.3, the proposed shape optimization

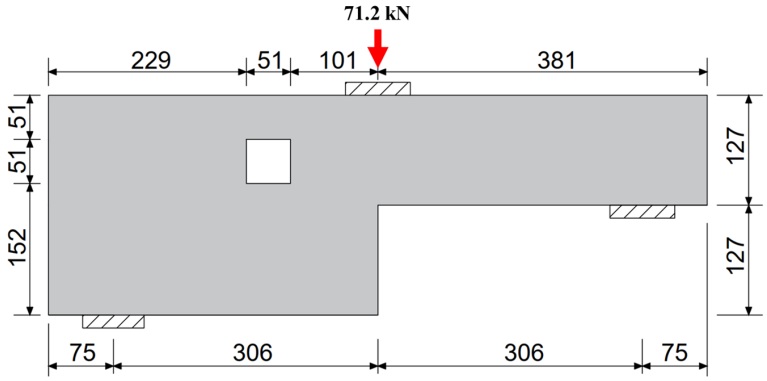

Figure 3.1: The dapped-end beam design problem (mm).

method to generate adequate ST models based on the extracted truss-like structures is presented.

3.2.1. TOPOLOGY OPTIMIZATION PHASE

Since the landmark work by Bendsøe and Kikuchi [23], continuum TO methods have been investigated broadly, and have become powerful and creative approaches for a wide variety structural design applications. Specifically in the conceptual design phase, TO methods provide a systematic procedure to find optimized material distributions of a given domain with specific load and support conditions.

The classical SIMP TO method [22] is adopted here to optimize material distributions of given problems. Note that various other TO methods could be used in this phase, as reviewed in the preceding section. Although we employ a classical TO approach, its main steps are discussed here for completeness; for additional details, the reader is referred to Bendsøe and Sigmund [22]. Topology optimization variables, so called densities $\boldsymbol{\rho}$, are assigned to all elements in the FEM model. Based on FEM analysis results and sensitivity information, densities are updated at each optimization iteration until the process converges.

Based on the SIMP method, the mathematical formulation of the compliance minimization TO problem is:

$$\begin{aligned} &\text{minimize: } C(\boldsymbol{\rho}) = \boldsymbol{F}^{\mathrm{T}}\boldsymbol{U}(\boldsymbol{\rho}) \\ &\text{subject to: } \boldsymbol{K}(\boldsymbol{\rho})\boldsymbol{U} = \boldsymbol{F} \\ &\qquad\qquad V(\boldsymbol{\rho}) \leq \alpha \bar{V} \\ &\qquad\qquad \boldsymbol{\varepsilon} \leq \boldsymbol{\rho} \leq \mathbf{1} \end{aligned} \tag{3.1}$$

In this optimization problem, C is the compliance of the structure, $\boldsymbol{F}$ and $\boldsymbol{U}$ are the nodal force vector and the nodal displacement vector respectively. $\boldsymbol{\rho}$ is the density vector which elements are in the range between ε (denoting void) and 1 (solid). The lower limit ε is a

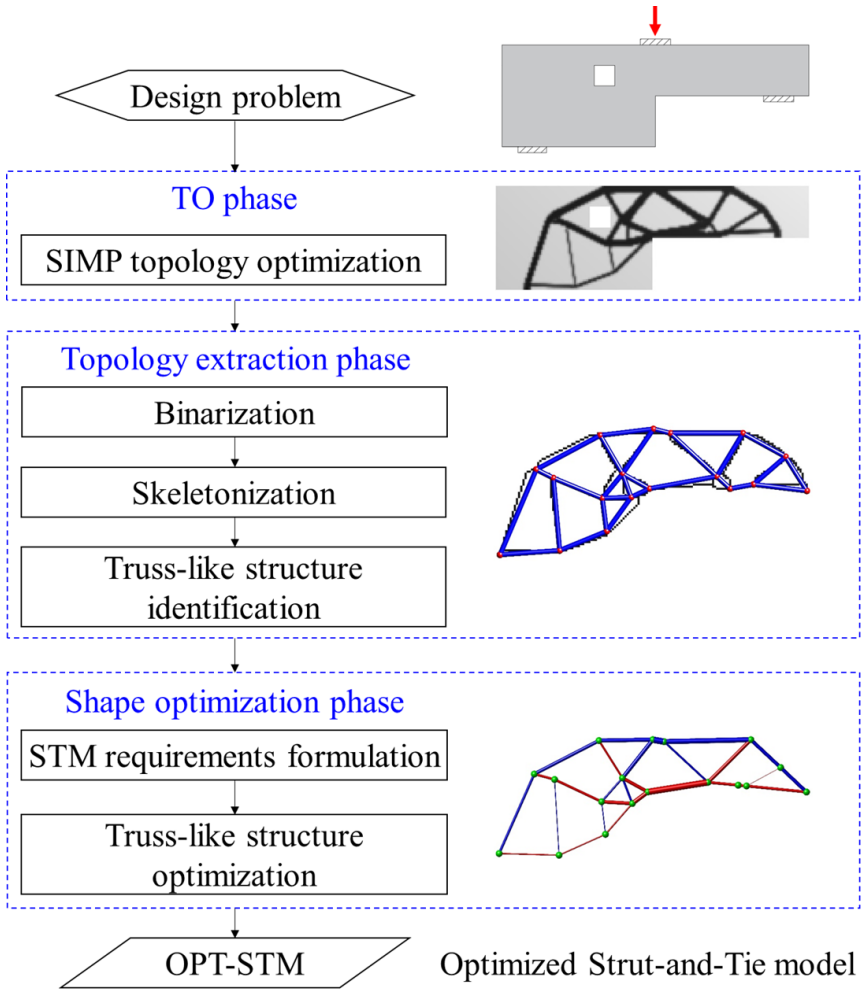

Figure 3.2: Flowchart of the OPT-STM generation method.

small value (10^{-4}) which prevents singularity of $\boldsymbol{K}$, which is the structural stiffness matrix depending on densities $\boldsymbol{\rho}$ as discussed below. $V(\boldsymbol{\rho})$ and $\bar{V}$ are the material volume and the total volume of the full domain respectively. $\alpha \in [0,1]$ is a specific volume fraction for limiting the material utilization of optimized results.

In this research, conventional four-node bilinear finite elements under plane stress assumption are adopted to perform the finite element analysis in all 2D examples. In the SIMP TO method, the Young's modulus $E(\rho_i)$ of element i is scaled by the associated density ρ_i raised to the power p:

$$E(\rho_i) = \rho_i^p E_0, \tag{3.2}$$

where E_0 is the prescribed Young's modulus. The element stiffness matrix $\boldsymbol{K}_i$ is calculated

based on the penalized modulus $E(\rho_i)$, and then assembled to the global stiffness matrix $\boldsymbol{K}$, defined as:

$$\boldsymbol{K}(\boldsymbol{\rho}) = \sum_{i=1}^{n} \boldsymbol{K}_i. \tag{3.3}$$

The gradient-based Method of Moving Asymptotes (MMA) [135] is used to update the densities in every optimization iteration. The design sensitivities of the structural compliance $C(\rho_i)$ and volume constraint $V(\rho_i)$ are required. The sensitivity of the volume constraint $\partial V/\partial \rho_i$ simply equals the volume of the i-th element V_i. Following the adjoint method, the sensitivity of the compliance is given by:

$$\frac{\partial C}{\partial \rho_i} = -\boldsymbol{U}^{\mathrm{T}} \frac{\partial \boldsymbol{K}}{\partial \rho_i} \boldsymbol{U}. \tag{3.4}$$

Based on the element-wise assembly of global stiffness matrix $\boldsymbol{K}$ (Eq.(3.3)) and given the SIMP material interpolation (Eq.(3.2)), this simplifies to the following expression on element level:

$$\frac{\partial C}{\partial \rho_i} = -p(\rho_i)^{(p-1)} \boldsymbol{U}_i^{\mathrm{T}} \boldsymbol{K}_0 \boldsymbol{U}_i, \tag{3.5}$$

where, $\boldsymbol{U}_i$ is the element nodal displacement vector, and $\boldsymbol{K}_0$ is the original element stiffness matrix of a fully solid element.

In order to avoid mesh dependence and checker-board problems [127] in the optimization process, a density filter is adopted. The densities are filtered as:

$$\bar{\rho}_i = \frac{\sum_{j=1}^{n} h(i,j)\rho_j}{\sum_{j=1}^{n} h(i,j)}. \tag{3.6}$$

Here, h is the convolution kernel defined as:

$$h(i,j) = \max(0, r_0 - r(i,j)), \tag{3.7}$$

where r_0 is a specific radius and $r(i,j)$ indicates the centroid distance between the element i and the element j. Based on the filtered densities $\bar{\rho}$, the chain rule is used to obtain consistent sensitivities. The optimization process terminates when the relative compliance difference between two subsequent iterations is less than a given threshold (0.1 % in this research) and the volume constraint is satisfied.

Based on the design problem in Figure 3.1, a FEM model with 180×60 elements is generated. Concrete material properties are adopted of which the Young's modulus is 30 GPa and the Poisson ratio is 0.15. In the TO process, the density power is $p = 3$, the volume constraint is taken as $\alpha = 25\%$ and the filter radius is $r_0 = 1.5 \times$ (mesh size). After 103 TO optimization iterations, the optimized topology of this example is obtained, as shown in Figure 3.3.

3.2.2. TOPOLOGY EXTRACTION PHASE

The purpose of this phase is to extract a truss-like structure from the obtained TO, as the next step towards an OPT-STM model. There have been several studies on extracting

Figure 3.3: Optimized topology of the dapped-end beam. Black and grey pixels indicate the solid and void regions.

designs from TO results for different purposes, which we briefly review here. Lin and Chao [89] used several shape templates to represent holes in the TO results. Hsu and Hsu [64] adopted B-splines to describe the boundaries of TO results. Chou and Lin [39] and Yi and Kim [156] identified the geometrical features of TO results, and proceeded with shape and size optimization-based on the obtained features. Cuillière et al. [44] and Yi and Kim [156] extracted 3D TO results to CAD-friendly models for the further utilization. However none of these methods was dedicated to extract ST models from the TO results. In this section, an automatic extraction method is proposed, which is specifically conceived to extract truss-like models from continuum TO results for the STM method. The method is a refinement of the method we have presented in an earlier study [152], and in particular the robustness of the connectivity identification is improved.

The proposed extraction method contains three steps (Figure 3.2): 1) transforming TO results to binary data; 2) Thinning TO results into image skeletons; 3) Identifying nodes and their connections for the generation of truss-like structures. These three steps are described in more detail below.

1. Transforming TO results to binary data. Although TO results largely denote void/solid regions of structural domains, some of the densities have intermediate values. Clear binary data is required in Step 2, thus TO results are transformed to binary data by setting a threshold. In order to maintain the original topology in the binary data, in this research the threshold is set to 0.1. All densities below this value are converted to the void state, and the remainder is set to solid. The binary image generated from the optimized topology (Figure 3.3) is shown in Figure 3.4.

2. Thinning TO results for skeletons. In order to extract truss-like structures effectively, optimized topologies are simplified through the thinning process introduced by Zhang and Suen [166]. The binary images are skeletonized by iteratively removing boundary pixels until no further pixels can be removed without changing the topology. In the thinning process, pixel-wise elimination rules are applied to determine the boundary pixels which are removable without changing the topology. Next, based on elimination rules, every pixel is marked to remove or remain, depending on the values of its eight neighbour pixels. The whole binary image is thinned iteratively in this manner. For the detailed elimination rules and further discussion of this thinning process, the reader is referred to

Figure 3.4: The binary image based on the TO result.

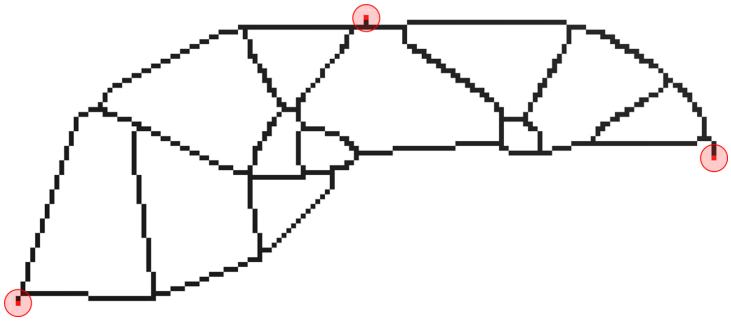

Figure 3.5: The skeleton after the thinning process. The pixels marked in red circles are load and support points, and they are unremovable.

Zhang and Suen [166]. Moreover, in our study, the load and support points are taken as unremovable pixels in the thinning method, as these must remain in the final ST model. The obtained skeleton of the adopted example (Figure 3.4) is shown in Figure 3.5. Note that the topology is unchanged, and members are represented by single-pixel curves.

3. Identifying nodes and connections for the generation of truss-like structures. The ST model is a truss-analogy model consisting of a network of nodes and their connections. Moreover, this truss-analogy model uses the axial-equilibrium forces to indicate the assumed force flow of a structure. Based on the obtained skeleton from the previous step, the truss-like structure generation method proceeds by identifying nodes and their connections. The detailed extraction procedures are introduced below.

First, nodes are detected based on the binary skeleton. Since the obtained skeleton curve is at most a single pixel wide, node detection rules are defined to identify candidate nodes by checking every pixel in the skeleton. The node detection patterns are presented in Figure 3.6. Note that Patterns 1-4 include four rotationally equivalent cases, as is shown for Pattern 1 only. Every pixel in the skeleton and its eight neighbouring pixels is probed, and if the pattern matches one of these sets, it is identified as a candidate node. Moreover, the load and support points are taken as candidate nodes as well. The candidate nodes of the example (Figure 3.5) are presented in Figure 3.7a in red. Based on the node detection

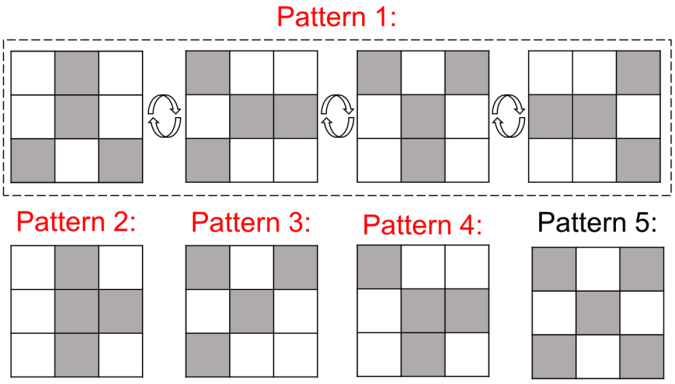

Figure 3.6: Node detection patterns. Red patterns indicate that they have rotationally equivalent cases.

pattern, several candidate nodes may cluster in a small region, and a reduction method is used to eliminate redundant candidate nodes. In this research, if the distance between two candidate nodes is smaller than 1.5 × the mesh size, they are replaced by a single node at the rounded-averaged location in the skeleton. The reduced set of candidate nodes exclusively contains the identified nodes and is shown in Figure 3.7b.

After identifying the nodes, their connections are required for the generation of a truss-like structure. Since all detected nodes are attached to the one-pixel wide skeleton, a recursive method is proposed to generate node connections. The method node-wisely checks every identified node. By iteratively detecting the skeleton pixels from the eight neighbouring pixels, a path from the considered node to other nodes connected by the skeleton curve is determined. This path defines a connection between two nodes, and is replaced by a bar in the truss-like structure. The generated truss-like structure of the example is presented in Figure 3.8. Note that the curved lines in the skeleton are now replaced by straight bars, while maintaining the original topology.

The initially generated truss-like structure may have various short bars. These short bars, while structurally insignificant, are adverse for the generation of ST models. They increase the number of optimization variables in the subsequent shape optimization phase and can produce internal mechanisms in the truss model, which hamper in finding a static equilibrium state for the STM method. A merging method is proposed to eliminate these short bars. In the method, iteratively the lengths of all bars in the generated truss-like structure are checked. A typical situation is shown in the conceptual example in Figure 3.9. Here the short bar B_i has two nodes, N_1 and N_2. In order to eliminate this short bar, a new node $\bar{N}_1$ is created replacing nodes N_1 and N_2 by their average. In the dapped-end beam example, considering a merging length $L_0 = 25.4\,\text{mm}$ (10 % of the smallest outside dimension of the beam), the refined truss-like structure after removing 10 short bars is shown in Figure 3.10. Note that the topology simplification leads to a structure that does not fully correspond to the TO result. A possible increase in compliance will however be counteracted in the final shape optimization phase.

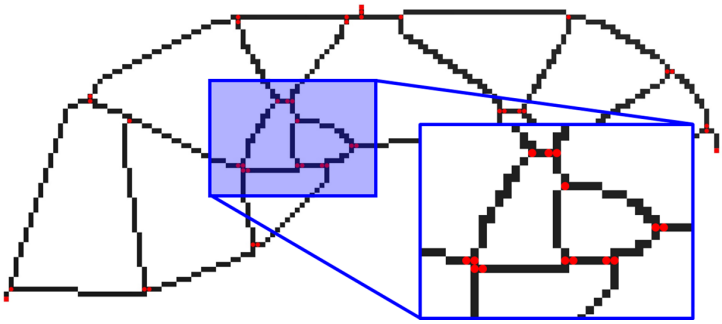

(a) Candidate nodes generated based on the skeleton, indicated in red

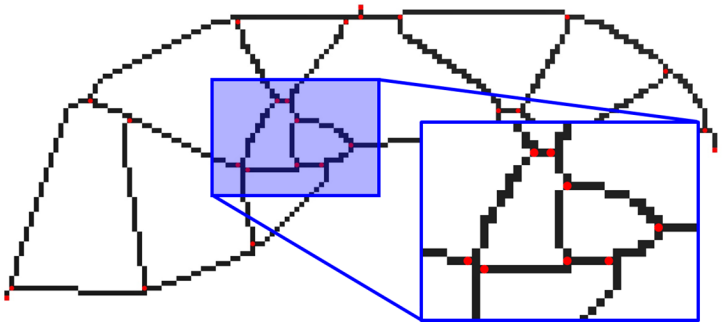

(b) Identified nodes by eliminating redundant nodes, indicated in red

Figure 3.7: Node identification of the truss-like structure.

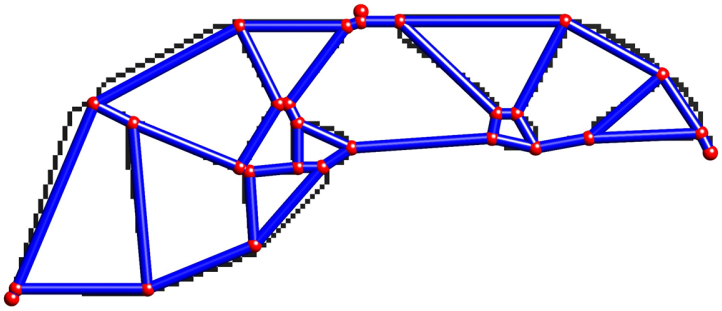

Figure 3.8: The generated truss-like structure. Red points indicate the identified nodes and blue lines indicate their connections.

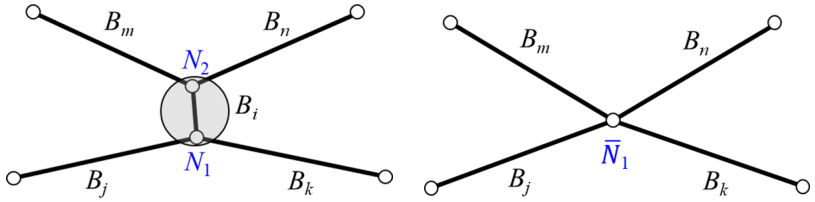

(a) Before merging

(b) After merging

Figure 3.9: The example of merging a short bar.

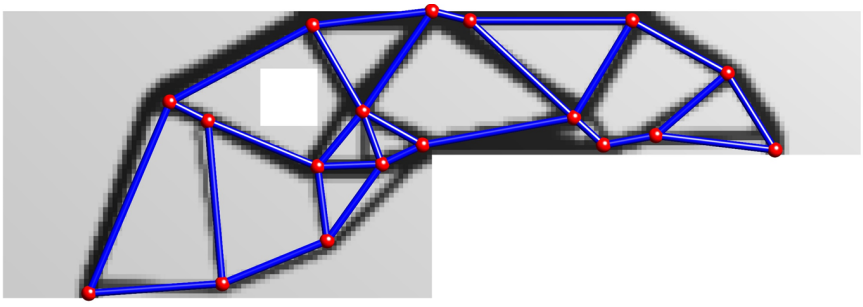

Figure 3.10: The refined truss-like structure.

3.2.3. SHAPE OPTIMIZATION PHASE

In most cases, the generated truss-like structures are statically and kinematically unstable structures, and their equilibrium forces cannot be calculated through truss analysis. In order to obtain equilibrium forces of the generated truss-like structures, instead of truss elements the classical beam element with a high slenderness (height/length = 0.001) is used. However, the obtained equilibrium forces cannot guarantee the generated truss-like structures can be used as ST models, because of the existence of shear forces. Based on the lower bound theory in the STM method, a pure axial force equilibrium state is required and shear forces should be zero. Thus, the generated truss-like structures can only be applied as ST models if a network of axial equilibrium forces is obtained. In this section, a shape optimization procedure is proposed to obtain an axial-force equilibrium while satisfying the geometry requirements. The generated truss-like structures are adjusted in the shape optimization process by modifying the internal node positions. After this process, a statically stable truss is obtained, referred to as the optimization-based Strut-and-Tie model (OPT-STM). The detailed steps are presented below.

PURE AXIAL-FORCE EQUILIBRIUM REQUIREMENT

In order to quantify the closeness of the generated truss-like structures to a pure axial force equilibrium state, the Suitable Truss Structure (STS) index has been proposed based on axial and shear forces obtained from beam analysis with slender beams and rigid joint connections [152], defined as:

$$\mathrm{STS} = \frac{1}{n}\sum_{e=1}^{n}\frac{|N_e|}{|N_e|+|V_e|}, \tag{3.8}$$

where, N_e is the element axial force, V_e is the element shear force, and n is the number of elements. The STS index has range [0,1]. When STS = 1, all members in the truss-like structure are subjected to axial forces only and it can be used as-is in the STM method. The STS index of the illustrative example (Figure 3.10) is 0.933.

INCLUDING GEOMETRIC REQUIREMENTS

Several geometric requirements that are important for practical application of the STM method are considered in this shape optimization process. Minimum required cover depths apply for the positions of the ties. Also the struts should have a minimum distance to the outer surface of the concrete element to ensure sufficient widths of these struts. This also applies to holes in the structure. These aspects were not taken into account in the TO phase, and the truss-like structure obtained after Step 2 may not be admissible.

A geometrical constraint is formulated to quantify these requirements, assuming rectangular impermissible areas. More complex regions can be represented by combinations of rectangles, a generalization to arbitrary shapes is left as a future extension. Two geometrical conditions are presented in Figure 3.11, in which the grey areas denote the impermissible areas. In the first condition the bar, that is the line segment along the blue line, is crossing the rectangle, but its endpoints (nodes) are outside. In the second condition a bar crosses an edge of the rectangle, and one of its nodes lies in the impermissible region.

In the first case, bar-to-corner distance vectors are used to formulate a geometrical constraint for the shape optimization procedure. Constraint violation is measured by the perpendicular distance from the bar to the nearest corner of the impermissible region. As a result, during optimization the bar will move towards this corner and out of the rectangle. In Figure 3.11a, $\boldsymbol{v}_i$ are five vectors from the four corners ($i = 1$ to 4) and the centre point ($i = 0$) of the impermissible area to an endpoint of the bar. The five vector distances $\boldsymbol{d}_i$ between the centre and corner points of the impermissible area and the bar vector $\boldsymbol{v}_*$ are calculated as:

$$\boldsymbol{d}_i = \left(\mathrm{I} - \frac{\boldsymbol{v}_* \otimes \boldsymbol{v}_*}{\|\boldsymbol{v}_*\|^2}\right)\boldsymbol{v}_i, \tag{3.9}$$

where I is the identity matrix and $\otimes$ denotes the dyadic tensor product. In this case, the geometrical constraint is defined by the scalar distance using d, defined as:

$$d = \sum_{i=1}^{4} \min[0, \mathrm{sign}(\boldsymbol{d}_0 \cdot \boldsymbol{d}_i)]\,\|\boldsymbol{d}_i\|. \tag{3.10}$$

In this equation, $\mathrm{sign}(\boldsymbol{d}_0 \cdot \boldsymbol{d}_i)$ is the sign operator applied on the inner product of distance vectors. If the bar passes the corner of the rectangle at the same side as it passes the centre point then $\mathrm{sign}(\boldsymbol{d}_0 \cdot \boldsymbol{d}_i) = 1$, otherwise -1 is obtained. A negative d indicates that the bar is crossing the rectangle. If the bar lies outside the impermissible area then $d = 0$.

In the second case (a bar node that is within the impermissible area), next to the distance calculated from the first condition, the penetration length is considered to evaluate the constraint violation. The bar is thus steered to move out of the impermissible area along the bar direction. The intersecting line segment of the bar with the impermissible area is presented as $\boldsymbol{l}$ in Figure 3.11b. Note that when the bar entirely falls inside the impermissible area, $\boldsymbol{l}$ equals the full bar length. The geometry constraint is given by the length l, defined as:

$$l = -1 \cdot \min(\|\boldsymbol{l}\|, |d|). \tag{3.11}$$

Combining the two conditions together, the geometry constraint g_m^n of the bar n with respect to the impermissible area m is calculated as:

$$g_m^n = \begin{cases} d & \text{Condition 1} \\ l & \text{Condition 2} \\ 0 & \text{Outside the area} \end{cases}. \tag{3.12}$$

Based on this constraint measure, g_m^n is zero when bar n and rectangle m do not overlap or intersect (Figure 3.11c), and $g_m^n \leq 0$ otherwise. In the illustrative example, six impermissible regions are introduced to ensure sufficient cover and maintain the opening, as presented in Figure 3.12.

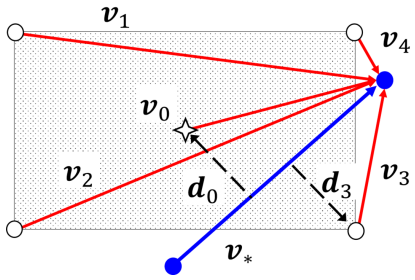

(a) Condition 1

- Inside the area:

$$\begin{cases} \text{sign}(\boldsymbol{d}_0 \cdot \boldsymbol{d}_3) = -1 \\ d = -||\boldsymbol{d}_3|| \end{cases}$$

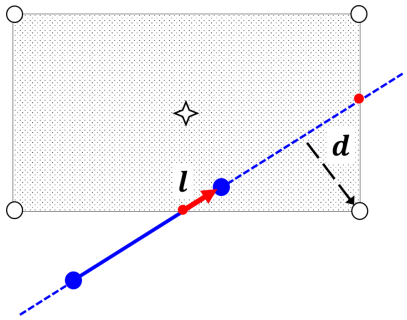

(b) Condition 2

- Inside the area:

$$\begin{cases} ||\boldsymbol{l}|| < ||\boldsymbol{d}|| \\ l = -||\boldsymbol{l}|| \end{cases}$$

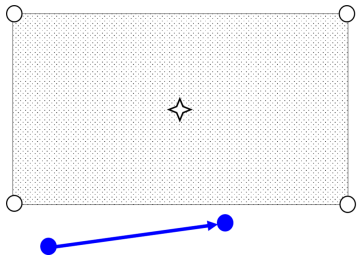

(c) Outside the impermissble area

- Outside the area:

$$\begin{cases} d = 0 \\ l = 0 \end{cases}$$

Figure 3.11: Example illustrating the geometry constraint. Blue points indicate two nodes of a bar. Black circles and stars indicate the four corners and the centre point of a rectangular impermissible area respectively. Red points indicate the intersection points.

THE SHAPE OPTIMIZATION PROBLEM

Based on the above aspects, and continuing with the same objective as used in Phase 1 (Eq.(3.1)), the mathematical formulation of the shape optimization problem is given by:

$$\begin{aligned} &\text{minimize: } C(\boldsymbol{x}) = \boldsymbol{F}^{\mathrm{T}}\boldsymbol{U}(\boldsymbol{x}) \\ &\text{subject to: } \boldsymbol{K}(\boldsymbol{x})\boldsymbol{U} = \boldsymbol{F} \\ &\qquad \text{STS} \geq 1-\varepsilon \\ &\qquad \sum_{j=1}^{n} g_m^j \geq 0 \quad (m = 1,2...) \\ &\qquad \boldsymbol{x}_{\min} \leq \boldsymbol{x} \leq \boldsymbol{x}_{\max} \end{aligned} \tag{3.13}$$

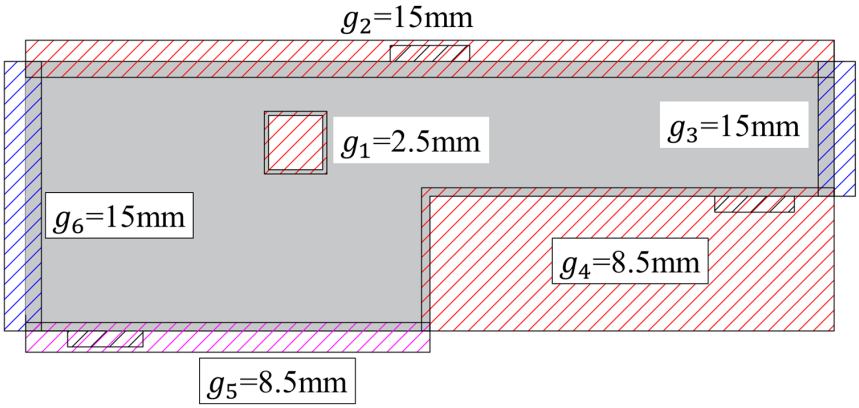

Figure 3.12: The geometry constraint regions. Six rectangular regions defining the required cover layers and the opening are highlighted with dashed lines.

where $\boldsymbol{x}$ is a vector containing the coordinates of the nodes of the generated truss-like structure, which are used as optimization variables. $\boldsymbol{x}_{\text{min}}$ and $\boldsymbol{x}_{\text{max}}$ are the minimum and maximum coordinates of the structural domain. Furthermore, m is the index of an impermissible area and n is the number of bar elements. C, $\boldsymbol{F}$, $\boldsymbol{U}$ and $\boldsymbol{K}$ here represent the compliance, nodal forces, nodal displacements and the stiffness matrix based on the beam finite element model. STS is the axial force equilibrium indicator introduced in Eq.(3.8). Note that in this shape optimization, a tolerance ε is allowed. Bending moments and shear forces are inevitable when using beam elements. Therefore, ε is taken as 0.005 in this study in order to obtain nearly purely axial equilibrium forces. The inequality $\sum_{j=1}^{n} g_m^j \geq 0$ is the constraint with respect to region m to guarantee geometry requirements. Summing all constraints per region into a single inequality reduces the computational costs in the optimizer due to a large number of optimization constraints.

Similar to the TO phase, the MMA optimization algorithm is used to solve this problem. Central finite differences are used to calculate sensitivities. The perturbation is taken as a value at 0.1 % of the mesh size of the continuum elements. The problem defined by Eq.(3.13) is a nonconvex constrained optimization problem. In order to ensure robust convergence, a move limit of 10 % of the mesh size of the continuum elements is imposed on the design variables.

The result after shape optimization of the example problem is shown in Figure 3.13, and the difference compared to the previous model is shown in Figure 3.14. The convergence history of the objective value and constraints (g_2, g_4 and g_5 regions are shown in Figure 3.12) is presented in Figure 3.15. Some oscillation in constraint g_4 is observed which is due to the non-smoothness of the geometrical constraints, but the applied move limit is effective in stabilizing the optimization process. Although small node position differences are observed in Figure 3.14, the suitability for the STM method is improved significantly in this final shape optimization step. After 70 optimization iterations, the compliance con-

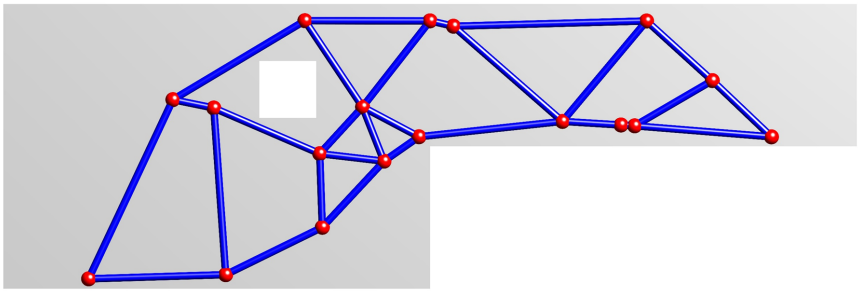

Figure 3.13: The generated truss-analogy model after the shape optimization phase.

verges after a considerable improvement, and the STS index has increased from 0.933 to 0.9997 while the geometry constraints g_2, g_4 and g_5 are reduced to 0 mm. g_1, g_3 and g_6 remained zero for all iterations. This indicates that a near ideal axial force configuration has been obtained, that also meets all geometrical requirements. With all three phases combined, the automated generation process took about 4 minutes for the considered example. The generated OPT-STM is shown in Figure 3.16 which can be used for STM analysis.

STM ANALYSIS

To complete the process, an STM analysis is conducted for the generated OPT-STM based on the European code [36] while disregarding partial safety factors. The average concrete compressive strength is 62.8 MPa (from the experiment by Oviedo et al. [106]). The limit strength of struts and node zones is defined as:

$$\sigma_{\max} = k\nu f_{\mathrm{cm}}, \tag{3.14}$$

where f_{cm} is the concrete compressive strength and ν is the concrete effectiveness factor determined as, with f_{cm} in MPa:

$$\nu = 1 - f_{\mathrm{cm}}/250. \tag{3.15}$$

In Eq.(3.14), k is a reduction factor which is 1 or 0.85 for the concrete compressive strength of the C-C-C nodes (nodal zones bounded by three or more struts) and C-C-T nodes (nodal zones bounded by two or more struts and a tie) respectively. All nodal zones with large compressive forces are checked, as illustrated in Figure 3.17. In the strength checking of struts, $k = 0.6$ for the strut with transverse tension is used, otherwise $k = 1$. Based on the given dimensioning, a summary of the strut checking results is given in Table 3.1. The generated OPT-STM satisfies the STM stress requirements.

For the ties, it is assumed that all reinforcements in the STM designs are fully activated. The reinforcement cross-sectional areas are determined based on a 100 % strength utilization and omitting partial safety factors.

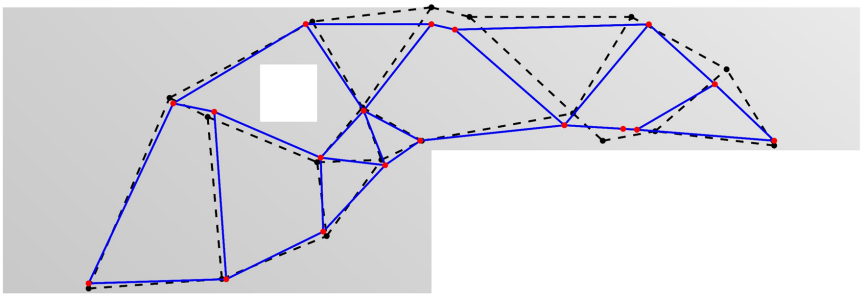

Figure 3.14: Comparison of two models. The blue solid lines present the model after shape optimization, while the black dashed lines present the truss obtained after Step 2.

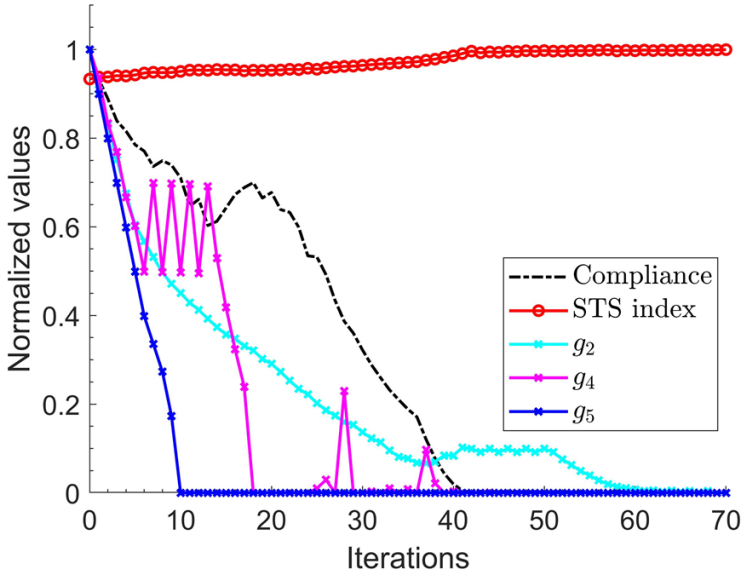

Figure 3.15: Shape optimization convergence history.

3.3. STRUT-AND-TIE MODEL EVALUATION METHOD

The intuition of engineers alone is not effective for evaluating the performance and capacities of complex ST models. In order to investigate the suitability of the generated OPT-STMs, an evaluation method based on Nonlinear Finite Element Analysis (NLFEA) is proposed in this section. Nonlinear phenomena such as concrete cracking and crushing and steel yielding and rupturing are considered in the NLFEA. Firstly, simulating RC structures by NLFEA is validated with experimental data, as presented in the following section. Next, the NLFEAs based on the ST models are used to obtain the structural performance. The structural responses are compared in terms of crack distribution, failure load and

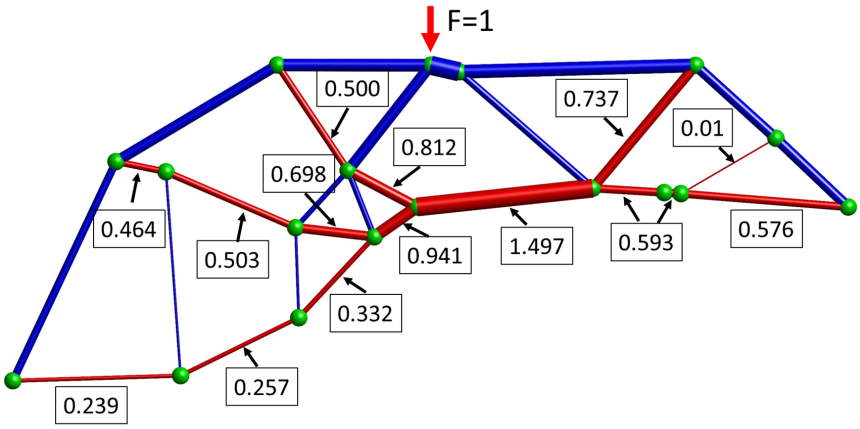

Figure 3.16: The generated OPT-STM. The blue and red lines indicate struts and ties respectively. The line width indicates the magnitude of axial forces. Normalized tensile forces (for a unit loading) are presented.

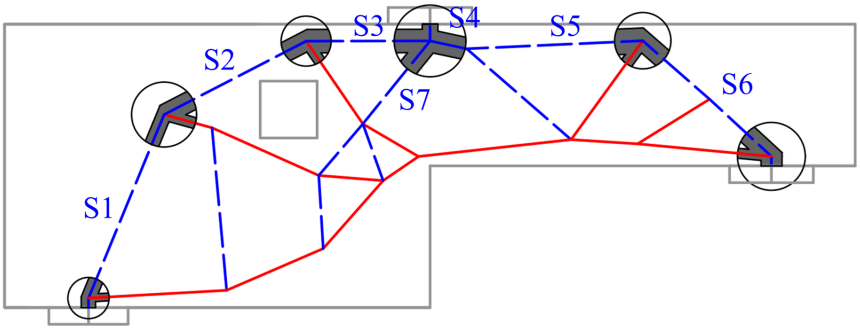

Figure 3.17: Node regions of the generated OPT-STM model after STM analysis.

Table 3.1: Summary of strut geometry and forces for STM

Strut	Force (kN)	k	Width (mm)	Strength utilization (%)
S1	39.9	0.6	13	91
S2	57.5	0.6	18	94
S3	69.2	0.6	21	97
S4	108.7	1.0	20	96
S5	75.9	0.6	23	97
S6	56.8	0.6	18	93
S7	59.7	0.6	18	98

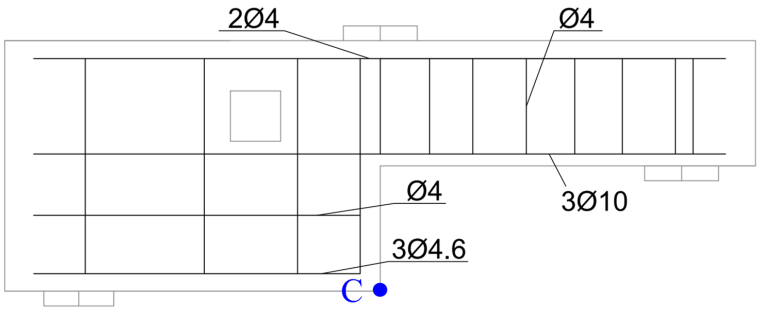

Figure 3.18: Reinforcement layout of specimen A in Oviedo et al. [106] (mm).

failure mode to evaluate various ST models. Note that this NLFEA procedure is included here to investigate and demonstrate the performance of the OPT-STM model generated by the proposed method, instead of being part of that method.

3.3.1. NONLINEAR FINITE ELEMENT ANALYSIS OF RC STRUCTURES

The NLFEA has been broadly applied in simulating RC structures, and several guidelines have been produced to select suitable solution strategies, see e.g. in fib [49] and Belletti et al. [20]. In this section, to validate the simulation an experiment conducted by Oviedo et al. [106] is simulated by NLFEA. The considered specimen is based on the same dapped-end beam of the previous section (see Figure 3.1), and its reinforcement layout in the experiment is shown in Figure 3.18. The steel has been placed horizontally and vertically, reflecting a conventional RC structure.

In order to conduct the NLFEA simulation, various aspects are considered, such as material models, finite element discretization, iteration scheme and convergence criteria. According to the solution strategy by Belletti et al. [20] and based on the compressive strength 62.8 MPa obtained from the 28-day cylinder test in the experiment, the derived concrete properties are summarized in Table 3.2. The properties of steel reinforcements from the experiment are presented in Table 3.3. The steel stiffness, E_s, is 200 GPa. They are simulated by fully-bonded embedded truss elements connected to the concrete continuum elements. The other analysis choices are presented in Table 3.4.

The analysis model is shown in Figure 3.19. The load and support plates are simulated using a linear material model with stiffness E_s and Poisson ratio 0.3, and interface elements are inserted between the steel plate and the concrete. The load-displacement curves of this simulation and the experimental result by Oviedo et al. [106] are presented in Figure 3.20. The displacement is measured vertically at the middle-bottom point of the beam (C point in Figure 3.18). The peak load of the simulation and experimental results are 119.0 kN (Point A in the curve) and 117.7 kN respectively. In the ultimate state (Point B), the structure fails due to steel rupturing. The strain in the steel and the rupturing location are presented in Fig(3.21), and the crack patterns predicted by the simulation are shown in Figure 3.22. The crack development of the simulation matches the observation

Table 3.2: Concrete properties

Mean compressive strength:	$f_{cm} = 62.8$MPa
Mean tensile strength:	$f_{ct} = 4.21$MPa
Fracture energy:	$G_F = 0.154$N/mm
Compressive fracture energy:	$G_C = 38.45$N/mm
Young's modulus:	$E_c = 39666$MPa
Poisson ratio:	$\nu = 0.15$

Table 3.3: Reinforcement properties

Diameter (mm)	Yield stress (MPa)	Ultimate stress (MPa)	Ultimate strain (%)
4	522	604	10
4.6	508	603	15
10	625	650	11.5

Table 3.4: NLFEA solution strategies [20]

- Finite element discretization:	8-node plane stress elements for concrete Embedded truss elements for reinforcement Mesh size: 7.5 mm
- Constitutive relation:	**Concrete**: • Rotating smeared crack model • Hordijk model for tensile behavior • Parabolic model for compressive behavior (reduction model by Vecchio and Collins [146], 0.6) **Reinforcement**: •Bi-linear strain-stress relation •Perfect bonded with concrete [48]
- Iteration method:	Newton-Raphson method
- Convergence criteria:	Displacement norm: 0.01 Force norm: 0.01
- Loading scheme:	Displacement control (Step size: 0.05 mm)

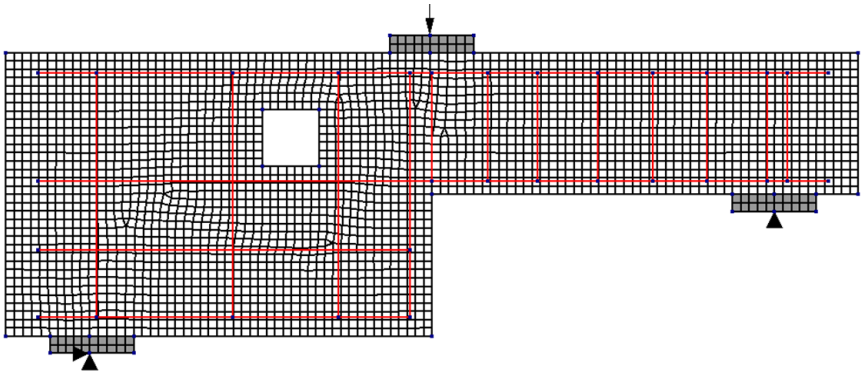

Figure 3.19: Finite element model of the experimentally tested dapped-end beam.

in the experiment [106]. While cracking patterns, ultimate capacity and failure mode show good agreement with the experimental findings, the numerical analysis shows substantially smaller deformations than the experiments (Figure 3.20). This can be attributed to a too high estimate of the Young's modulus in the analysis, inadequate modelling of the stiffness of the support and loading systems, which possibly included felt or plywood layers, or deformations within the loading frame. It is likely that these aspects only influence the prediction of the deformation capacity. Considering the lack of experimental data on these aspects, and the fact that the main use of the NLFEA is to predict the loading capacity and failure mode, no further efforts are considered to improve the displacement predictions. The current solution strategy is used to evaluate Strut-and-Tie models.

3.3.2. NLFEA-BASED EVALUATION METHOD OF STRUT-AND-TIE MODELS

In order to evaluate the performance of complex ST models, NLFEA is used. It is assumed that reinforcement bars are located corresponding to the ties in the ST model. In this way, practical reinforcement detailing aspects are excluded from the procedure and all NLFEAs are based on the same principle and the obtained responses can be used for comparing various ST models. The cross sections of these bars are based on full utilization of the yielding stress at the design load. The yield strength of steel is set to 580 MPa, without hardening effects and applying a rupturing strain of 10 %.

Based on the obtained forces of the OPT-STM from the illustrative example (Figure 3.16), the resulting finite element model is shown in Figure 3.23. The total steel volume is 87452 mm^3. In the NLFEA, the same solution strategies as in the previous section are used to calculate structural responses. The obtained load-displacement curve through the NLFEA is presented in Figure 3.24. The ultimate capacity reaches 81.7 kN while the design load for the STM analysis is 71.2 kN. The crack pattern and steel strain at the ultimate state (Point A) are shown in Figure 3.25. Most reinforcements are yielding, and the structure collapses due to steel rupturing at the ultimate state and results in a flexural failure mode.

The evaluation process demonstrated here on this OPT-STM model is used in the later sections to evaluate various other ST models. We also define a dimensionless ratio

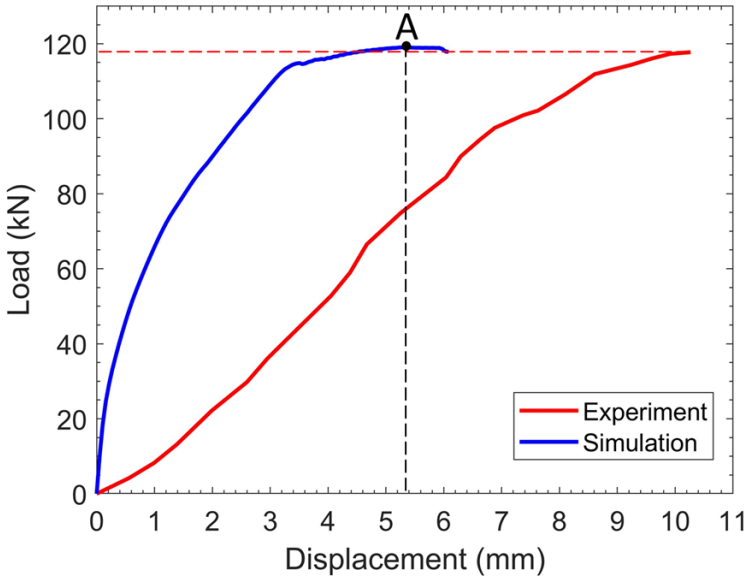

Figure 3.20: Load-displacement curves of the experimentally tested dapped-end beam.

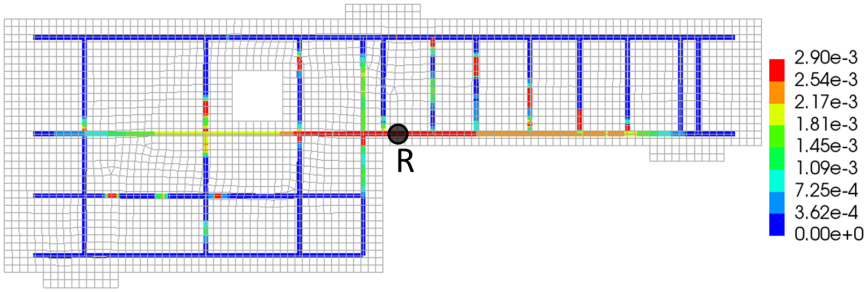

Figure 3.21: Steel strain distribution at the ultimate state B (Point R indicates the rupturing location).

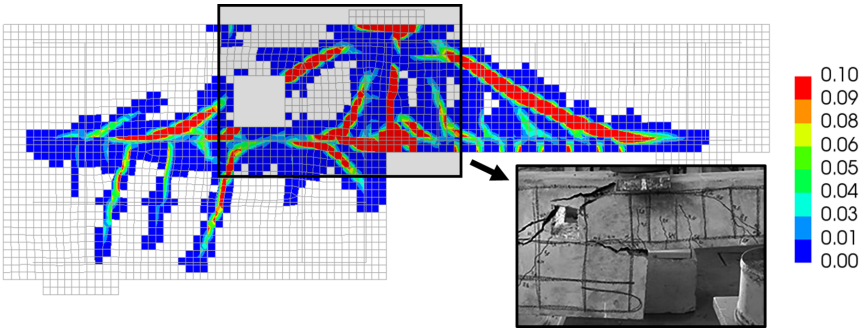

Figure 3.22: Simulated and experimental (inset) crack patterns and widths (mm) at the ultimate state B of the experimentally tested dapped-end beam. The inset is adapted from Oviedo et al. [106].

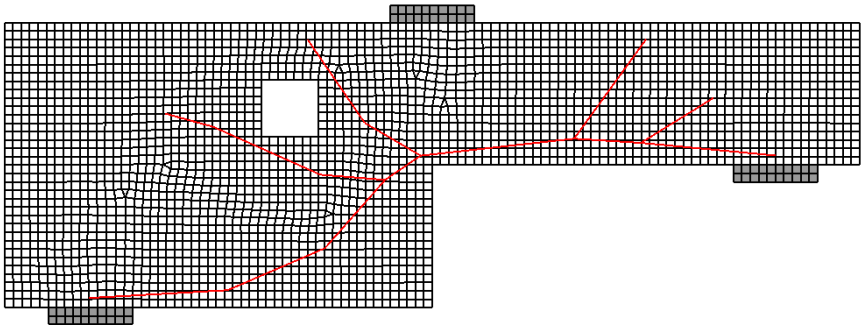

Figure 3.23: Finite element model based on the generated OPT-STM for the dapped-end beam.

that expresses the degree of utilization of the steel reinforcement for later comparisons. This ratio, named PV ratio, is given by:

$$PV = \frac{P_{\text{load}} L_k}{V f_y}, \tag{3.16}$$

where P_{load} is the peak load obtained from the NLFEA, V is the total steel volume, f_y is the steel yield strength and L_k is a characteristic length of the structure. In this research, L_k is taken as the smallest height of the structure. In the presented OPT-STM example, L_k equals to 127 mm and the resulting PV ratio is 0.205. Before using the measures introduced in this section for a comparative evaluation of OPT-STM designs against classical ST models, they are applied in the next section to study several aspects of the proposed generation process.

3.4. THREE ASPECTS OF THE AUTOMATED DESIGN METHOD FOR OPT-STM MODELS

In this section, three main aspects influencing the generation of OPT-STM models are discussed. Different settings and parameters in the generation method will affect generated OPT-STM models. Firstly, in the TO phase (Section 3.2.1), TO is conducted to generate optimized material distributions. The volume fraction and filter radius affect the optimized topology and thus influence the generated OPT-STM models. The influence of these two factors will be demonstrated and discussed. Next, in the topology extraction phase (Section 3.2.2), the merging of short bars (Figure 3.9) simplifies the extracted truss-like structures. However, by adopting different merging lengths the generated OPT-STM models are affected. The influence of the merging length will be demonstrated and discussed. Thirdly, regarding the ST model generation phase, the importance of satisfying the axial force equilibrium is discussed.

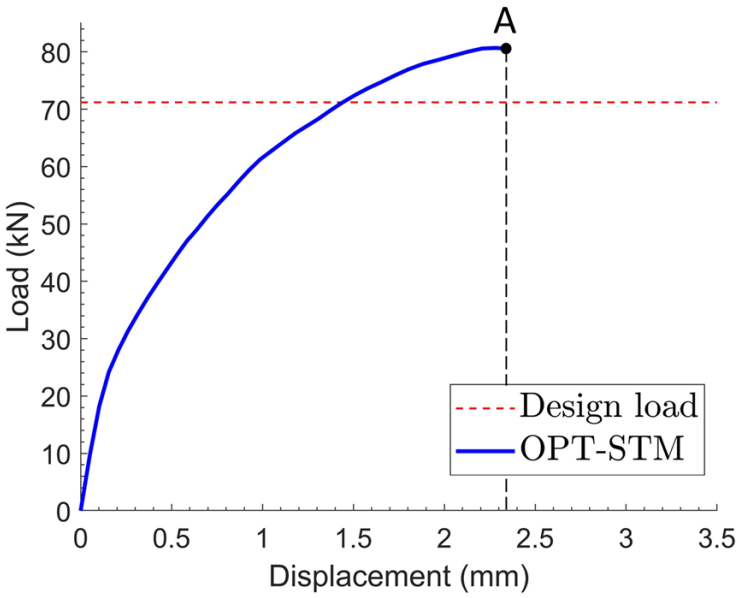

Figure 3.24: Load-displacement curve of the OPT-STM based design.

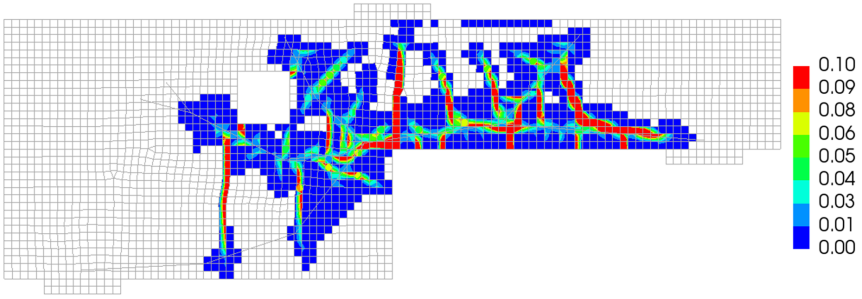

(a) Simulated crack patterns and widths (mm) at the ultimate state A

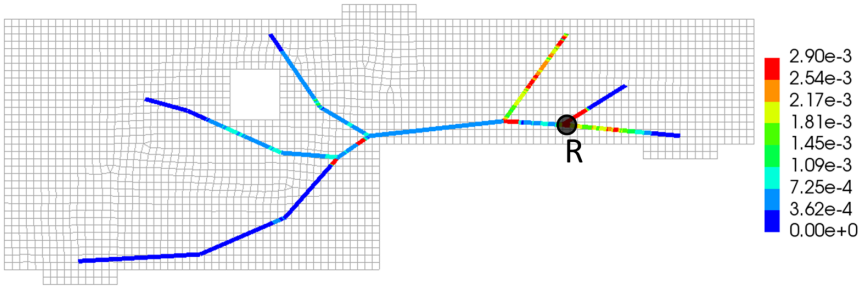

(b) Steel strain distribution (Point R indicates the rupturing location)

Figure 3.25: NLFEA simulation results of the OPT-STM based design.

3.4.1. INFLUENCE OF VOLUME FRACTION AND FILTER RADIUS IN THE TOPOLOGY OPTIMIZATION PHASE

The volume fraction (α) affects the number of members and their width in the topology results. The topological changes will influence the generated OPT-STM models and their performance. Next to the volume fraction, the filter radius (r_0) smoothens the TO results to prevent mesh dependency and checker-board problems in the TO process. With a large filter radius, a TO result with fewer members is obtained. In order to investigate the influence of these parameters, OPT-STM models of the illustrative example with various volume fractions and filter radii are generated, and their performance is evaluated using both the PV ratio and the load-displacement curve obtained through NLFEA.

In the illustrative example, the OPT-STM model is generated with volume fraction $\alpha = 25\%$ and filter radius $r_0 = 1.5$. Here, four other OPT-STM models are generated based on a one-factor-at-a-time sensitivity analysis. In these four models the volume fraction is $\alpha = 15\%$ and $\alpha = 35\%$ and the radius is $r_0 = 2.5$ and $r_0 = 3.5$ respectively. The topology optimization results and the resulting OPT-STM models are shown in Figure 3.26. All OPT-STM models have STS indices larger than 0.995 and satisfy the geometry constraints. The evaluation results based on the proposed evaluation method are presented in Table 3.5. The load-displacement curves are presented in Figure 3.27.

Based on the calculated PV ratios of changing volume fractions (Figure 3.26 (a), (b) and (c)), we observe that the OPT-STM model with $\alpha = 15\%$ performs better than the other two cases regarding the ultimate capacity and steel usage. The variations of OPT-STM models for a changing filter radius are presented in Figure 3.26) (b), (d) and (e). The OPT-STM model performs better with a relatively small radius ($r_0 = 1.5$). NLFEA shows that all designs based on these OPT-STM models provide higher capacities than the design load, as seen in Figure 3.27. This observation confirms that STM results in conservative designs. Although different material distributions are obtained in the TO results, all models show similar load-displacement curves and the resulting structures fail due to steel rupturing. However, the models with a relatively large volume fraction and filter radius have lower PV ratios. Moreover, from results not shown in this research, it has been found that adopting even larger volume fractions ($\alpha = 50\%$) or larger filter radii ($r_0 = 6$) leads to unclear topologies, which do not allow generation of truss-like structures and the OPT-STM models. Therefore, a relatively small volume fraction and filter radius are suggested in the TO phase.

3.4.2. INFLUENCE OF MERGING LENGTH IN THE TOPOLOGY EXTRACTION PHASE

The merging length L_m is used to eliminate short bars in the topology extraction phase. This simplification will influence the accuracy of extracted truss-like structures in representing TO results and thus influence the performance of the resulting OPT-STM models. The merging length L_m is taken as: r_L times the smallest outside dimension of the illustrative example. A fraction $r_L = 10\%$ results in a merging length of 25.4 mm for the considered beam example. The corresponding reference result is shown in Figure 3.26b. In this section, in order to investigate this parameter, two more OPT-STM models are generated with fractions $r_L = 15\%$ and $r_L = 25\%$ respectively. The generated OPT-STM

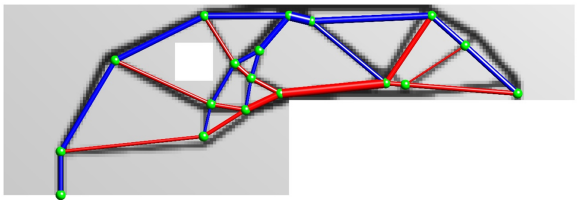

(a) $\alpha = 15\%$ $r_0 = 1.5$

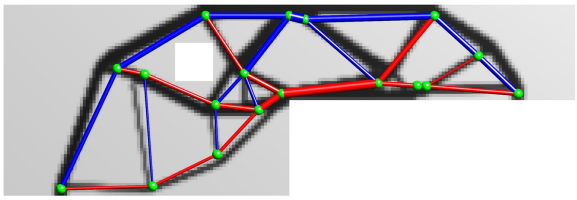

(b) $\alpha = 25\%$ $r_0 = 1.5$

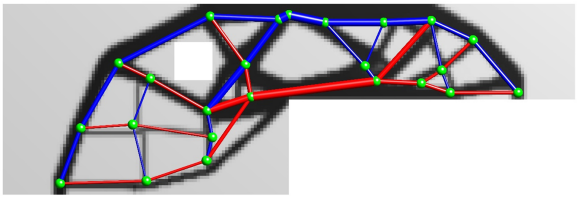

(c) $\alpha = 35\%$ $r_0 = 1.5$

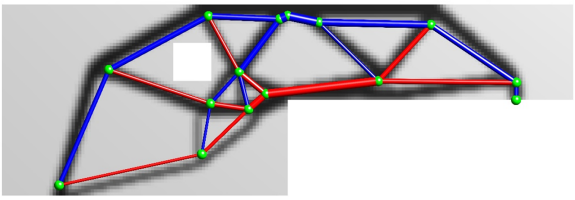

(d) $\alpha = 25\%$ $r_0 = 2.5$

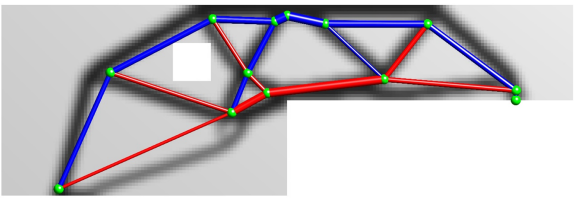

(e) $\alpha = 25\%$ $r_0 = 3.5$

Figure 3.26: The generated OPT-STMs with different parameters. Black pixels present the TO result. The blue and red lines indicate struts and ties respectively. The line width indicates the magnitude of axial forces.

Table 3.5: Peak load, steel volume and PV ratio of evaluated OPT-STM models

α (%)	r_0 (mesh size)	Peak load(kN)	Steel volume (mm^3)	PV (%)
15	1.5	82.10	**86630**	**20.9**
25	1.5	81.73	87452	20.5
35	1.5	79.08	92693	18.2
25	2.5	**84.17**	91116	20.2
25	3.5	82.95	92927	19.5

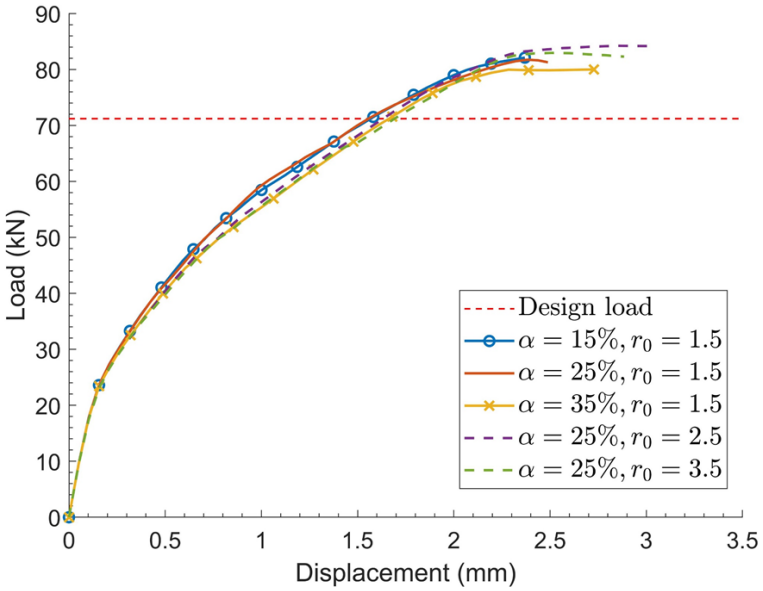

Figure 3.27: Load-displacement curves of evaluated OPT-STM models.

models are presented in Figure 3.28.

The obtained results for these models are shown in Table 3.6. The complexity of the OPT-STM models is reduced with increasing merging lengths. Regarding the evaluation results of $r_L = 10\%$ and $r_L = 15\%$, we observe similar PV ratios. By reducing the merging length, a more accurate and detailed truss-like structure is obtained in the topology extraction phase, and the resulting OPT-STM has a higher PV ratio. The OPT-STM generated with $r_L = 25\%$ has an obviously different truss analogy model than the other two cases. In this case, the structure fails due to steel rupturing, as shown in Figure 3.29. The limited steel ductility and concrete plasticity are not able to re-distribute stresses to fully

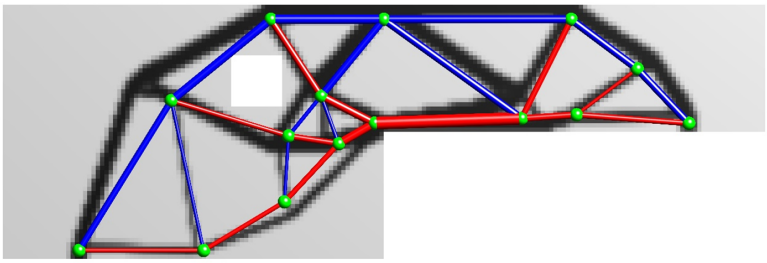

(a) $r_L = 15\%$

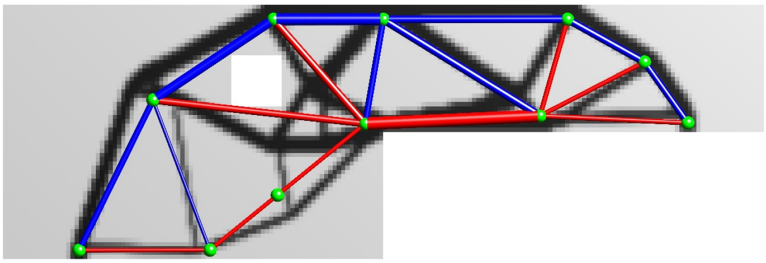

(b) $r_L = 25\%$

Figure 3.28: Generated OPT-STMs with two merging lengths. Black pixels present the TO result. The blue and red lines indicate struts and ties respectively. The line width indicates the magnitude of axial forces.

Table 3.6: Peak load, steel volume and PV ratio of evaluated OPT-STM models

r_L (%)	Peak load (kN)	Steel volume (mm^3)	PV (%)
10	**81.73**	87452	**20.5**
15	79.45	**85799**	20.3
25	65.89	88929	16.2

utilize the steel, therefore the ultimate capacity is lower than the design load (71.2 kN).

These findings confirm that the merging length affects the extracted truss-like structures. Although large merging lengths reduce the complexity of OPT-STM models, the generated models are no longer representative of the TO results, and a poor performance is obtained which has a lower capacity, a higher steel usage and a lower PV ratio. By choosing suitable lengths, the generated OPT-STM models are effective in representing the TO results and have good performance.

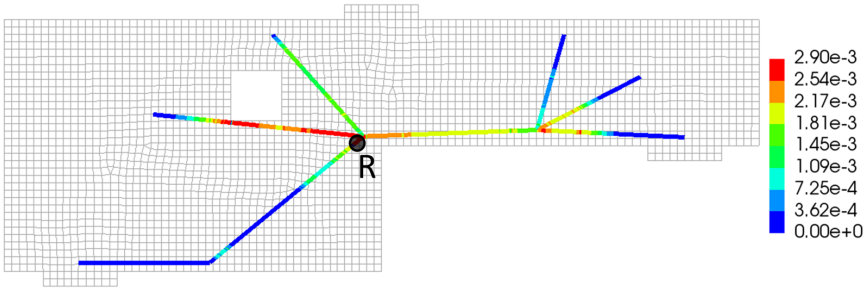

Figure 3.29: Steel strain distribution of the model ($r_L = 25\%$) (Point R indicates the rupturing location).

Table 3.7: Peak load, steel volume and PV ratio of evaluated models

Cases	STS index (%)	Peak load (kN)	Steel volume (mm^3)	PV (%)
Truss-like structure	93.3	43.98	78029	12.4
OPT-STM	99.97	81.73	87452	20.5

3.4.3. IMPORTANCE OF SATISFYING THE AXIAL FORCE EQUILIBRIUM

Axial force equilibrium states of truss-analogy models are required in the STM method. The designs based on the STM method are conservative which is an important aspect in practice. The extracted truss-like structures are usually statically and kinematically unstable structures in which the calculated STS indices (Eq.(3.8)) are substantially smaller than 1. Through shape optimization, the final OPT-STM structure closely approximates a pure axial force system. In order to investigate the importance of this shape optimization step and of satisfying the axial force equilibrium, the extracted uncorrected truss-like model excluding the shape optimization phase is analyzed, as shown in Figure 3.10. The STS index of this truss-like structure is 93.3 %. After the beam analysis, only axial forces are used to design cross sections of the reinforcement in the NLFEA model. The evaluation results are summarized in Table 3.7, and load-displacement curves are presented in Figure 3.30.

The evaluation result of the uncorrected truss-like structure shows a capacity significantly below the design load, which is supposed to be a lower bound. The shear force diagram of the truss-like structure is presented in Figure 3.31, and the crack patterns and the steel strain in the ultimate state are presented in Figure 3.32. Due to the large shear forces, the structure fails in a shear failure mode without steel rupturing. The satisfaction of the STS index requirement is important to guarantee that the generated models are suitable for the STM method, and lead to safe designs.

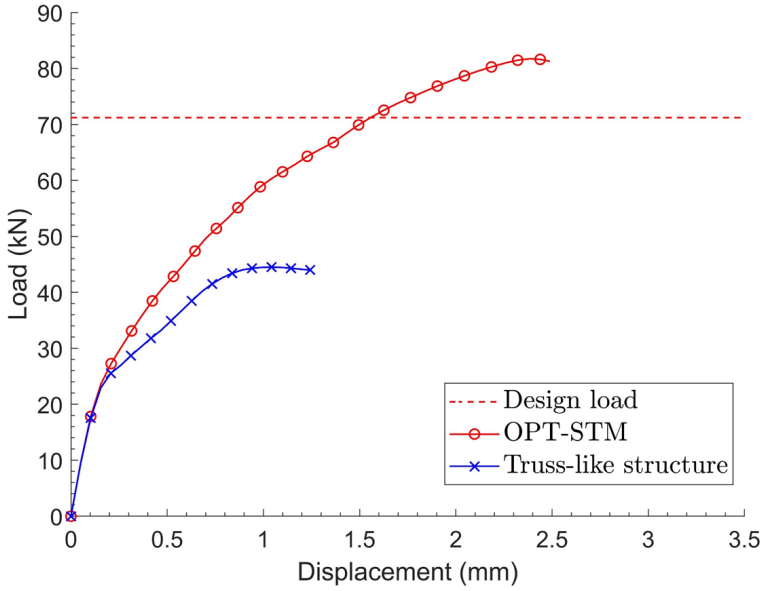

Figure 3.30: Load-displacement curves of the OPT-STM and the uncorrected truss-like model.

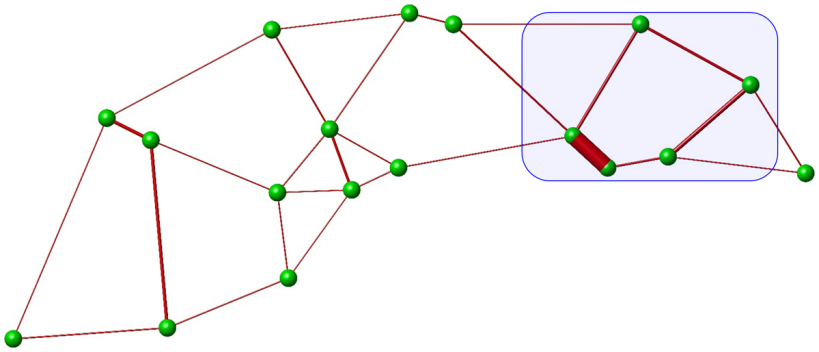

Figure 3.31: The shear force diagram of the uncorrected truss-like structure. The bar width indicates the magnitude of shear forces.

3.5. APPLICATIONS OF THE GENERATION METHOD FOR TWO D-REGIONS

In this section, the generated OPT-STM models and 11 manually generated ST models from literature for two D-regions are evaluated. The first case (Case A) is the dapped-end beam which has already been used as illustrative example throughout the previous sections. The second case (Case B) is an irregular deep beam with an opening. Based on NLFEA results of these ST models, the load capacity, steel usage, PV ratios

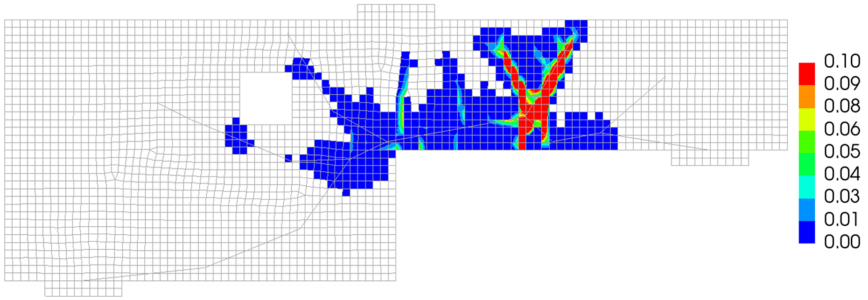

(a) Simulated crack patterns and widths (mm)

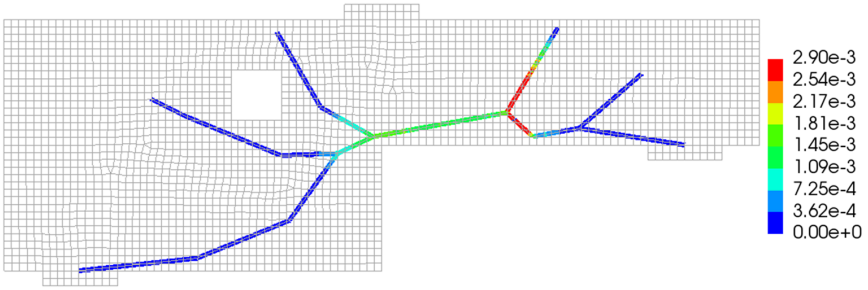

(b) Steel strain distribution

Figure 3.32: Structural response of the uncorrected truss-like structure in the ultimate state.

and failure modes are compared to evaluate the relative effectiveness of the generated OPT-STM models.

3.5.1. PROBLEM DESCRIPTION AND STRUT-AND-TIE MODELS

Case A was introduced in Figure 3.1 in Section 3.2. Case B is based on Example Problem 4 of ACI SP-208 [114]. The experimental investigation of this problem was by Ley et al. [84]. The geometry and loading conditions are presented in Figure 3.33. The thickness of this structure is 38 mm.

Following the proposed generation method, and using the recommended settings obtained in Section 4 (volume fraction $\alpha = 25\%$, filter radius $r_0 = 1.5$, merging length $r_L = 10\%$), the OPT-STM model for this irregular deep beam is generated, as shown in Figure 3.34. It has an STS index equal to 0.999, and is presented in Figure 3.35.

The evaluated ST models of Case A from previous studies in literature are presented in Figure 3.36. The OPT-STM model for this case is the same model as obtained in Section 2, Figure 3.16. Four additional ST models from previous studies, as shown in Figure 3.36 (b)-(e) with corresponding references, are also evaluated. STM-A1, STM-A2 and STM-A3 have a similar right-hand side part, however the force transmission in the left-hand side part differs between these models. Model STM-A4 has been generated based on a topology optimization result with manual adjustments.

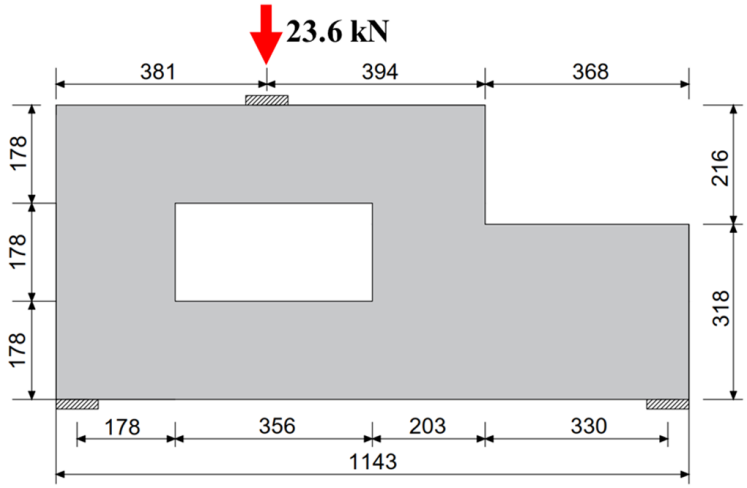

Figure 3.33: Irregular deep beam with an opening (mm).

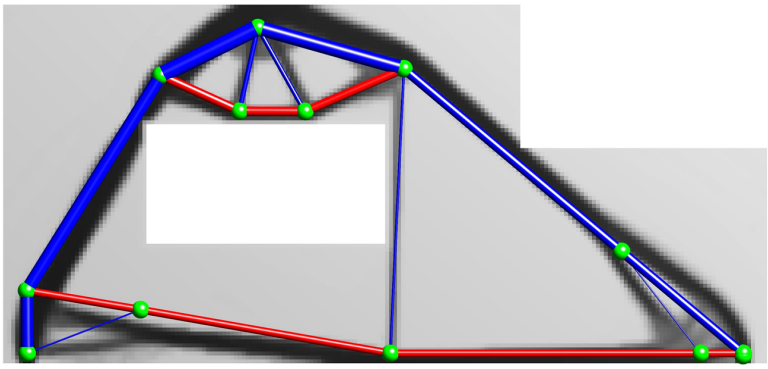

Figure 3.34: The generated OPT-STM of the irregular deep beam.

As for Case B, seven previously proposed ST models are evaluated and compared against the generated OPT-STM model, as shown in Figure 3.37. In this example, STM-B1 simulates two beams which are placed in the upper and lower part of the structure. STM-B2 simulates the force transmission as a portal frame with a hinge at the top. STM-B3 was proposed following the load path method. Compared to STM-B1, STM-B4 uses a deeper truss at the right-hand side. The motivation of the proposed STM-B5 is to provide a large amount of ductility. The stresses in the bottom part of the beam are neglected. STM-B6 and STM-B7 are created based on TO results, followed by manual interpretation. However, a large difference is observed between the TO result reported in Zhong et al. [169] and the resulting STM-B7.

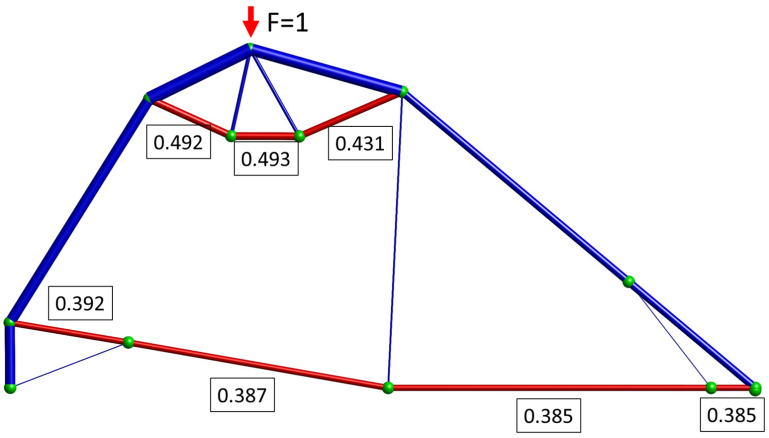

Figure 3.35: The generated OPT-STM of the irregular deep beam. The blue and red lines indicate struts and ties respectively. The line width indicates the magnitude of axial forces. Normalized tensile forces (for an unit loading) are presented.

3.5.2. EVALUATION RESULTS AND DISCUSSIONS

Based on the evaluation method from Section 3, the aforementioned ST models are evaluated by NLFEA. The solution strategy for Case A is the same as in the illustrative example. In Case B, the concrete properties are calculated based on a mean compressive strength as 21.4 MPa from the experiment by Ley et al. [84]. The step size is 0.01 mm in displacement control and the mesh size for the FEM model is 12 mm. Other aspects of the solution strategy remain the same as in the first example. All axial equilibrium forces of evaluated ST models are calculated based on the design load to determine cross-sectional areas for the reinforcements. The STS indices for the classical ST models approach 1, indicating pure axial loading. Given the high STS indices for both OPT-STM models, there is no difference between all models in this respect.

The obtained load-displacement curves of Case A are shown in Figure 3.38. The ultimate load and steel usage are summarized in Table 3.8. The models with best and worst PV ratios have line markers in the load-displacement curves. In this example, all models fail due to steel rupturing and they have a peak load larger than the design load (71.2 kN). Moreover, the load-displacement curve shows that the OPT-STM model is generally stiffer than other models. It has the largest PV ratio which indicates the most economical design. STM-A2 has the lowest PV ratio, indicating a relatively costly design. Since STM-A4 was inspired by a TO result, a relatively large PV ratio is obtained compared to the other classical ST models. The proposed automated ST model generation process is superior to this hand-tuned model in both capacity and PV ratio, however in terms of absolute reinforcement volume the STM-A4 model has a slight advantage. Moreover, the peak loads of all models are reached when the reinforcement reaches the ultimate strain.

In Case B (irregular deep beam), the load-displacement curves of all evaluated models are presented in Figure 3.39. The ultimate load and steel usage are summarized in Table 3.9. Similar as in the first example, the OPT-STM has the best PV ratio. STM-B6

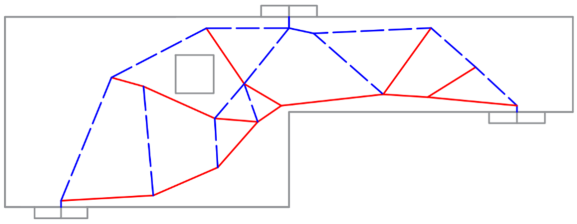

(a) OPT-STM-A

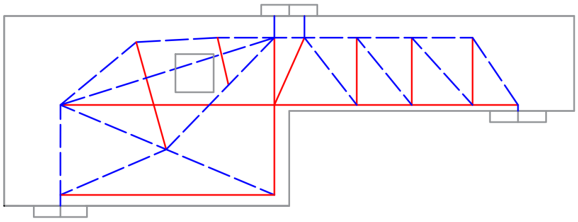

(b) STM-A1 [106]

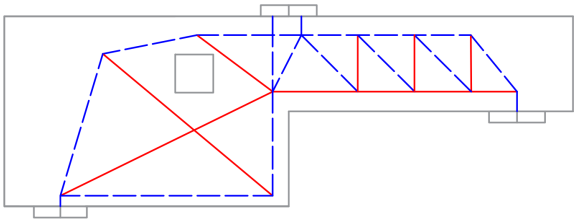

(c) STM-A2 [37]

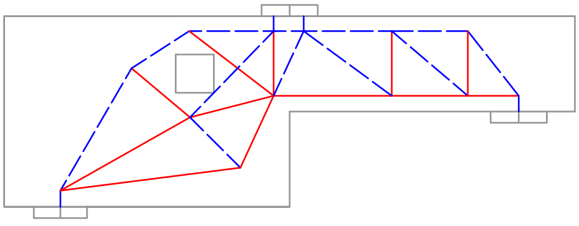

(d) STM-A3 [37]

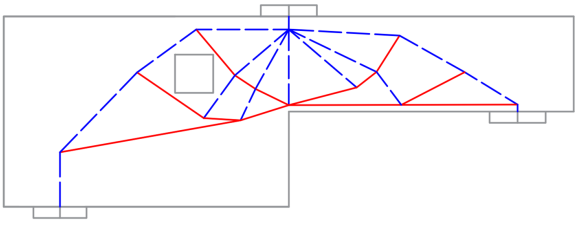

(e) STM-A4 [63]

Figure 3.36: ST models for Case A (the dapped-end beam).

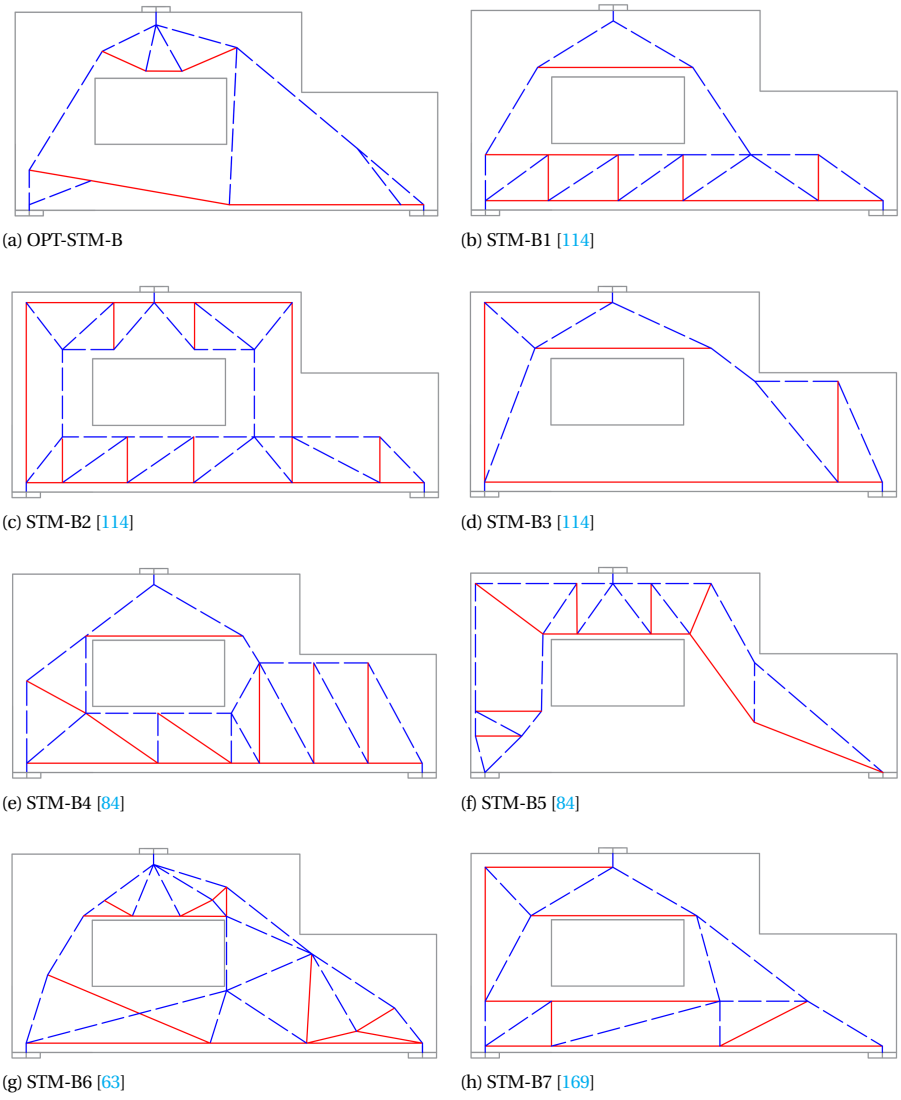

(a) OPT-STM-B (b) STM-B1 [114]

(c) STM-B2 [114] (d) STM-B3 [114]

(e) STM-B4 [84] (f) STM-B5 [84]

(g) STM-B6 [63] (h) STM-B7 [169]

Figure 3.37: ST models for Case B (irregular deep beam).

is inspired by a TO result and also leads to a relatively good PV ratio. Because of the large differences between STM-B7 and its TO result, a lower PV ratio is obtained for STM-B7.

In this example, the peak loads of other models are considerably larger than the design load (23.6 kN) apart from STM-B5. The design of STM-B5 shows a brittle behaviour in which the reinforcement cannot be fully activated due to the limited plasticity of concrete. In this case, most ST models (except STM-B2 and STM-B5) fail due to steel rupturing. Because of stress redistribution, the designs of OPT-STM-B and STM-B3

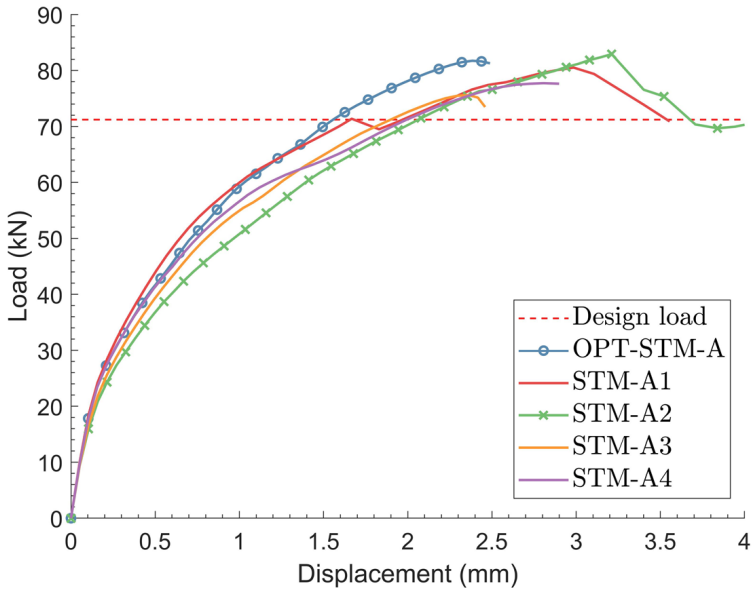

Figure 3.38: The load-displacement curves for the ST models of Case A (dapped-end beam).

Table 3.8: The ultimate load and steel usage of ST models of the Case A (dapped-end beam)

Cases	Peak load(kN)	Steel volume(mm^3)	PV(%)
OPT-STM	81.73	87452	**20.5**
STM-A1	80.50	134202	13.1
STM-A2	82.91	189422	**9.6**
STM-A3	80.58	105979	16.6
STM-A4	77.72	84781	20.0

exhibit restabilization after the occurrence of critical cracks in the first peak load point. All models have a similar stiffness before developing the initial cracks. Only the designs of OPT-STM-B and STM-B1 reach the peak load at the moment of steel rupturing. Other models show ductility after reaching the peak load. In terms of steel economy and avoiding an overly conservative design, the automatically generated OPT-STM-B model outperforms both hand-tuned designs based on TO results, as well as all other ST models proposed for this problem. It is also noted, that through the very efficient use of steel, less ductile behavior is observed.

Based on evaluation results of two D-region problems under considered concrete and steel properties, large PV ratios are found for the generated OPT-STM model. More-

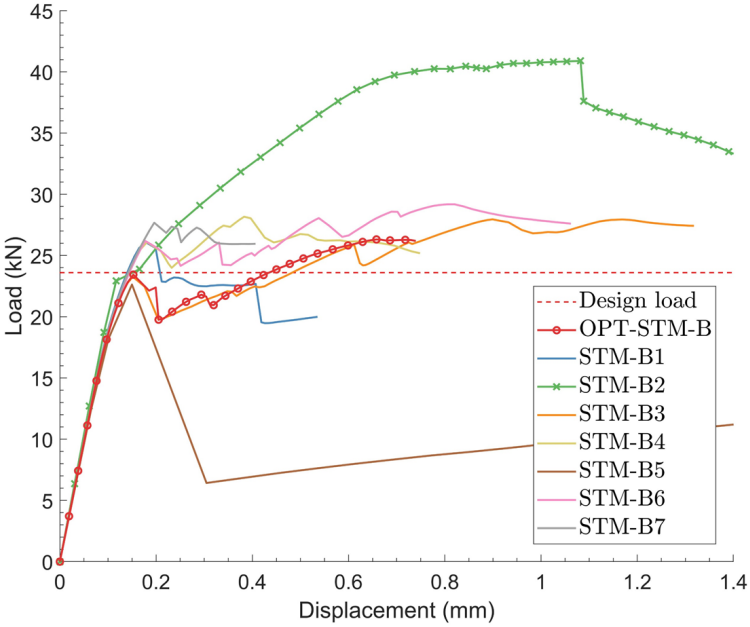

Figure 3.39: The load-displacement curves for the ST models of Case B (irregular deep beam).

Table 3.9: The ultimate load and steel usage of ST models of the Case B (irregular deep beam)

Cases	Peak load(kN)	Steel volume(mm^3)	PV(%)
OPT-STM-B	26.51	24467	**59.4**
STM-B1	26.80	42715	34.38
STM-B2	40.90	152440	**14.7**
STM-B3	27.95	39994	38.3
STM-B4	28.12	43657	35.4
STM-B5	22.63	73639	16.8
STM-B6	29.18	27378	58.4
STM-B7	27.68	42554	35.6

over, the resulting design reaches the peak load in the ultimate state, in which the structure fails due to steel rupturing. This indicates that more suitable ST models are generated, which are more accurate in representing the force flows in the D-region. Comparing TO inspired ST models (STM-A4 and STM-B6) with other manually created models, it is clear that the topology inspired models have relatively large PV ratios. However, by avoiding the manual interpretation of TO results, the PV ratios are most improved in the

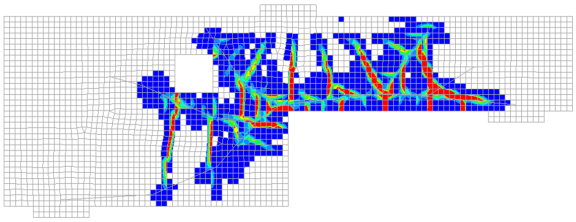

(a) Dapped-end beam

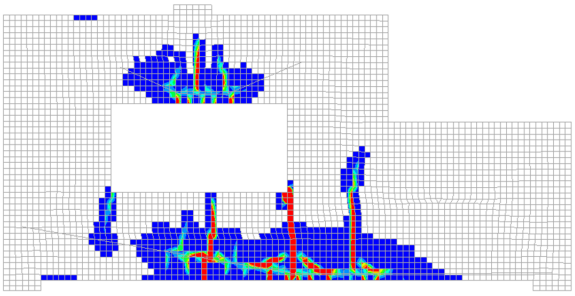

(b) Irregular deep beam

Figure 3.40: Crack plots for the OPT-STM models at the ultimate state.

generated OPT-STM models. The crack plots of the two OPT-STM models are presented in Figure 3.40. The OPT-STM models lead to flexural failure modes due to rupture of the reinforcement. By using a more suitable ST model, the usage of reinforcements is reduced and a more accurate design model for D-regions is obtained.

3.6. CONCLUSION

In this chapter, a method is proposed to automatically generate optimization-based Strut-and-Tie (OPT-STM) models. In order to generate suitable models for the STM method, the proposed method includes three phases. The topology optimization results of the compliance minimization problem are obtained in the first phase. Next, in the topology extraction phase, truss-like structures which represent the TO results are generated. Finally, in the shape optimization phase, the requirements of the STM method on the axial-force equilibrium and geometrical conditions such as openings and cover thicknesses are considered. The entire procedure, depending on the selected resolution, typically produces a valid OPT-STM model in a few minutes.

In order to evaluate the generated OPT-STM models, in this study NLFEA is used to simulate the structural performance. Steel usage, peak loads and failure modes are used to evaluate the suitability of the used ST models. Based on obtained steel usage and peak loads, the PV ratio is defined to quantify the degree of utilization of steel reinforcement for further comparison. Two D-region design cases are investigated. In addition to two generated OPT-STM models, 11 ST models from previous studies are evaluated. Based

on the present investigation, the conclusion is summarized as follows:

1. The proposed method successfully generates valid OPT-STM models for D-regions automatically and without manual adjustments. Recommendations for the settings of several parameters are provided based on parameter studies.

2. Detailed NLFEA simulation of RC structures based on OPT-STM models show a high stiffness and sufficient, yet not overly conservative load capacity. Compared with manually generated ST models, the OPT-STM models lead to the most economical steel usage relative to load capacity. The desired flexural failure mode is obtained.

3. Given these findings, the proposed ST model generation method can be recommended for practical use. It removes variability due to manual ST model construction from the design process and replaces this with safe and economical designs. When implemented in the engineering practice, significant savings in design time and steel usage can be expected.

4

Optimization-Based Three-Dimensional Strut-and-Tie Model Generation for Reinforced Concrete

Strut-and-Tie modelling (STM) is an effective and widely used method to design D-regions of reinforced concrete structures. Among the various steps of STM, finding a suitable truss analogy model is the most challenging part. Even for experienced engineers it is difficult to find representative models for complex D-regions, and this task is even harder for three-dimensional (3D) D-regions. To date, only a few 3D ST models have been proposed by researchers for several complex D-regions, which leaves practitioners with little guidance. In order to solve this problem, a method is proposed to automatically generate 3D optimization-based Strut-and-Tie (3D-OPT-STM) models. The generation method comprises a compliance-based topology optimization (TO) process which generates optimized structural forms by maximizing stiffness, a topology extraction method and a shape optimization method. In this study, three 3D-OPT-STM models are generated for typical 3D D-regions, and their performances are compared to manually created ST models. The generated 3D-OPT-STM models result in more economical designs. Moreover, geometrical and loading parameter studies demonstrate the applicability and robustness of the proposed method.

Contents of this chapter have been published in Computer-Aided Civil and Infrastructure Engineering (2020) [153].

4.1. INTRODUCTION

It is a challenge for engineers to design disturbed regions (D-regions) of reinforced concrete (RC) structures due to their highly non-linear strain distributions. The Strut-and-Tie Modelling (STM) has been established as an effective tool to design D-regions. STM was first generalized by Schlaich et al. [122] and Schlaich and Schafer [121] as a versatile tool for designing RC structures. In the STM analysis, the flow of forces is idealized by abstracting concrete struts, reinforcement ties and their connecting nodes. By using truss analogy models which indicate the force and stress distribution, STM improves designers' insights for designing complex D-regions. STM is based on the limit lower-bound theory [16, 47, 105, 159] and leads to conservative designs in case the structure has adequate ductility for the assumed struts and ties to develop. STM procedures have been implemented in the current codes to facilitate designers in practice, e.g. British Standards [34], Canadian Standards [43], code requirements from the American Concrete Institute [4], fib Model Code for Concrete Structures [51], the American Association of State Highway and Transportation Officials [2] and European Code [36]. However, in current codes design guidances are provided for relatively simple D-regions only, such as deep beams. For relatively complex D-regions, current codes can only give limited directions. This evidently applies even more to disturbed three-dimensional (3D) domains than to disturbed 2D domains.

In the STM method, the first step is to simplify D-regions by discrete truss analogy models to represent the force transfer mechanism. Various models can be used to design a single D-region and they can lead to significantly different performances [47]. It has been broadly accepted that finding a suitable truss analogy model is an important part to guarantee that Strut-and-Tie (ST) models will perform well [31, 78, 87, 108, 121]. While all ST models result in conservative designs, with an ill-chosen truss analogy model the resulting design can be overly conservative, i.e. uneconomical in terms of its steel usage.

Several approaches have been applied in the past decades to find suitable ST models. For example, load path methods were used to determine suitable truss-analogy models in Palmisano and Elia [107], Schlaich and Schafer [121]. Using stress field approaches, Schlaich and Schafer [121] suggested to conduct a linear finite element analysis and form ST models based on the calculated stress field. Muttoni et al. [101] applied a similar concept. With increasing complexity of D-regions, the difficulties of generating suitable ST models also increase. In this regard, the use of topology optimization (TO) methods for ST model generation has become one of the most popular directions in this field. Researchers have proposed various TO methods for STM, e.g., the ESO (evolutionary structural optimization) method [10, 79, 87], the isoline method [147], the full-homogeneous method [63] and the SIMP (solid isotropic material with penalization) method [31–33, 71]. Optimization techniques have also been widely applied in the structural design beyond STM. Various applications have been reported in the field of the civil engineering. To name a few examples, Vantyghem et al. [144] applied a TO method together with 3D printing to produce post-tensioned concrete structures. Stromberg et al. [131] used continuum-beam integrated topology optimization method to design laterally braced frames. Aldwaik and Adeli [7] used a genetic algorithm to design highrise buildings. Talischi et al. [137] applied the polygonal element in the TO process. Shape

optimization techniques have been applied in designing truss structures [5, 6, 134] and shell structures [75, 76, 117, 150].

Up to date, most investigations of finding ST models have focused on 2D D-regions. Compared to 2D ST models, there are much fewer studies on 3D ST models. One main reason is the increased difficulty of determining suitable ST models in 3D. However, as a result of the increased complexity of 3D D-regions, finding suitable 3D ST models is even more important. Cai [35] proposed a 3D indeterminate ST model for a footing system. Leu et al. [83] applied a refined ESO TO method to obtain optimized material layouts for creating 3D ST models. Similarly, based on the ESO TO methods, He and Liu [62] generated ST models for anchorage diaphragms, Shobeiri and Ahmadi-Nedushan [124] applied a bi-directional ESO method to obtain optimized material distributions for several 3D D-regions, and Zhong et al. [168] used a micro-truss based ESO method for 3D ST models. Yun et al. [164] generated 3D ST models by using a grid-based approach. Dey and Karthik [45] analyzed several pile-cap designs based on 3D compatible ST models. Several investigations [95, 129, 165] were conducted to investigate suitable 3D ST models for pile-cap design problems.

Among different approaches, TO-based methods have the potential to provide a systematic procedure to generate suitable ST models. However, in current state, TO approaches only provide optimized material distributions as inspirations for ST models. Manual and subjective interpretations and adjustments are required to transform TO results (material distributions) to ST models (truss analogy models). On the one hand, these subjective interventions hamper the systematic generation of ST models; on the other hand, the created ST models may not exhibit the required axial-force equilibrium state. These problems have been demonstrated in our previous review [152]. Therefore, in order to fill this gap and move towards in developing a systematic STM method, an automatic generation method to generate suitable truss analogy models for 3D STM is proposed in this chapter. To the best of our knowledge, it represents the first method of its kind to address 3D ST model generation.

The method is developed based on our previously proposed OPT-STM generation method [151], which was focused on two-dimensional problems only. The proposed method in this chapter includes three main steps: 1) the 3D compliance-minimization-based TO, 2) the topology extraction which automatically generates truss-analogy models based on 3D TO results, 3) the shape optimization which generates valid truss-analogy models for STM. In this research the framework of the method is repeated briefly for convenience, while highlighting the modifications made for making the method applicable, effective and robust for 3D D-regions. Key innovations this research introduces in comparison to the 2D method to enable the treatment of 3D cases are:

- Various measures reducing the computation costs for the computationally demanding 3D TO process,
- Proposing a novel robust procedure in extracting 3D truss-like structures,
- Extending the STM shape optimization procedure for 3D models, including a continuous minimum length constraint.

Through the integrated optimization process, three-dimensional optimization-based STM (3D-OPT-STM) models can be generated in an automated manner, which simplifies the design process in engineering practice. Thus a systematic method for generating suitable 3D ST models for 3D D-regions is devised. Based on the proposed generation method, 3D-OPT-STM models for three typical D-regions (four-pile cap, corbel and box girder) are generated and compared with the manually created ST models. The proposed generation method enables to further investigate three factors in the STM method systematically:

- A geometrical parameter study reveals the transition from one optimal topology to another as 3D aspect ratios are varied,
- A loading parameters study shows the effect of adding out-of-plane load components on optimal transfer mechanisms,
- Discretizing distributed loads is an essential step in the STM method. The effect of different load discretization schemes of surface loads in 3D is investigated.

Along with the variation studies, the applicability and robustness of the 3D-OPT-STM is demonstrated. It is emphasized that practical requirements, such as steel detailing and constructability aspects, are outside the scope of the current study.

The remainder of the chapter is organized as follows: The 3D-OPT-STM generation method is introduced in Section 4.2. 3D-OPT-STM models for three typical D-regions are generated in Section 4.3. The performance of the generated ST models is evaluated by Nonlinear Finite Element Analysis (NLFEA) simulations. In Section 4.4, the three factors of the 3D STM are investigated by adopting the generation method. Finally, the conclusion of this chapter is given in Section 4.5.

4.2. AUTOMATIC GENERATION METHOD FOR THREE-DIMENSIONAL OPTIMIZATION-BASED STRUT-AND-TIE MODELS

In this section, a generation method is proposed to automatically generate 3D-OPT-STM models, which forms a generalization of our previously proposed method limited to 2D cases [151]. The proposed method comprises three steps: 1. Compliance minimization-based 3D TO, 2. Topology extraction, 3. STM-based shape optimization. The optimized material layouts for various design problems can be obtained in the TO phase. Next, in the topology extraction phase, the obtained 3D TO results are transformed to truss-like structures which comprise a network of connected straight bars. Because the extracted truss-like structures are usually unstable structures, 3D beam elements are used to analyse their force distributions. In order to satisfy the requirement of axial force equilibrium for STM analysis, 3D shape optimization is conducted for the truss-like structures to generate adequate ST models in the last step. The flow chart of the proposed method is presented in Figure 4.1. The extensions and improvements of each step are presented in following sub-sections.

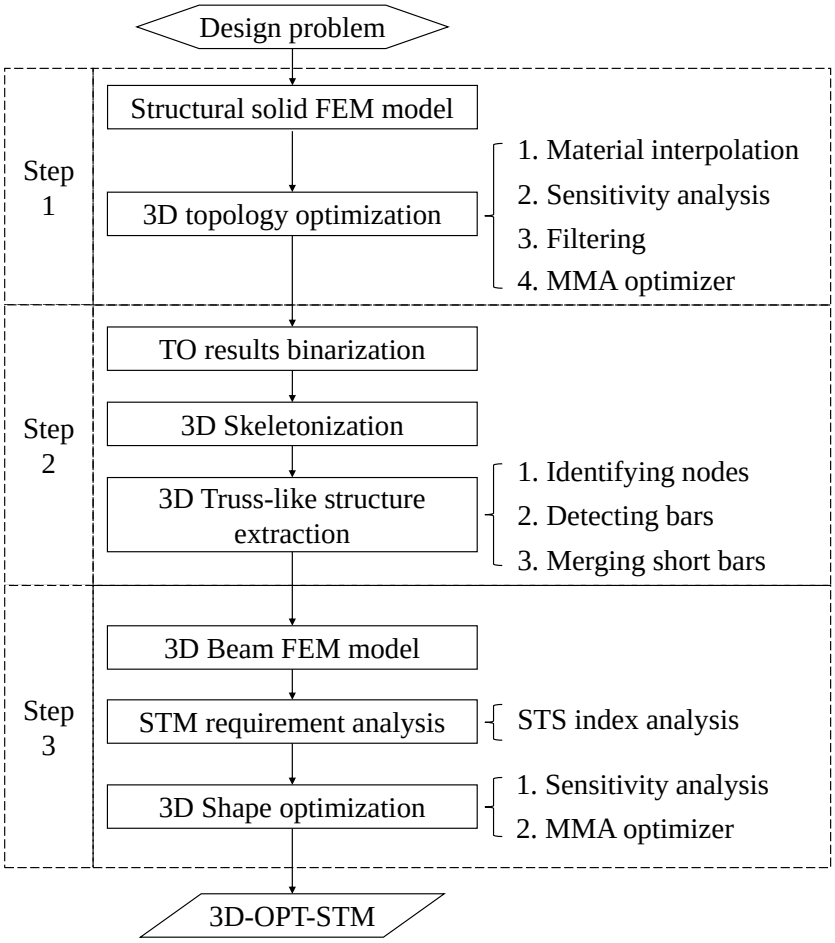

Figure 4.1: Flowchart of the 3D-OPT-STM generation method

4.2.1. STEP 1: 3D TO OPTIMIZATION

Topology optimization provides numerical material distributions for conceptual designs without specific shapes. Various methods and applications of TO methods have been reported after the initial work by Bendsøe and Kikuchi [21]. In this research, we apply the classical and popular SIMP (solid isotropic material with penalization) method [22] for the compliance minimization problem. The adopted SIMP method for 3D problems is a natural extension of our previous 2D work [151], where the SIMP parameter settings were introduced and their influences to the generated ST models have been discussed. For compactness of the research, only the modifications to apply the TO method in 3D are presented. For further details, readers are referred to Xia et al. [151] and the book by Bendsøe and Sigmund [22].

Table 4.1: Computation time by adopting three measures individually and jointly (s)

Mesh	Without measures	Parallel assembling	PCG method	Reducing redundant DOFs	With three measures
$10\times10\times10$	1.17	0.59	0.95	0.93	**0.29**
$20\times20\times20$	69.36	10.10	63.95	61.33	**3.02**
$30\times30\times30$	784.56	129.49	689.03	652.28	**27.81**

Compared to the TO procedure in 2D, the design structure (or full domain) is discretized by trilinear hexahedral structural finite elements for implementation convenience and numerical efficiency. The computational cost of 3D FEM analysis combined with iterative optimizations needs to be considered. In order to conduct the TO process within reasonable time, additional measures are taken. In assembling the global stiffness matrix $\boldsymbol{K}$, because the components in the matrix are calculated independently and individually, the assembling process can be programmed in a parallel manner [123], making use of multiple processing cores. For solving the governing equation ($\boldsymbol{K}(\boldsymbol{\rho})\boldsymbol{u}(\boldsymbol{\rho})=\boldsymbol{f}$, where $\boldsymbol{\rho}$, $\boldsymbol{u}$ and $\boldsymbol{f}$ indicate element densities, nodal displacement and nodal force respectively), the preconditioned conjugate gradient method is adopted to iteratively solve this large, sparse linear system of equations. In this way, the required random access memory (RAM) can be significantly reduced for 3D FEM analysis in comparison to matrix factorization that was applied in 2D. The efficiency of applying the iterative solvers in the TO process has been discussed by Amir and Sigmund [13]. Finally, the dimension of the global stiffness matrix $\boldsymbol{K}$ is reduced during the optimization process. The degrees of freedom (DOFs) that are solely linked to void elements ($\rho_i = 10^{-4}$) are detected. A small number is used as the void density in TO to prevent singularity of the system matrix without affecting the TO result. The components $\boldsymbol{K_i}$ associated with these detected DOFs are eliminated in $\boldsymbol{K}$, which also speeds up the topology optimization process.

In order the verify the effectiveness of these measures, the computation time of analyzing 3D FEM models of various meshes are presented in Table.(4.1). Without these measures, the computation time increases exponentially. Each measure improves the computation performance, and the most efficient procedure is obtained by adopting all of them. In the case of $30\times30\times30$ elements, the computation time of adopting three measures is reduced to 3.5 % of the original one.

4.2.2. STEP 2: TO EXTRACTION

The obtained TO results (voxel meshes and densities) of Step 1 cannot be directly used for defining ST models. Postprocessing steps are usually required to convert TO results into required models for manufacturing purposes [90]. For a review of 2D TO extraction techniques, the reader is referred to our previous research [151]. For 3D TO results, CAD-friendly models were extracted from TO results in Cuillière et al. [44] and Yin et al. [158]. None of these methods is dedicated to, or suited for, obtaining ST models. In

order to address this gap, in our previous study [151], an automatic extraction method was developed to convert 2D TO results into truss-like models. In this section, the extraction method is extended and improved to generate truss-like models in the 3D setting.

The TO extraction method includes three substeps (Step 2 in Figure 4.1). The obtained TO densities show intermediate values. By setting a threshold value (0.1), all densities larger than this value are set to 1 and the remainder is set to 0. In this way, the noise in the thinning process by the intermediate densities is avoided. The densities are transformed into binary data for the subsequent skeletonization step.

Based on the binary density and voxel mesh information, the raw TO results are simplified by a 3D digital thinning method. The thinning method reduces a large amount of TO data to a simple centerline pattern (skeleton) which preserves the topology. Based on the obtained skeleton, the subsequent truss-like model identification step can be implemented effectively. The pattern-based thinning method in our previous 2D work Xia et al. [151] cannot be extended to 3D, since the prescribed patterns are not able to describe all elimination conditions in 3D while preserving topology. In this research, therefore the 3D thinning method developed by Lee et al. [81] is adopted. The invariance of the Euler characteristic and the preservation of the connectivity are considered in 3D thinning. The Euler characteristic refers to the number of connected objects, holes and cavities, which quantifies the topology of a given voxel model (Figure 4.3a). The obtained skeleton must have the same Euler characteristic as the original voxel model to preserve the topology. The thinning method iteratively eliminates border voxels until obtaining a one-voxel width skeleton. A skeleton of a table-like model after the thinning process is shown in Fig(4.2). Note that, the loaded and support points in our study are taken as unremovable voxels; they remain the same in generated ST models.

The truss-like model consists of a 3D network of nodes and connected bars. The extraction procedure in our previous 2D work is not suitable for 3D conditions. The previous extraction method may lead to overly complex 3D skeletons containing superfluous members. In this research, a new procedure is proposed to extract 3D truss-like structures. In the procedure, the nodes of a 3D truss-like model are first identified, next their connections (i.e. the bars of the truss-like model) are determined, and finally short bars are removed to avoid difficulties in later STM shape optimization. While these general steps are similar to the 2D version [151], there are important differences in the details as described below.

The nodes of a 3D truss-like model are identified based on element-wise detection of skeleton voxels. Each 3D skeleton voxel is surrounded by 26 neighbouring voxels. If the number of solid neighbouring voxels is larger than 2, this skeleton voxel is taken as a node (see in Figure 4.3a). Different from the procedure in our 2D work, clustered nodes are allowed in a small region. They will be removed in a following merging step while preserving the topology. After determining the nodes, the presence of direct connections via the skeleton indicates the bars of a truss-like model. In order to identify these connections, a 3D recursive detecting method is proposed, because the complexity of 3D topologies makes our previous 2D connection identification process infeasible. The method node-wisely takes every identified node as the starting point for a connecting

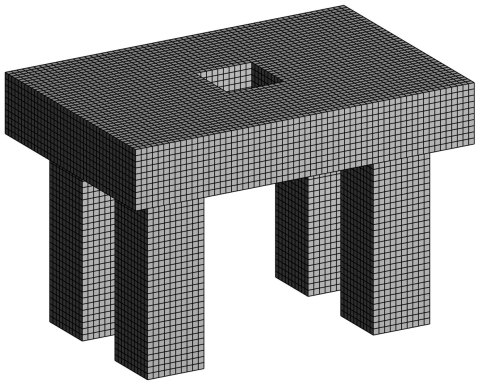

(a) The original model

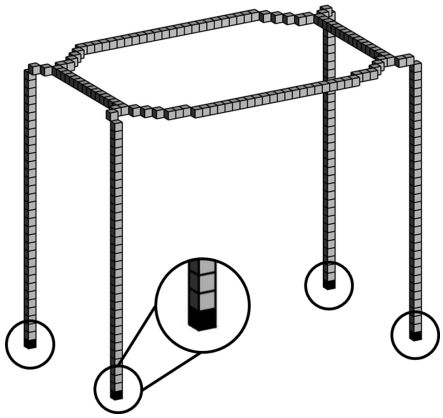

(b) Thinning skeleton (black voxels within circles are the prescribed unremovable members)

Figure 4.2: The thinning process applied to a table-like model

bar. By tracing the skeleton via the 26 neighbouring voxels of each visited voxel, a path along the skeleton to another identified node can be found, which is taken as the bar end point (see in Figure 4.3b). Therefore, a bar of a truss-like model can be created by a straight line connecting the identified start and end nodes. The initial generated truss-like model may have various short bars which are impractical and insignificant for the ST model. Therefore, a merging method is proposed to eliminate these short bars. In the method, a minimum length is set to check all bars. If the bar length is smaller than the prescribed value, the short bar and its end nodes are replaced by a new node at its center location. Based on the proposed extraction method, a truss-like model of the table-like model (Figure 4.2) is generated, as shown in Figure 4.4. The robustness of the proposed procedure is demonstrated by various case studies in the later sections.

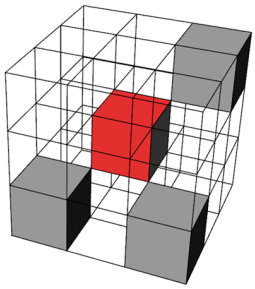

(a) Candidate voxel and its 26 neighbouring voxels. Red and grey cubes indicate candidate voxel and neighbouring skeleton voxels respectively, which here renders the candidate voxel as a node.

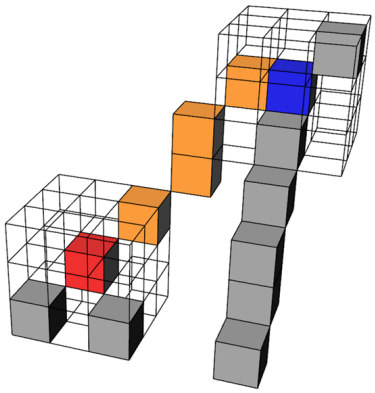

(b) Detecting node connections. Red and blue cubes indicate end nodes of a bar. The orange cubes indicate direct connection via skeleton voxels. The remaining grey cubes indicate other skeleton voxels.

Figure 4.3: Process of identifying nodes and their connections for the generation of a 3D truss-like model from a voxel-based skeleton

4.2.3. STEP 3: STM SHAPE OPTIMIZATION

The STM method is a truss-analogy based method: axial force equilibrium is necessary. The importance of the satisfaction of axial equilibrium has been demonstrated in Xia et al. [151]. Since the generated truss-like structures from the previous phase are usually statically and kinematically unstable structures, their equilibrium forces cannot be calculated through truss analysis [152]. In this research, 3D beam elements with high slenderness (height/length = 10^{-3}) are used to calculate the equilibrium forces of the generated truss-like structures. Although equilibrium forces are obtained with beam analysis, the existence of non-marginal shear forces does not satisfy the requirement of the STM method. Thus the generated truss-like structure cannot be used as a Strut-and-Tie model without obtaining a pure axial force equilibrium. In order to obtain a suitable model, a 3D shape optimization method is introduced in this section.

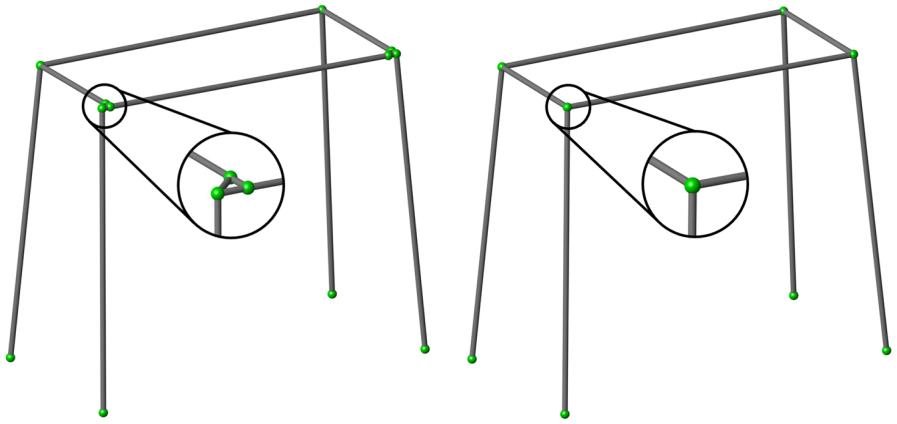

(a) The initial model without merging short bars. The short bars are indicted in circles.

(b) The refined model after merging short bars. The minimum length for merging is taken as 5 voxels.

Figure 4.4: The generated truss-like models generated by the proposed extraction process based on the table-like model (see in Figure 4.2)

In the shape optimization, the node positions of the generated truss-like structure are adjusted to optimize the structure. The mathematical formulation of this shape optimization is shown as:

$$\begin{aligned} \text{minimize: } & C(\boldsymbol{x}) = \boldsymbol{f}^{\mathrm{T}}\boldsymbol{u}(\boldsymbol{x}) \\ \text{subject to: } & \boldsymbol{K}(\boldsymbol{x})\boldsymbol{u}(\boldsymbol{x}) = \boldsymbol{f} \\ & \mathrm{STS} \geq 1-\varepsilon \\ & L(\boldsymbol{x}) \geq L_{\min} \\ & \boldsymbol{x}_{\min} \leq \boldsymbol{x} \leq \boldsymbol{x}_{\max} \end{aligned} \tag{4.1}$$

where $\boldsymbol{x}$ is a vector containing the coordinates of the nodes of the generated truss-like structure, which are used as optimization variables. C, $\boldsymbol{f}$, $\boldsymbol{u}$ and $\boldsymbol{K}$ here represent the compliance, nodal forces, nodal displacements and the stiffness matrix based on the beam finite element model.

There are two more considerations in the shape optimization: the axial equilibrium force state and the minimum bar length. They are considered through the constraints in the optimization process. Firstly, the Suitable Truss Structure (STS) index is a dimensionless number which indicates the closeness of a beam structure to a pure axial force equilibrium state [152]. For a structure consisting of 3D beam elements, STS is given as:

$$\mathrm{STS} = \frac{1}{n}\sum_{e=1}^{n}\frac{|N_{\mathrm{e}}|}{|N_e| + \sqrt{V_{e,1}^2 + V_{e,2}^2}}, \tag{4.2}$$

where, N_{e} is the element axial force, V_{e} indicate the element shear forces in two orthogonal transverse directions, and n is the number of elements. STS = 1 indicates that a pure

axial force equilibrium state is obtained for a specific beam structure. Since shear forces are inevitable in the beam analysis, in this chapter, a tolerance $\varepsilon = 0.05$ is used to relax the STS requirement in the optimization process. Secondly, in the inequality constraint $L(\boldsymbol{x}) \geq L_{\min}$, $L_{\min}$ is the given minimum bar length to avoid short bars. $L(\boldsymbol{x})$ measures the minimum length of all bars. Different from the previous 2D method, this constraint prevents the generation of short bars which would lead to convergence difficulties. By using a p-norm formulation, the measure of the minimum bar length is calculated as:

$$L(\boldsymbol{x}) = 1 / \left[\sum_{e=1}^{n} \frac{1}{(L_e)^p} \right]^{\frac{1}{p}}, \tag{4.3}$$

where L_e indicates the element length and n is the number of elements and the exponent is set to $p = 10$. The continuous minimum length constraint facilitates solving the STM shape optimization problem using gradient-based optimizers.

The shape optimization problem given in Eq.(4.1) is solved using the gradient-based Method of Moving Asymptotes (MMA) [135]. Central finite differences are used to calculate sensitivities. The perturbation is taken as 0.1 % of the mesh size of the continuum elements. In order to ensure robust convergence of the nonconvex shape optimization problem, a move limit of 50 % of the mesh size of the continuum elements is imposed on the optimization variables. Moreover, with the shape optimization, the structural compliance is further improved by correcting the differences caused by simplifying TO continua to discrete structures.

In order to briefly illustrate the effectiveness of the shape optimization, two simple cases are presented as shown in Figure 4.5. The first case (Figure 4.5a) is topologically a line with a helical shape under compression. The resulting STS index is 0.42. After the 3D shape optimization, as expected, a straight structure (Figure 4.5b) is obtained that carries the load by axial compression. The STS index of the optimized structure is 0.99 after 51 iterations. The second case (Figure 4.5c) is an irregular planar frame with two vertical forces and two hinges at two bottom points. It is a modification of a classical ST model (see Schlaich and Schafer [121]) by shifting all members and adding redundant nodes. The STS index of this structure is 0.73. After 25 shape optimization iterations, the optimized model (Figure 4.5d) results in STS=0.98 and it has a similar shape as the classical ST model. Since the shape optimization involves a computationally inexpensive beam model, the whole optimization process takes less than a minute.

4.3. THREE-DIMENSIONAL OPTIMIZATION-BASED STRUT-AND-TIE MODELS FOR THREE TYPICAL D-REGIONS

In this section, the proposed generation method is applied to three typical D-regions: a four-pile cap, a corbel and a box girder. Apart from the generated 3D-OPT-STM models, also three manually created ST models are considered. In all cases the strength of the struts is verified and the strength of the ties is ensured by providing sufficient reinforcement in the direction of the ties. The capacities of the 3D nodal zones are considered as sufficient. In order to demonstrate the effectiveness of the generated 3D-OPT-STM

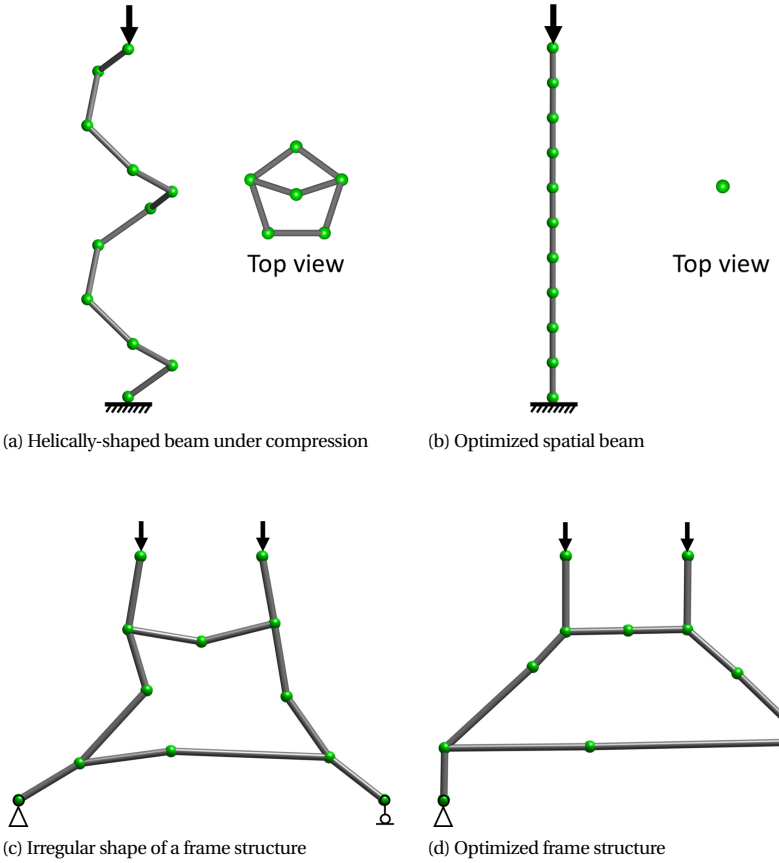

(a) Helically-shaped beam under compression

(b) Optimized spatial beam

(c) Irregular shape of a frame structure

(d) Optimized frame structure

Figure 4.5: Two simple cases and resulting structures after the 3D shape optimization

models, the STM designs are simulated by NLFEA to obtain structural performances, in particular load-displacement curves and insight in structural failure modes.

In NLFEA, nonlinear phenomena, such as the cracking and crushing of concrete and the yielding and rupturing of steel, are considered. The simulation results include the loading capacities and failure modes, which are used to evaluate the ST models. In the NLFEA models, we assume that reinforcement bars are located corresponding to the ties in the ST model and their cross sections are based on full utilization of the yielding stress at the design load. A similar solution strategy of NLFEA is used in our previous work [151] for 2D ST models. The embedded truss elements are used for rebar, assuming perfect bonding with concrete. The Hordijk model and the parabolic model are used to present the tensile and compressive behaviour of concrete respectively, and thhe rotating smeared crack model is adopted to indicate the crack initiation [20]. In this research, 20-node quadratic solid elements are used. The concrete has a mean

Table 4.2: Concrete properties

Mean compressive strength:	$f_{cm} = 30$MPa
Mean tensile strength:	$f_{ct} = 2.896$MPa
Fracture energy:	$G_F = 0.135$N/mm
Compressive fracture energy:	$G_C = 33.662$N/mm
Young's modulus:	$E_c = 31008$MPa
Poisson ratio:	$\nu = 0.15$

compressive strength of 30 MPa and its derived properties are given in Table (4.2). The steel has a yield strength of 580 MPa without hardening effects and ruptures at a strain of 10 %. The Young's modulus and Poisson ratio of steel are 200 GPa and 0.3 respectively.

The structural efficiency is defined as the ratio between load capacity and steel usage. Finally, the steel usage, analyzed structural performances and structural efficiency between the generated 3D-OPT-STM models and manual created ST models are compared.

4.3.1. FOUR-PILE CAP CASE

Reinforced pile caps are widely used in bridges to transfer loads from piers to the pile foundation. They are common structures and previous studies have also proposed ST models for them. Here we first consider this case to verify that the proposed method generates a suitable and high-quality ST model. Subsequently, in Section 4.4.1, with our systematic generation method, we explore ST models of a wide range of pile caps with different aspect ratios.

The geometry and load conditions of the evaluated four-pile cap case are shown in Figure 4.6. In the figure, L, W and H indicate the length, width and height of the structure respectively. In the considered model, the structure is subjected to a concentrated load of 700 kN and supported with 4 ball joints.

Figure 4.7 illustrates the various steps of the generation method of obtaining the 3D-OPT-STM for this case. The FEM model of the design problem is presented in subfigure (a), with a mesh size of 12 mm and 62500 solid elements. Concrete material properties are used: the Young's modulus is 30 GPa and the Poisson ratio is 0.2. In the TO process, only linear finite element analysis is conducted. A volume constraint of 5 % and a filter radius of 250 mm (2.5 × (mesh size)) are adopted. The binary TO result is presented in subfigure (b). The skeleton after the thinning process and the truss-like structure after the identification process are shown in subfigure (c) and subfigure (d) respectively. The obtained 3D-OPT-STM is shown in subfigure (e) with an increase of STS index from 0.77 to 0.99, which is close to a pure axial force equilibrium state. In this case, by using a PC with an Intel Core 4 3.5 GHz processor and 16 GB memory, the overall computational time is about 40 minutes. The 3D TO step uses about 95 % of the total time, the extraction step is the second-most expensive step and followed by the shape optimization, which takes less than 1 minute, but offers crucial improvements that enable the use of the generated model in the STM method. Based on 3D-OPT-STM, the force diagram can be

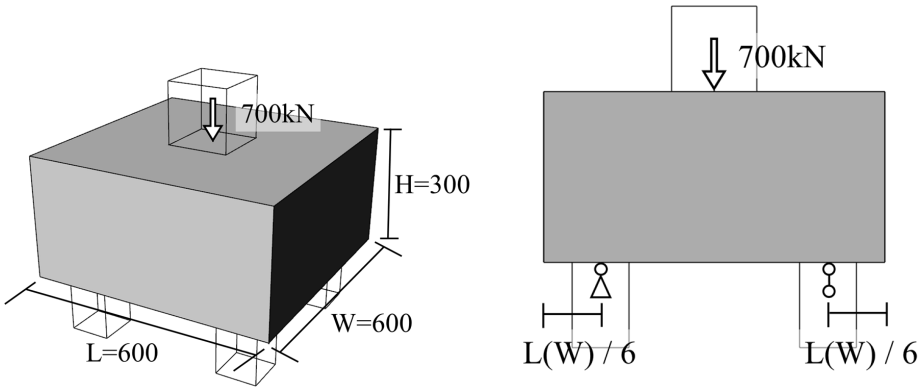

(a) Axial view (mm)

(b) Left-side view

Figure 4.6: Geometry, load and supports of the four-pile cap

calculated as shown in subfigure (f). It can be used for the subsequent STM analysis.

In this research, a manually created ST model is used for comparison, which is similar to the models in Dey and Karthik [45], Souza et al. [129], Yun et al. [165], as shown in Figure 4.8. It has the same node positions as the generated 3D-OPT-STM, but a different topology, and results in an STS index of 0.98. Based on the obtained tensile forces, bar lengths and steel yielding strength (580 MPa), the required steel according to the two ST models can be calculated.

In order to gain further insight into the structural performance of these two ST models, two NLFEA models are created and analyzed to obtain their structural performances. The NLFEA model of the 3D-OPT-STM design for the four-pile cap is shown in Figure 4.9. A nodal displacement of 0.1 mm for a single load step is applied vertically on the top steel plate. Four steel plates are used to support the cap. For the steel plates, a linear material model is adopted. Similarly, the analysis model of the manually created ST model was created by modifying the rebar while the concrete remained unchanged.

Based on NLFEA results, load-displacement curves of these two STM designs based on the NLFEA results are shown in Figure 4.10. In these, the displacement is measured vertically at the middle-bottom point of the cap. The 3D-OPT-STM model results in a peak load of 876.6 kN and the classic ST model leads to a peak load of 830.1 kN. Both peak loads are larger than the design load (700 kN). In the figure, Point A indicates the onset of cracking, and Point B and C indicate the steel yielding of the 3D-OPT-STM model and the classic ST model respectively. It is observed that both structures fail due to steel rupturing.

Based on the generated ST models, the steel ratio of the generated 3D-OPT-STM and the manually created ST model are both equal to 0.39 %. Although the topologies are different, they lead to the same steel ratio in this case. In Blévot and Frémy [27] and Clarke [40], the similar performance of these two designs was observed in their experiments. By comparing the ratio of peak load and steel usage, 2.081 N/mm^3 and 1.971 N/mm^3 for the

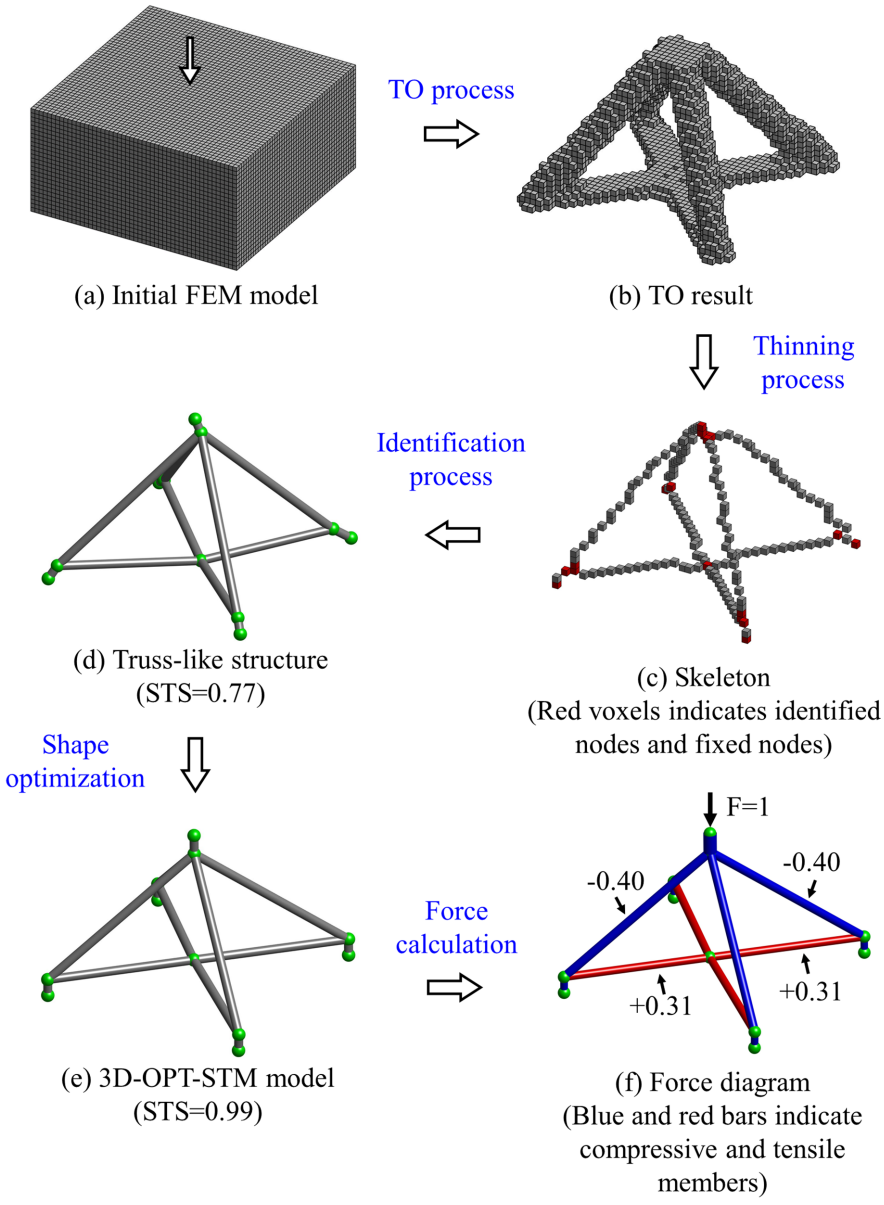

Figure 4.7: Processes figure of obtaining the 3D-OPT-STM model of the four-pile cap

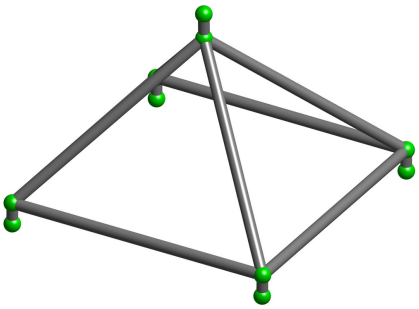

Figure 4.8: The manually created ST model

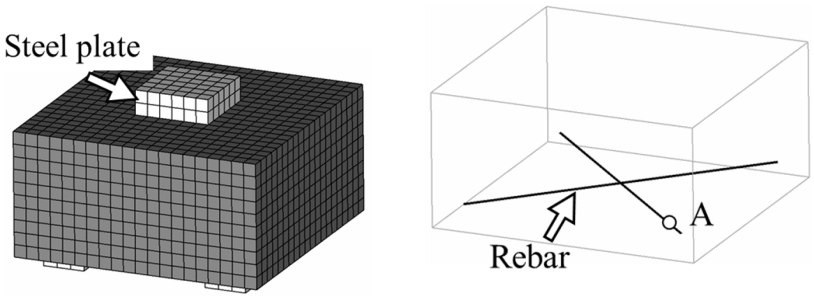

(a) Finite element model (b) Rebar location

Figure 4.9: NLFEA model of the 3D-OPT-STM design of the four-pile cap. Point A indicates the yielding point of steel.

3D-OPT-STM and classic model respectively, more efficient steel usage is observed in the 3D-OPT-STM design. In a later section (Section 4.1), further investigations on applying the generation method for the four-pile cap with various geometrical parameters are presented.

4.3.2. CORBEL CASE

Reinforced concrete corbels are common D-regions used in building structures to support floors or precast beams. Here we first verify the proposed method to generate a suitable ST model for this case. In addition to the plane load conditions, corbels may be loaded in out-of-plane direction, which will be studied in Section 4.4.2 as well. For this research, the FEM model and structural conditions of the evaluated corbel are shown in Figure 4.11. The corbel is fixed at the top and bottom ends and a concentrated load of 300 kN is applied. The FEM model consists of 14337 solid elements with a mesh size of 33 mm. Similar as for the four-pile cap case, concrete material properties are used.

In the TO process, the corbel is optimized with a 10 % volume constraint and a 49.5 mm filter radius (1.5 × (mesh size)). After 107 TO iterations, the TO result of this corbel case is shown in Figure 4.12a. The resulting 3D-OPT-STM is obtained after 26 shape optimization iterations and is shown in Figure 4.12b. The STS index has increased from

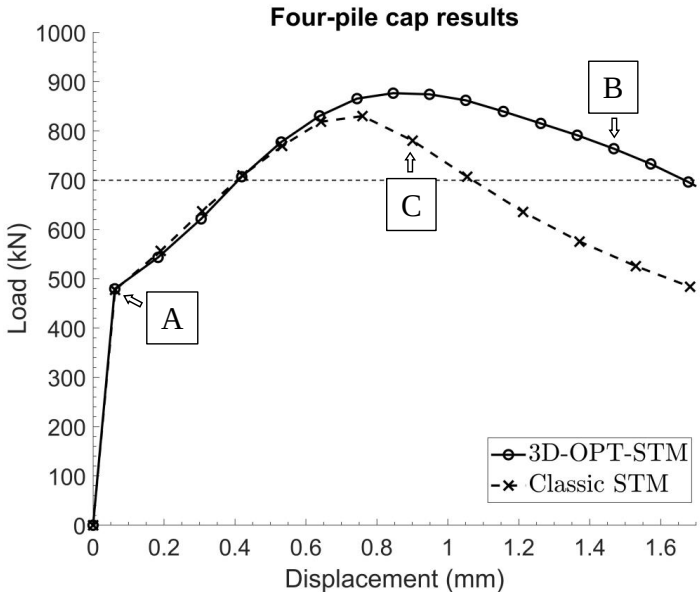

Figure 4.10: Load-displacement results of the 3D-OPT-STM design and classic STM design of the four-pile cap.

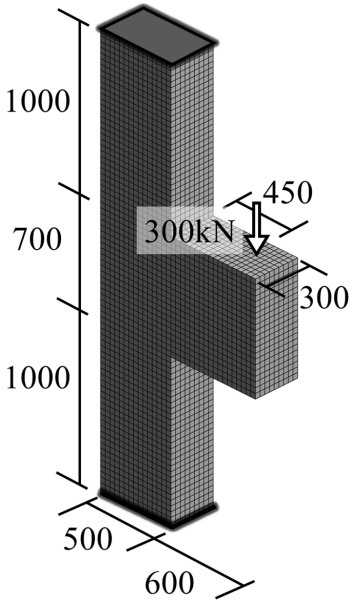

Figure 4.11: The FEM model of the corbel case (mm)

0.84 to 0.97. Based on the calculated tensile forces and steel yielding strength (580 MPa), the required steel ratio of this corbel is 0.18 %. The overall computational time of this case is about 10 minutes. Similar as for the four-pile cap case, the TO step accounts for 95 % of the computational time.

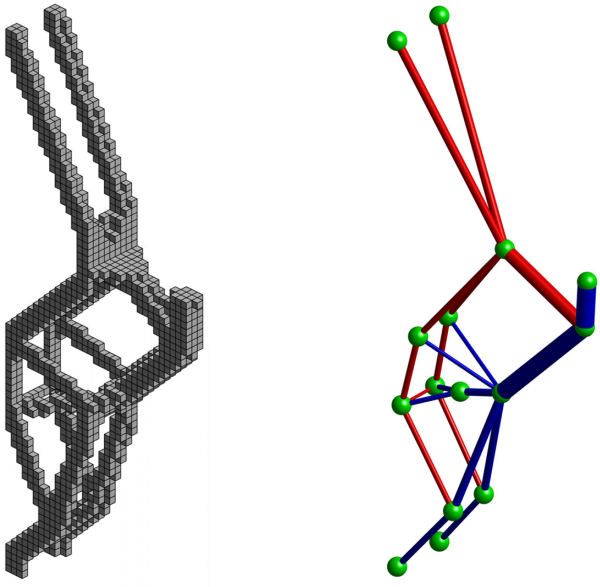

(a) TO result (b) 3D-OPT-STM model

Figure 4.12: Generation results of the corbel case. Red and blue bars indicate tensile and compressive members respectively. The bar width indicates the force magnitude.

In Figure 4.13a, an ST model based on a two-dimensional model by Schlaich et al. [122] is manually created for this corbel case. This manually created ST model is formed by a stable truss and results in an STS index of 1. The calculated equilibrium forces are presented in Figure 4.13b, and this design leads to a required steel ratio of 0.22 %. Compared to the manually created ST model, the 3D-OPT-STM design has a steel ratio of 0.18 % and thus results in a reduction of 0.04 % (percentage points of steel ratio) of steel usage and offers a more economical design. This corresponds to a relative reduction of 18 %.

Corresponding NLFEA models of these two ST models are created. The NLFEA model of the 3D-OPT-STM design for the corbel is shown in Figure 4.14. A nodal displacement of 0.1 mm for a single load step is applied vertically on the steel plate. The corbel is fixed at the top and bottom surfaces. The model for the classic STM design is created by modifying the rebar.

The resulting load-displacement curves are shown in Figure 4.15. The displacement is measured at the middle-bottom point of the outer end of the corbel. Based on the NLFEA results, the peak loads of the 3D-OPT-STM model and the classic ST model are

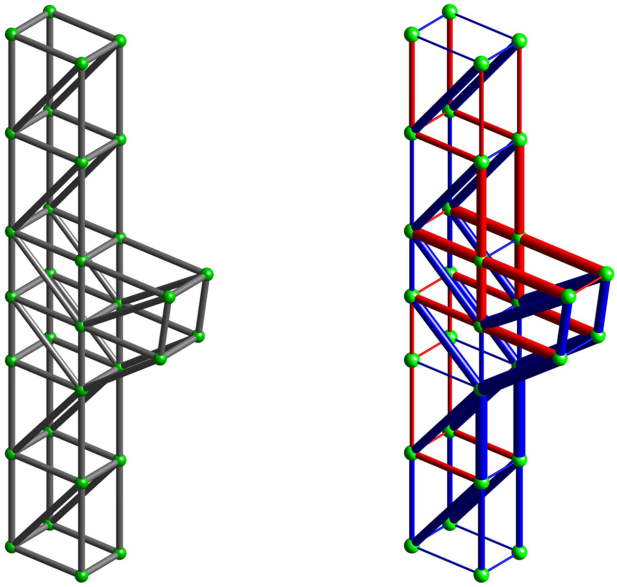

(a) ST model (b) Force diagram

Figure 4.13: The manually created ST model of the corbel. Red and blue bars indicate tensile and compressive members respectively. The bar width indicates the force magnitude.

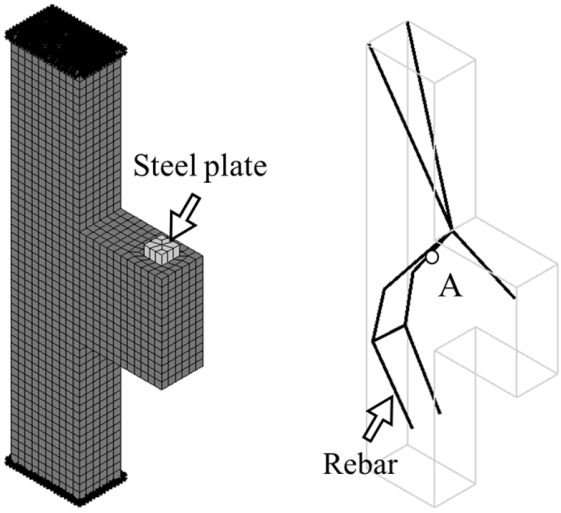

(a) Finite element model (b) Rebar location

Figure 4.14: NLFEA model of the 3D-OPT-STM design of the corbel. Point A indicates the yielding point of steel.

336.1 kN and 378.0 kN respectively. The ultimate capacity of both designs is larger than the design load (300 kN). The concrete starts cracking at Point A shown in Figure 4.15. The steel yields at Point B for the classic ST model, and at Point C for the 3D-OPT-STM model. Both designs exhibit steel rupturing in the final stage. Although the classic STM design results in a larger peak load, by comparing the ratio of peak load and steel usage, 0.342 N/mm^3 and 0.319 N/mm^3 for the 3D-OPT-STM and classic model respectively, a more efficient steel usage is observed in the 3D-OPT-STM design.

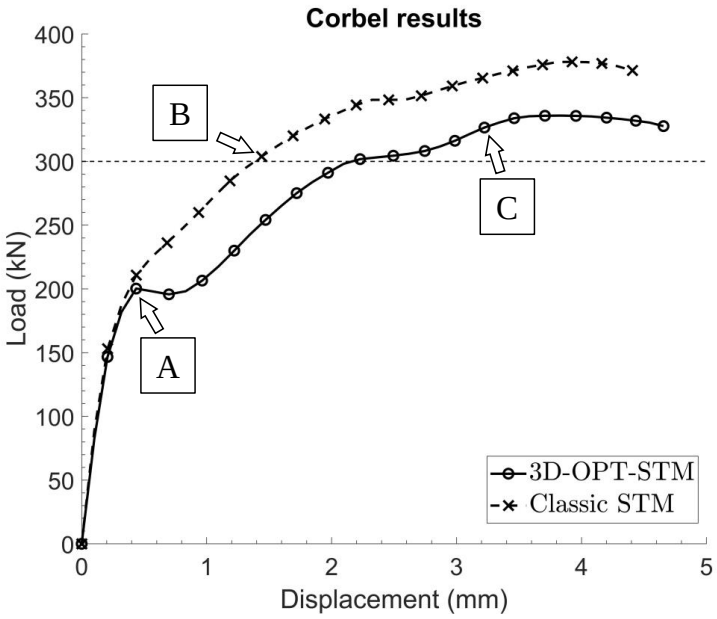

Figure 4.15: Load-displacement results of the 3D-OPT-STM design and classic STM design of the corbel.

4.3.3. BOX GIRDER CASE

Box girders are often used in bridge structures. Compared to common I-shape or H-shape beams, box girders provide larger load resistance capability, especially in resisting torsion. There is no standard ST model available for this fully 3D case. Firstly, the effectiveness of the proposed method is verified through the generated ST model. Subsequently, the influence of complex load combinations (in Section 4.4.2) and load discretization (in Section 4.4.3) for the ST models are explored for the box girder based on the proposed method. The FEM model of an evaluated box girder is shown in Figure 4.16. The box girder is subjected to 9 concentrated vertical forces of 300 kN, which represent a discretization of a uniformly distributed load on the top flange. The structure is constrained in axial direction at the end surface and is supported additionally by two ball joints. The FEM model has 118400 solid elements with a mesh size 50 mm and has the same concrete material properties as the four-pile cap case.

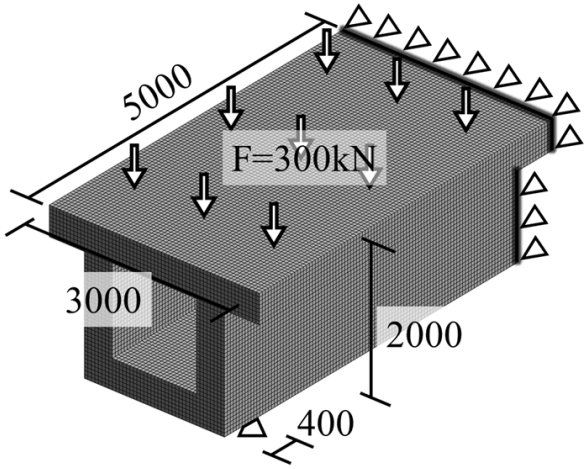

(a) Axial view

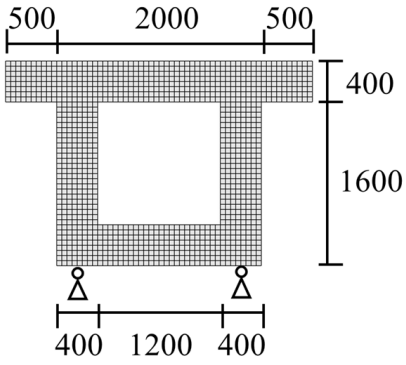

(b) Front view

Figure 4.16: The FEM model of the box girder case (mm)

In the TO process, the box girder is optimized with a 10 % volume constraint and a 125 mm filter radius (2.5 × (mesh size)). After 134 TO iterations, the TO result of this corbel case is shown in Figure 4.17a. The resulting 3D-OPT-STM is obtained after 57 iterations of the shape optimization and is shown in Figure 4.17b. The optimization procedure leads to an increase of the STS index from 0.77 to 0.98. Based on the calculated tensile forces and steel yielding strength (580 MPa), the required steel ratio of this box girder design is 0.175 %. The overall computational time of this case is about 250 minutes. In this case, the TO step accounts for about 95 % of the computational time.

As the manually created ST model for this box girder we use the spatial truss structure as shown in Figure 4.18a. The manually created ST model results in an STS index of 0.97. The calculated equilibrium forces are shown in Figure 4.18b. This STM design

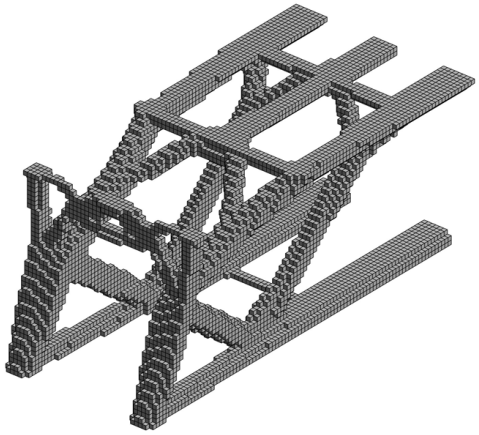

(a) TO result

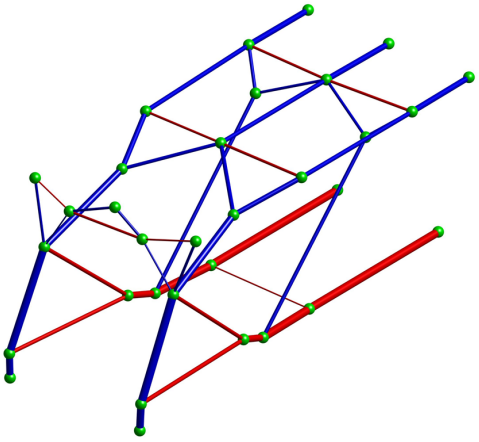

(b) 3D-OPT-STM model

Figure 4.17: Generation results of the box girder case. Red and blue bars indicate tensile and compressive members respectively. The bar width indicates the force magnitude.

leads to a steel ratio of 0.245 %. Compared to the manually created STM design, the 3D-OPT-STM design thus resulted in a reduction of 0.070 % of steel usage (percentage points of steel ratio). This corresponds to a relative reduction of 29 %.

The NLFEA model of the 3D-OPT-STM design for the box girder is shown in Figure 4.19. In this case, a vertical equally distributed load of 0.3 MPa is applied to the nine surfaces (200mm × 200mm) on the top. A similar NLFEA model is created for the manually created ST model by modifying the rebar.

Based on NLFEA results for the two ST models, load-displacement curves are presented in Figure 4.20, where the displacement is measured at the middle-bottom point at the free edge. In the curves, Point A indicates the initial cracking of concrete and Point B

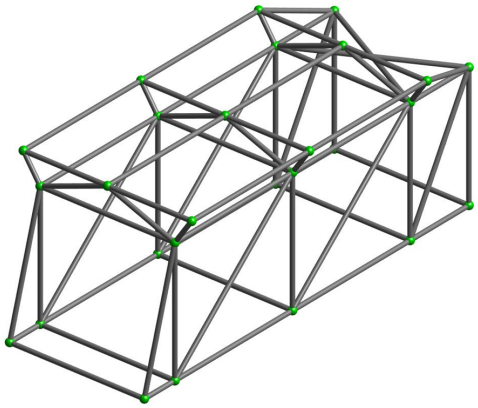

(a) ST model

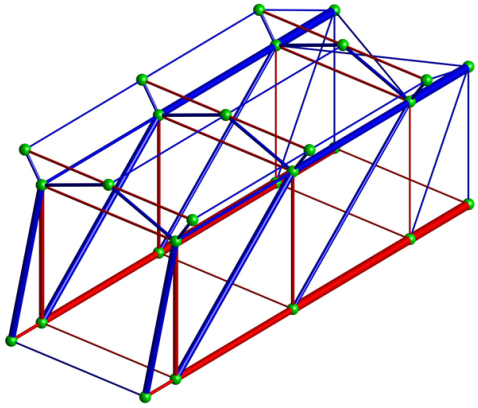

(b) Force diagram

Figure 4.18: The manually created STM of the box girder. Red and blue bars indicate tensile and compressive members respectively. The bar width indicates the force magnitude.

and C indicate the steel yielding points of the 3D-OPT-STM design and the manually created STM design respectively. Both models reach the design load level of 2700 kN. After obtaining the design load, the models indicate a rapid failure due to steel rupturing. The manually created ST model results in a slightly larger peak load, however substantially more steel is required. The ratios of peak load to steel usage of the 3D-OPT-STM and manual ST models are 0.114 N/mm^3 and 0.0775 N/mm^3 respectively. Also in this case, the 3D-OPT-STM design produces a more economical design than the manually created STM design. With these findings, the generation method can be considered capable of generating high-quality STM designs, in a practical timeframe.

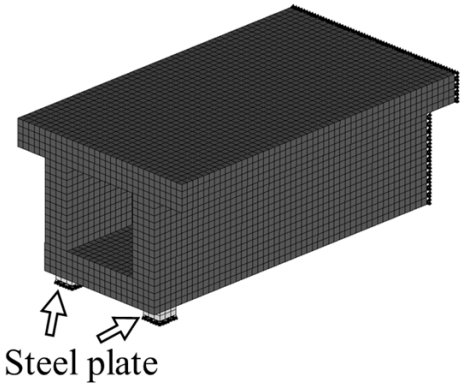

(a) Finite element model

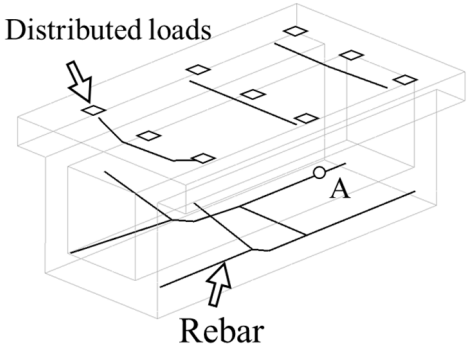

(b) Rebar location

Figure 4.19: NLFEA model of the 3D-OPT-STM design of the box girder. Point A indicates the yielding point of steel.

4.4. THREE IMPORTANT FACTORS IN GENERATING 3D STRUT-AND-TIE MODELS

The generated ST models will vary due to changes in input parameters and problem setting, such as the geometry of a specific case, the load conditions and the load discretization. Based on the proposed generation method, these factors can be investigated in a convenient and systematic manner. Here this capability is demonstrated for three different 3D cases. Firstly, various 3D-OPT-STM models are generated by varying geometrical parameters of the four-pile cap. The steel usage of the generated 3D-OPT-STM models is compared with that of classical ST models. Secondly, the load conditions influence TO results and consequently affect the generated 3D-OPT-STM models. Generating 3D-OPT-STM models considering alternative load conditions is investigated. Thirdly, load discretization is a prerequisite of the STM and affects the generated ST models. Therefore, the influence of the load discretization for the generated 3D-OPT-STM models is discussed.

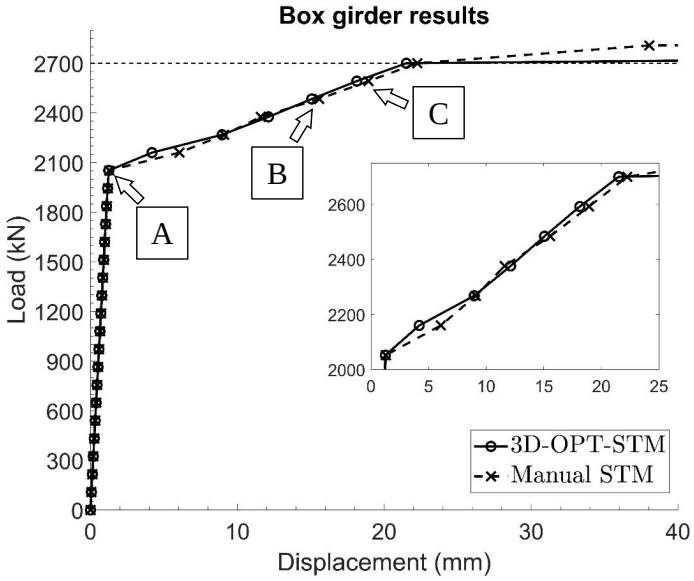

Figure 4.20: Load-displacement results of the 3D-OPT-STM design and classic STM design of the box girder.

4.4.1. PARAMETRIC INVESTIGATION FOR THE FOUR-PILE CAP

Four-pile caps with various geometries are used in practice. In this section, 25 3D-OPT-STM models are generated by adjusting the width and height of the four-pile cap, represented by (W,H) in Figure 4.6a. In the various models the length (L=600 mm) is fixed. The width and height are modified accordingly using 5 variations, as H/L=[2/6, 3/6, 4/6, 6/6,12/6] and W/L=[2/6, 3/6, 4/6, 5/6, 6/6] respectively. By varying these parameters, the span-depth ratio and plane shape of the cap are changed. The parametric settings of the evaluated case in Section 4.3.1 are H/L=3/6 and W/L=6/6.

Following the same generation process with the four-pile cap case (Section 4.3.1), the obtained 3D-OPT-STM models are shown in Figure 4.21. The required steel ratios for all 3D-OPT-STM designs are given. Accordingly, classical ST models are evaluated which have the same topology as the model shown in Figure 4.8. Comparing the required steel ratio of 3D-OPT-STM designs with classical STM designs, the differences are shown in Figure 4.21. The green and red numbers indicate the reductions and increases of steel ratios by applying the automatically generated 3D-OPT-STM designs respectively.

Based on the calculated steel ratios, we observe that by increasing the H/L ratio, which indicates a reduction of the span-depth ratio of the structure, the steel ratios reduce. By increasing H the internal level arm becomes larger, making the longitudinal reinforcement more efficient. For very large values of H, the results show a direct load transfer between the loaded point and supports. By reducing the W/L ratio, the load transfer is approaching a one-way system (i.e. beam action). Although the steel ratio increases, this is caused by the reduction in the structural volume, the total steel usage

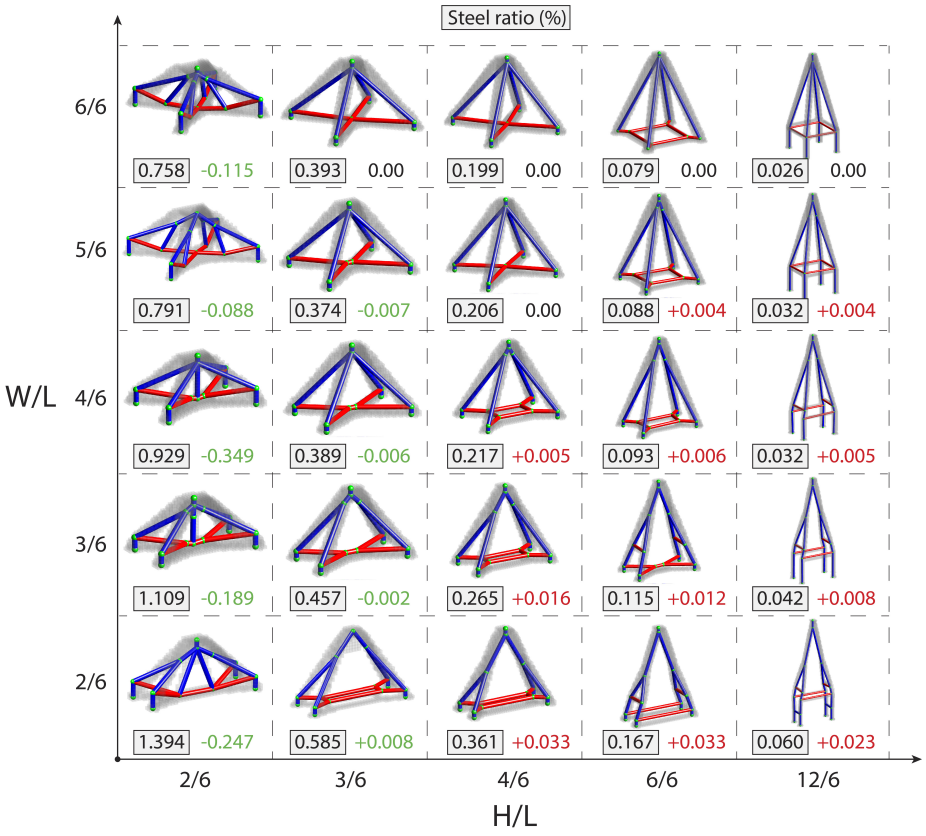

Figure 4.21: Generated 3D-OPT-STM models of various geometries. The grey voxels in each model indicate TO results. L, W and H indicate the length, width and height of the four-pile cap respectively. The numbers in the grey boxes indicate the steel ratio, in percent. Right of those, the green/black/red numbers indicate the difference (also in percent) compared to ST models with a classical topology given in Figure 4.8.

is reduced. Compared to classical ST models, the 3D-OPT-STM models reduce the steel usage in the situation of the larger span-depth ratios. In cases where the 3D-OPT-STM models have higher steel ratios, the differences are very small. In most cases, the 3D-OPT-STM models have a similar performance in terms of steel usage as the classical ST models.

Based on the obtained results, the best scenario in reducing steel usage is obtained in the model of (W/L,H/L) = (4/6,2/6). Compared to the classical ST model, the 3D-OPT-STM design results in a reduction of the steel ratio of 0.349 % (percentage points of steel ratio). Especially for low and wide pile caps, using the ST models generated by our method instead of the classical one leads to significant steel savings. Note also that the proposed generation method enables performing a parametric investigation in an automatic and convenient manner.

4.4.2. THE INFLUENCE OF COMPLEX LOAD COMBINATIONS

In practice, D-regions are subjected to various loads. The suitable ST model depends on the considered load combinations. Especially in the 3D setting classical 2D ST models are definitely not applicable for cases with loads in out-of-plane directions. Clearly, in such cases considering the full 3D situation is necessary.

In order to investigate the influence of the complex load combinations, two cases are studied. The first case is based on the corbel problem (Section 4.3.2), and a horizontal load is considered, as shown in Figure 4.22a. This load may come from the supported structures, such as bridge girders and crane beams. They transfer the horizontal load to the corbel. By using the same settings of the generation method as in the previous case (Section 4.3.2), the 3D-OPT-STM model is obtained as shown in Figure 4.22b.

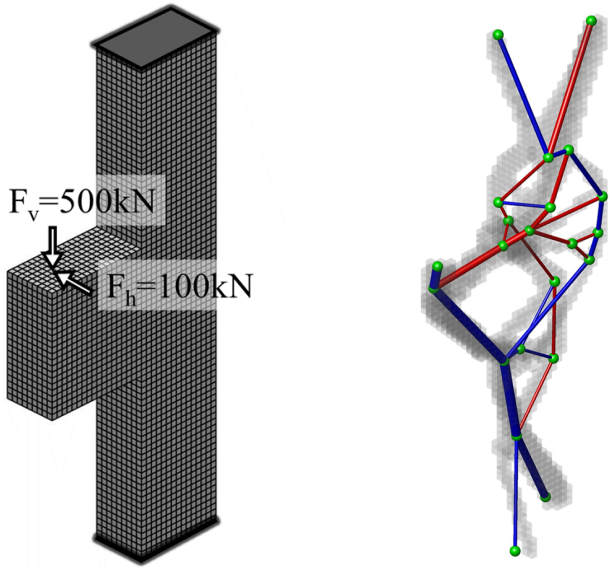

(a) Design problem (b) 3D-OPT-STM model

Figure 4.22: The corbel problem under complex load combination. The grey voxels indicate the TO results. Red and blue bars indicate tensile and compressive members respectively. The bar width indicates the force magnitude.

Compared to the 3D-OPT-STM model with one single load (Figure 4.12b), the model considering combined loads leads to an obviously different load transfer system. Although the obtained 3D-OPT-STM model has an irregular shape, it results in an STS of 0.97. The twisted shape of the obtained model is beneficial in resisting torsion caused by the horizontal force. The steel ratio based on this 3D-OPT-STM design is 0.239 % which is smaller than the single-load design (0.28 %). Apparently, with the right design less steel is required in the case with multiple loads, for this problem. However, more loads are transferred to the supports through compressive forces in struts. In this case, the corbel would fail by strut crushing under the combined load situation.

The second case is similar to the box girder problem (Section 4.3.3), as shown in Figure 4.23a. Here, two compressive forces are considered which represent applied prestressed tendons. The prestressed tendons are commonly used in box girders to improve structural service performance, such as reducing cracks and deformation. Similarly, based on the same generation settings with the single load problem, the generated 3D-OPT-STM model for the combined loads is shown in Figure 4.23b.

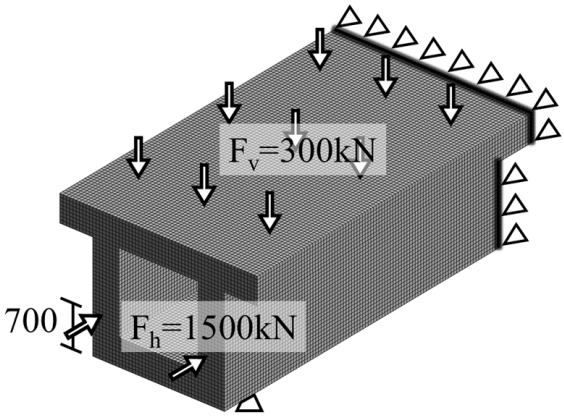

(a) Box girder problem

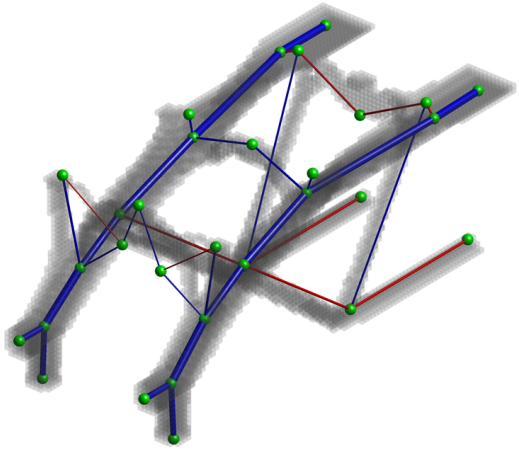

(b) 3D-OPT-STM model

Figure 4.23: The box girder problem under complex load combination. The grey voxels indicate the TO results. Red and blue bars indicate tensile and compressive members respectively. The bar width indicates the force magnitude.

The generated 3D-OPT-STM has a 0.98 STS index. Compared to the single-load 3D-OPT-STM model (Figure 4.17b), the load transfer system is different. Here the generated model has fewer tensile members. The loads are mainly transferred by compression through struts to the supports. The steel ratio based the generated model is 0.048 %

which is much lower than that of the single-load model (0.175 %). By applying the post-tensioned tendons, the required steel in the box girder is significantly reduced. However, if we account the steel usage of the prestressed tendon with the same yielding strength (580 MPa), the additional steel ratio of the tendon is 0.175 % and the total steel ratio is 0.223 %. This can be further improved by changing the position of prestressed tendons.

Based on the previous two cases, the effectiveness of the proposed generation method for complex combined loads has been demonstrated. The generated 3D-OPT-STM models under combined loads are different from the single-load models. In both cases the amount of reinforcement reduces, however this is not a general rule. The locations of steel reinforcement are clearly influenced by the presence of additional loads. Moreover, in these two cases, more compressive forces are obtained compared to the single-load situation. Therefore, the strut strength checking in the STM analysis becomes even more important.

In practice many loads and load combinations must be dealt with. In these cases, various 3D-OPT-STM models need to be generated. The proposed generation method facilitates the process in finding and exploring suitable ST models under various load situations, in limited time (up to a few hours for detailed models) and in an automated manner. Note that in the studied cases, all loads are assumed to occur simultaneously. For less predictable loads, such as earthquake or wind loads, a multi-loadcase formulation must be considered, which is an extension left for future research.

4.4.3. THE INFLUENCE OF LOAD DISCRETIZATION

Discrete loads are required in the STM. Different load discretizations affect the generated ST models and thus their performances. Especially in the 3D setting, the spatial distribution of discrete loads may have a significant influence on the generated ST models.

In order to investigate the influence of load discretization choices, three 3D-OPT-STM models of the box girder case (Section 4.3.2) are generated. In Section 4.3.2, the uniform vertical load is uniformly discretized into 3×3 concentrated loads of 300 kN. Now two more load discretization schemes are applied, 2×2 loads of 675 kN and 4×4 loads of 168.75 kN. The obtained TO results and 3D-OPT-STM models are shown in Figure 4.24.

The generated two 3D-OPT-STM models result in STS indices of 0.97. Based on the obtained tensile forces, the required steel ratio of three load schemes (2×2, 3×3 and 4×4) are 0.165 %, 0.175 % and 0.160 % respectively. In the 2×2 scheme the loads are aligned with the two webs of the box and the two supports. This results in a nearly 2D ST model. Similarly, the 2D-like performance is also observed in the model of the 4×4 scheme. The 3D-OPT-STM model of 3×3 scheme results in a slightly larger steel usage than the other two cases: additional steel in the top flange is required to transfer the load from the central loading points to both webs. The main tensile forces of three cases occur in the bottom flange, 1605 kN, 1593 kN and 1513 kN respectively, and their differences are small. However, the location and forces of the main c ompressive members are changed in these load conditions.

The proposed generation method enables fast and systematic exploration of the influence of various load discretization schemes. A suitable load discretization scheme

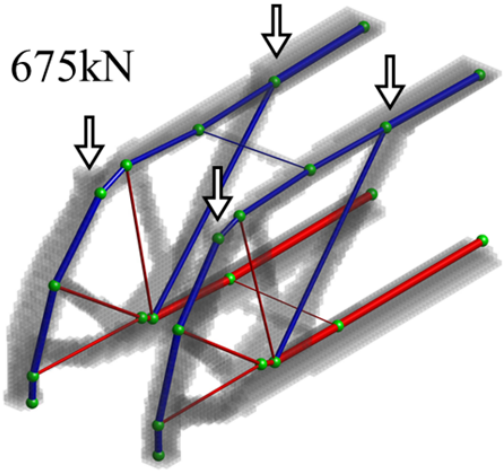

(a) 2×2 loads

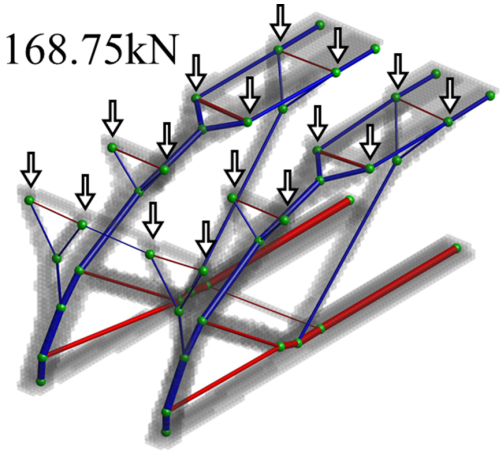

(b) 4×4 loads

Figure 4.24: Generated 3D-OPT-STM models of two additional load discretization schemes. The grey voxels indicate the TO results. Red and blue bars indicate tensile and compressive members respectively. The bar width indicates the force magnitude.

is required for a safe and robust STM design. In this box girder case, a more robust result would be obtained through the 3D-OPT-STM model with 3×3 discrete loads. It presents a more refined steel distribution on the top flange to resist the possible bending behaviour.

4.5. CONCLUSION

In this chapter, we propose a systematic method to automatically generate ST models in 3D. The proposed method integrates a topology optimization process, the topology extraction method and the shape optimization procedure to automatically generate suitable three-dimensional optimization-based Strut-and-Tie (3D-OPT-STM) models for the design of 3D D-regions. In the topology optimization, three measures (parallel matrix assembly, iterative solution techniques and removal of redundant DOFs) are combined to improve the computation efficiency. A new robust procedure is proposed to extract truss-like structures from 3D TO results. Subsequently, gradient-based 3D shape optimization is conducted to effectively obtain suitable 3D-OPT-STM models based on the extracted truss-like structures. Depending on the complexity of the model, within one or several hours an optimization-based ST model is produced.

Based on the proposed generation method, three 3D-OPT-STM models are generated for three typical 3D D-regions (four-pile cap, corbel and box girder) to demonstrate the effectiveness of the proposed method. Moreover, based on the generation method, three important factors in STM are discussed, including the parametric investigation for the four-pile cap, the influence of different load combinations and the load discretization. Based on the present investigation, the conclusion is summarized as follows:

1. The proposed method is effective in generating suitable 3D-OPT-STM models for 3D D-regions in an automatic manner. The generated and used ST models are simulated by NLFEA, and they are evaluated based on steel usage and the simulated structural performance. Compared to manually created ST models, the 3D-OPT-STM models were found to produce economically superior designs, especially for complex problems. It is reiterated that practical aspects, such as steel detailing and constructability were outside the scope of our study.

2. Parametric investigations can be conveniently conducted by the proposed method. It enables engineers to evaluate a larger range of design options, even at an early design stage. The change of the load transfer mechanism is observed through the generated ST models for different geometries.

3. The proposed method enables the systematic generation of valid 3D-OPT-STM models under different load conditions. Based on the obtained 3D-OPT-STM models, various load transfer systems are presented which can help the designer to conduct a more accurate STM analysis. In this study, all loads are assumed to occur simultaneously. In order to generate more robust and safer ST models, a multi-loadcase formulation is of interest for future research.

4. Load discretization schemes are important in 3D STM analysis and affect the generated 3D-OPT-STM models. A more robust design can be obtained by choosing a suitable load discretization. The suitability of various load discretization schemes can be readily and systematically studied by the proposed method.

5

PERSPECTIVES ON A SYSTEMATIC STRUT-AND-TIE MODELLING APPROACH

5.1. SUBJECTIVE CHOICES AND UNCERTAINTIES IN STRUT-AND-TIE MODELLING

In the past three decades, numerous investigations for STM have been conducted, aiming to develop a systematic D-region design approach. The intensive research has enabled the STM method to be widely applied. Many design codes have allowed STM methods to design D-regions. In addition, the STM method is not limited to the design of D-regions of reinforced concrete structures, and has been extended to analyze masonry structures [52] and reinforced concrete structures strengthened with carbon fibre-reinforced polymers [111]. Its simple implementation and the resulting safe designs are well-accepted advantages of the STM method. However, currently, it is still challenging for engineers to apply the STM method to more complex D-regions and D-regions under multiple load combinations. The current STM process involves a variety of human choices which are based on the designer's experiences and preferences. These subjective factors cause variations of the STM method and bring uncertainties to the STM analysis, thereby affecting the STM-based designs. There is a need to develop a systematic STM method which limits the subjective choices and uncertainties to a minimum. This will undoubtedly benefit the application of the STM method. In order to pave the path towards a systematic STM approach, in this section, the main sources of subjectivity and uncertainty are identified and directions for solutions are proposed and discussed.

The main steps of implementing the STM method (as introduced in Section 1.1.1) and a summary of important choices and uncertainties concerning the main steps are shown in Table 5.1. The detailed discussion of each item is provided in the following subsections. In Sections 5.2 and 5.3, two aspects of the identified uncertainties are investigated further. The first aspect concerns the generation of ST models considering multiple load combinations. The second one concerns the STM design considering different steel layouts to limit the construction complexity.

Table 5.1: Summary of the main steps and important uncertainties in the STM method

Step	Uncertainty
1. Preprocessing (Section 5.1.1)	- Load discretization - **Loading conditions** (Section 5.2)
2. Determining truss-analogy models (Section 5.1.2)	- Model generation - Suitability evaluation
3. Dimensioning and stress checking (Section 5.1.3)	- Member geometry - Effective strength
4. Designing steel layouts (Section 5.1.4)	- **Layout difference** (Section 5.3) - Performance influence

5.1.1. CHOICES AND UNCERTAINTIES IN PREPROCESSING

The design problem needs to specified and idealized, leading to a description of the mechanical problem. This step includes aspects, such as determining the geometry, loads and supports. Two main steps are identified here:

Load discretization: The load and reactions of the practical design problem need to be simplified to discrete forces in STM. For example, uniformly distributed loads are discretized by several concentrated forces. The load discretizations affect the generation of ST models and their performance. Only few studies on the influence of load discretizations have been conducted. Brown and Bayrak [30] conducted a series of experiments to investigate the influence of load configurations for deep beams. Based on the experimental results, they concluded that the two-load discretization is adequate in STM to design a deep beam under a uniform distributed load. The above research focused on standard deep beams, which are common but relatively simple D-regions. For more complex D-regions, the determination of an appropriate load discretization is equally important. To the best of our knowledge, no systematic investigation is conducted for such problems. In this thesis, we have conducted a preliminary investigation on the influence of load discretizations in Section **??**. The result shows that a more robust design can be obtained by choosing a suitable load discretization. However, a method for selecting the appropriate load discretization for a given case has not been developed, and further investigations are needed.

Loading conditions: Structures are subjected to various loads and combinations thereof. Also, the loading history might be of importance. Karthik et al. [73] addressed the latter topic by considering both monotonically increasing loads and alternating loads. In their so-called compatibility STM method the phenomenon of concrete softening of struts was considered to enable accurate modelling of the failure load. In addition, the analysis process was modified to enable the analysis in displacement control. The topic of dealing with multiple load cases was addressed by several researchers. To et al. [142] and Sritharan [130] created several ST models to design bridge tee joints considering a horizontal seismic load and vertical dead loads. Several ST models were created based on the selection of these load combinations. In order to generate ST models considering multiple load combinations, Bruggi [32] adopted a multi-load TO method to provide inspiration for the generation of a single ST model. In this thesis, we have conducted a preliminary investigation for the generation of ST models considering complex loads, as shown in Section 4.4.2. The result shows that the obtained layout of the reinforcements varies considerably with a relatively small change of the assumed load combinations. However, at present, no systematic and validated approach has been proposed for the ST model generation and the resulting steel design considering multiple load combinations. In order to obtain a robust and safe design, it is necessary to investigate possibilities for devising an ST model generation method that can deal with multiple load combinations. In Section 5.2, a preliminary investigation of the ST model generation considering multiple load combinations is presented based on the proposed generation method, as introduced in Chapter 3.

5.1.2. CHOICES AND UNCERTAINTIES IN DETERMINING TRUSS-ANALOGY MODELS

Finding a suitable force transfer model is a key part of the STM method. In the early stage of the STM method, the creation of a suitable ST model is largely dependent on the engineer's experience. In order to reduce the uncertainty in generating the truss-analogy model, as discussed in Section 3.1 and Section 4.1, numerous investigations have been conducted in the past three decades, but these still included a subjective interpretation step. In order to address this problem, we proposed a systematic method to automatically generate truss-analogy models in the previous chapters.

From the results shown in this thesis, it can be concluded that our automatic ST model generation approach is effective and also applicable to cases of higher complexity. The proposed generation method reduces the variability in ST model generation and thus paves the path to a systematic design approach for D-regions. With this in place, we can shift our attention to the subsequent steps of the STM procedure. Still, other factors could also be considered in this step, such as cost considerations or criteria related to constructability. The proposed generation method is expected to form a fruitful basis for future refinements.

5.1.3. CHOICES AND UNCERTAINTIES IN DIMENSIONING AND STRESS CHECKING

The STM method requires the resistance of all members to be larger than the limit strength without violating geometrical conditions. The generated model needs to satisfy the stress criterion, that is, the struts, ties and nodes must have sufficient strength. In order to calculate the stress in nodes and struts, the geometrical size of the struts and nodes needs to be specified. In the STM procedure of dimensioning and strength checking, there are uncertainties and multiple options. These aspects are discussed below.

Commonly, the dimensioning process starts with determining the geometry of nodes. By node-wisely determining the width of the connecting struts and ties, the geometry of ST models can be obtained. There are two typical categories of nodes: the hydrostatic nodes and the non-hydrostatic nodes. For a hydrostatic node, the stress on all faces of the node is equivalent and acting purely in the normal direction. In contrast, non-hydrostatic nodes allow for shear stresses along the faces of the node. The choice of node types will affect the geometry of the ST model and the calculated stress, thereby affecting the strength checking. Usually, the use of non-hydrostatic nodes is preferred since they give more flexibility to shape the ST model. This aspect is possibly even more relevant in 3D D-regions. However, the level of shear stresses in the nodes should be limited to allow for sufficiently accurate strength verifications [122].

Apart from the dimensioning process, there are numerous debates on the effective strength of struts and nodes. Through various researches [4, 36, 53, 60, 74, 92, 112, 119, 132, 162], many formulations and definitions have been proposed to determine the effective strength, usually formulated by the definition of a strength reduction factor. These formulations were proposed by considering various phenomena, such as

the concrete strength [53, 103, 112], the shape of struts [15, 118, 119, 128, 133, 162], the orientation of struts [53, 61, 112, 132, 133, 140], the influence of the concrete confinement [103, 120, 140] and the influence of adopting distributed reinforcement [139]. The performance of STM design is affected by the adopted procedures for dimensioning and stress checking. Currently, no decisive method is provided for these processes.

5.1.4. CHOICES AND UNCERTAINTIES IN DESIGNING STEEL LAYOUTS

The practical steel layouts are nearly always different from ties in the ST model. In practice, additional aspects, such as the constructability and anchorage length, are considered in designing steel layouts. Even in the more academic experimental investigations [37, 84, 94] on the suitability of ST models, the steel layouts of specimens are different from the STM designs. In the current state, no unique procedure for designing the steel layouts based on the proposed ST models has been established. In addition, the influence of the difference between practical reinforcements and STM designs is not clear. These uncertainties could cause unexpected performance of the realized structure as compared to the original STM design. In the later Section 5.3, a preliminary investigation of the STM design considering construction complexity is presented through a case study. The performance of different steel designs based on variations of the generated ST model is compared and discussed.

5.2. GENERATING STRUT-AND-TIE MODELS CONSIDERING MULTIPLE LOAD COMBINATIONS

In practice, engineers need to verify safety and performance of the design for several load combinations. These load combinations will comprise the permanent loads, frequently encountered loads and accidental loads, such as self-weight, traffic loads, seismic loads and wind loads. Building codes require engineers to verify a variety of load combinations, all with different load factors for each load. In current investigations of STM, the research mainly focuses on structures under a single load combination. It is an important safety aspect for a systematic STM approach to consider multiple load combinations.

The simplest way to consider multiple load combinations is to create different truss-analogy models for each (critical) load combination. Next, the corresponding ST models can be used for the steel design. This basic approach has a main disadvantage. As the number of load combinations increases, the number of generated truss-analogy models and resulting ST models increases also. This increases the difficulty in designing a single steel layout that is appropriate for all load combinations. In Figure 5.1, an example concerning three load combinations is used to illustrate this aspect. This illustrative example is further investigated in the next section. It is economically sensible that the ties of the obtained ST models are as much as possible overlapping under multiple load combinations, which will not always be the case. Struts, on the other hand, can vary in position, since they are supposed to form within the concrete where needed, without the demand for extra (steel) material. The generation of ST models considering multiple load combinations, which provides safe and design-convenient results, is identified as a key problem.

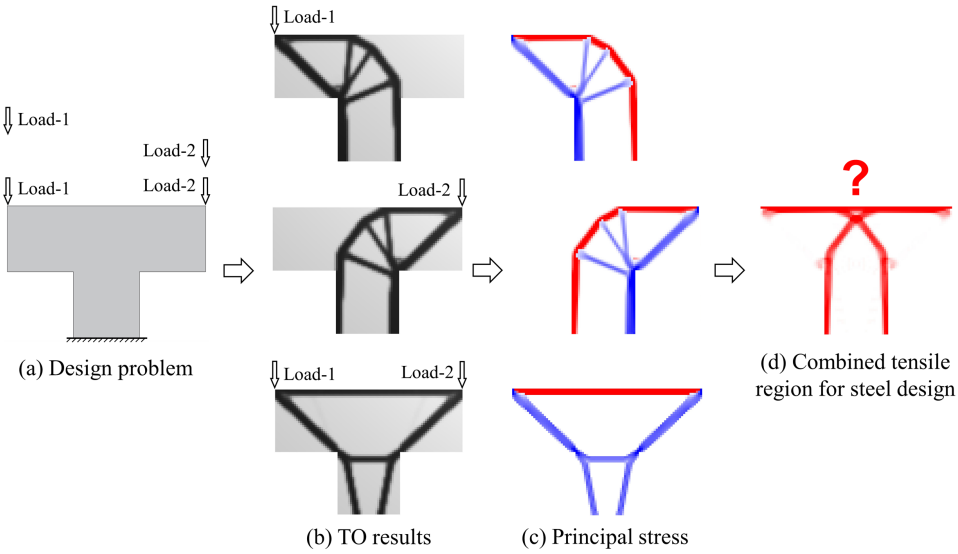

Figure 5.1: Tee joint case illustrating the basic approach for multiple load combinations. Three optimized topologies are generated based on the standard TO method. Red and blue parts indicate the tensile and compressive regions respectively. The intensity of the color indicates the stress magnitude. The challenge is combining the three results economically in one single steel design. The question mark indicates the difficulty for steel design.

For the identified problem, Bruggi [32] provided a promising direction. In this research, a multi-load TO formulation is used to obtain the optimized topologies considering the interactive effect of multiple load combinations. Several D-regions were investigated and their TO results were generated. For each D-region the proposed method resulted in one single TO result. This obtained TO result can be used as inspiration for the generation of ST models. In this section, similar to Bruggi's work [32], the multi-load TO formulation is used. Next, we incorporate this multi-load TO process into the framework of the OPT-STM generation method to further investigate the ST model generation considering multiple load combinations.

5.2.1. MULTI-LOAD TOPOLOGY OPTIMIZATION FOR STM

The multi-load TO process aims to improve the robustness of the generated TO results under multiple load combinations. Compared to the standard TO method, the multi-load TO method considers the interactive effect of various load combinations, and provides a unified optimized result with good performance for each considered load combination. In this case, the multi-load TO method can provide one TO result used for ST model generation with multiple load combinations.

To consider the multiple load combinations in the SIMP TO method, the mathemat-

ical formulation of the compliance minimization problem is:

$$\begin{aligned} &\text{minimize: } C(\boldsymbol{\rho}) = \sum_{i}^{m} \beta_i \boldsymbol{F}_i^{\mathrm{T}} \boldsymbol{U}_i(\boldsymbol{\rho}) \\ &\text{subject to: } \boldsymbol{K}(\boldsymbol{\rho})\boldsymbol{U}_i = \boldsymbol{F}_i \\ &\qquad\qquad V(\boldsymbol{\rho}) \leq \alpha \bar{V} \\ &\qquad\qquad \boldsymbol{\varepsilon} \leq \boldsymbol{\rho} \leq \mathbf{1} \\ &\qquad\qquad (i = 1,..,m) \end{aligned} \tag{5.1}$$

This mathematical formulation is a generalization of the formulation of the standard single-load TO problem, as given in Eq.(3.1). Here, $\boldsymbol{F}_i$ and $\boldsymbol{U}_i$ are the nodal force vector and the nodal displacement vector under the $i-$th load combination, respectively, C is the total compliance of the structure under m load combinations, β_i is the given weight for each load combination.

Here, a tee joint structure is optimized to demonstrate the difference of using this multi-load TO method compared to the standard TO method. A similar case was investigated by Bruggi [32]. The geometry of the tee joint structure is shown in Figure 5.2a. The structure is subjected to two concentrated forces on the top. These loads can occur individually or simultaneously. There are thus three load combinations: Load-1, Load-2 and Load-1&2. The finite element model is created with a mesh size of 20 mm, as shown in Figure 5.2b.

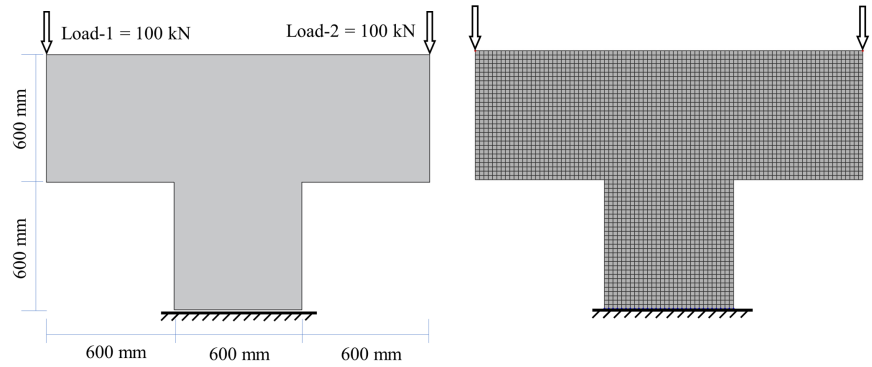

(a) Geometry and load conditions (b) Finite element model

Figure 5.2: Tee joint structure case considering three load combinations, Load-1, Load-2 and Load-1&2.

For this structure, both multi-load TO and standard TO are conducted. In the multi-load TO method all three load combinations are considered ($m = 3$), whereas only one load combination where both loads are applied simultaneously is considered in standard TO. The weighting factors β_i are set to 1 for the three load combinations in the multi-load TO case. A volume constraint of 25 % and a filter radius of 75 mm (1.5 × (mesh size))

are adopted for the two TO methods. The obtained TO results are shown in Figure 5.3. Clearly different topologies have been obtained.

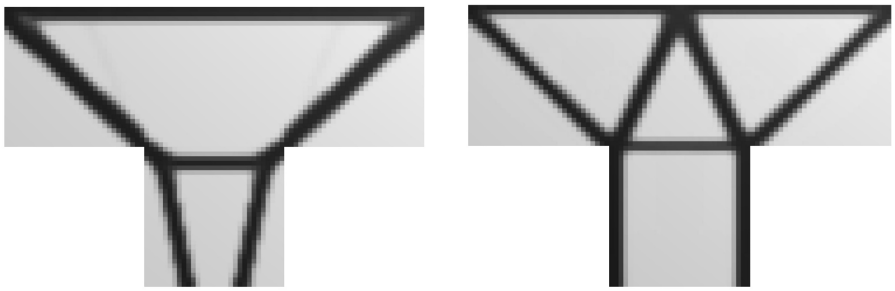

(a) Single-load TO result using the load combination where Load-1 and Load-2 act simultaneously

(b) Multi-load TO result using all three load combinations

Figure 5.3: Optimization results of the tee joint structure with respect to two TO formulations

In order to evaluate the performance of the obtained TO results, the principal stress for the three load combinations is plotted in Figure 5.4 and Figure 5.5. Based on the stress plots, the standard TO result shows pure tensile and compressive regions when subjected to simultaneous loads. However, bending regions are observed when only Load-1 or Load-2 acts on the structure (Figure 5.4b and 5.4c). These bending regions will likely hamper the generation of suitable ST models that satisfy axial force equilibrium. Compared to the standard TO result, the multi-load TO result leads to better overall performance with these load combinations (Figure 5.5). Less bending regions are observed in the multi-load TO result, for each of the load combinations, and in the bending regions that are present, the stresses have a relatively low magnitude.

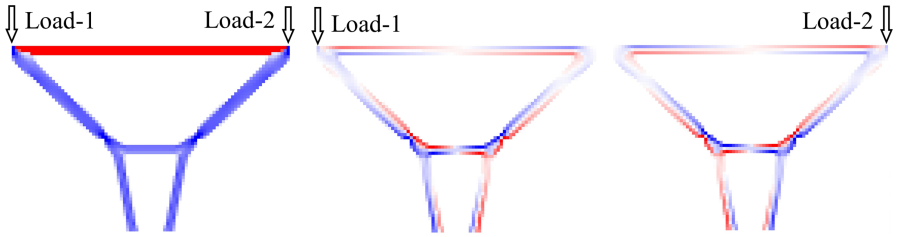

(a) Load-1&2 (b) Load-1 (c) Load-2

Figure 5.4: Principal stress distribution of the single-load TO result. Red and blue parts indicate the tensile and compressive regions respectively. The intensity of the color indicates the stress magnitude.

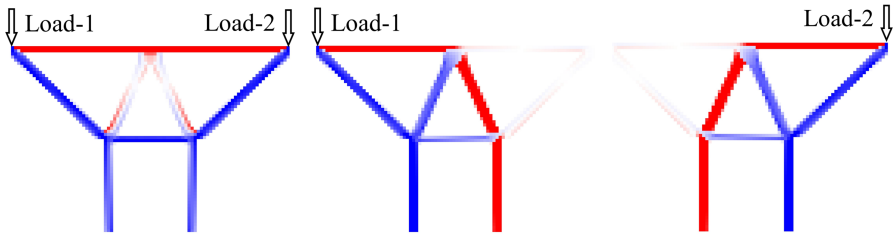

(a) Load-1&2 (b) Load-1 (c) Load-2

Figure 5.5: Principal stress distribution of the multi-load TO result. Red and blue parts indicate the tensile and compressive regions respectively. The intensity of the color indicates the stress magnitude.

5.2.2. GENERATING A UNIFIED STRUT-AND-TIE MODEL UNDER MULTIPLE LOAD COMBINATIONS

Based on the previous case study, using a multi-load TO method provides TO results that have overall more favorable stress distributions under multiple load combinations. In this case, a unified truss-analogy model for STM under multiple load combinations can be obtained based on the multi-load TO result. In this section, the suitability of using the obtained multi-load TO result to generate a unified truss-analogy model under multiple load combinations is discussed.

The obtained TO results of the tee joint structure, as shown in Figure 5.3, are used to investigate this problem. Following the proposed extraction method as described in Section 3.2, the extracted truss-like models are shown in Figure 5.6.

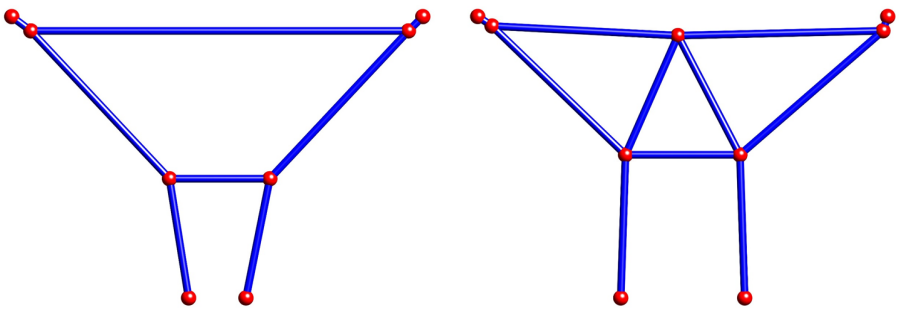

(a) Single-load result using the load combination where Load-1 and Load-2 act simultaneously (b) Multi-load result using all three load combinations

Figure 5.6: Extracted truss-like structures based on the optimized topologies of the tee joint structure

The obtained truss-like models cannot be directly used in STM. A shape optimization procedure is needed to obtain the required axial force equilibrium. With multiple load combinations, more constraints are imposed on the STS index in the shape optimization process. The mathematical formulation of the shape optimization considering

multiple load combinations is given by:

$$\begin{aligned} &\text{minimize: } C(\boldsymbol{x}) = \sum_{i}^{m} \beta_i \boldsymbol{F}_i^{\mathrm{T}} \boldsymbol{U}_i(\boldsymbol{x}) \\ &\text{subject to: } \boldsymbol{K}(\boldsymbol{x})\boldsymbol{U}_i = \boldsymbol{F}_i \\ &\qquad\qquad S_i(\boldsymbol{x}) \geq 1-\epsilon \\ &\qquad\qquad \boldsymbol{x}_{\min} \leq \boldsymbol{x} \leq \boldsymbol{x}_{\max} \\ &\qquad\qquad (i = 1,..,m) \end{aligned} \tag{5.2}$$

This formulation is extended and modified based on the previous one of the single load problem given in Eq.(3.13). Similar to the multi-load TO formulation, C is the total compliance of m load combinations; $\boldsymbol{F}_i$ and $\boldsymbol{U}_i$ are nodal forces, and nodal degrees of freedom (displacements and rotations) based on the beam finite element model for the $i-$th load combination.

We require axial force equilibrium in every load combination. Here, S_i indicates the STS index which quantifies the closeness of the truss-like structure to a pure axial force equilibrium state under the $i-$th load combination. Since not all members are significantly loaded under all load combinations, the members which have minor elemental forces are not relevant for the STS index. These inactive members are excluded in the STS calculation. The calculation of the STS index is given by:

$$S = \frac{1}{n} \sum_{e=1}^{n} \frac{|N_{\mathrm{e}}|}{|N_{\mathrm{e}}| + |V_{\mathrm{e}}|}, \tag{5.3}$$

where, N_{e} is the element axial force and V_{e} is the element shear force. Previously in Eq.(3.8), n denoted the total number of elements, however for the multiple load combinations, n indicates the number of active elements under the considered load combination. In this thesis, each element e for which holds that $(|N_{\mathrm{e}}| + |V_{\mathrm{e}}|) \geq 0.01 \max_{n}(|N| + |V|)$ is taken as an active element. This modified STS index also has the range $[0,1]$. When STS $= 1$, all active members in the truss-like structure are subjected to axial forces only, and the truss-like structure can be used as-is in the STM method. Since shear forces are inevitable in the beam analysis, a tolerance $\varepsilon = 0.05$ is used in Eq.(5.2) to relax the STS requirement in the optimization process.

5.2.3. CASE STUDIES

In this section, two cases are tested to validate the suitability of the generated structures for STM. The first case is the tee joint structure, already introduced earlier (Figure 5.2). The obtained TO results and the extracted truss-like structures are shown in Figure 5.3 and Figure 5.6, respectively. The second case is a column structure which has more loads. The geometry and loads are shown in Figure 5.7. The structure is subjected to five load combinations: Load-1, Load-2, Load-3, Load-4 and Load-1&2&3&4. Each load consists of a single concentrated force of 100 kN as indicated.

For the first case, the shape optimization is conducted for both the single-load and multi-load model. The optimized truss-like structures are shown in Figure 5.8, and the

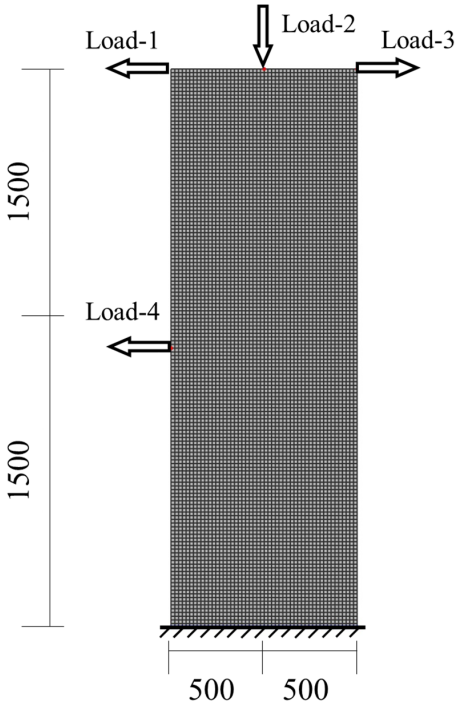

Figure 5.7: Finite element model of the column case (mm)

summary of STS indices is given in Table 5.2. It is found that for both cases, the STS indices have increased after the shape optimization. However, for the single-load model the STS indices for the two individual loads are still lower than the required number (0.95). In contrast, for the optimized result based on the multi-load TO result, all STS indices have improved and satisfy the requirement (STS $\geq$ 0.95). This indicates that a nearly pure axial force equilibrium is obtained for the considered load combinations, and this generated truss-like model can be used for STM. The inactive members of the multi-load model remains inactive after the shape optimization. Excluding these inactive members in the STS calculation increases the indices without affecting the calculated forces, as seen in Table 5.2. However, since all members are active in the single-load model, the STS indices remain the same.

In the column case, a volume constraint of 30 % and a filter radius of 40 mm (2 $\times$ (mesh size)) are used in the multi-load TO process. The obtained TO result is shown in Figure 5.9a. Using a similar shape optimization process as with the tee joint case, the optimized truss-like model is found as shown in Figure 5.9b. The summary of the STS indices before and after the shape optimization is shown in Table 5.3. Again, the STS indices of the generated model under multiple load combinations have improved and satisfy the requirement. This generated truss-like model can be used for STM.

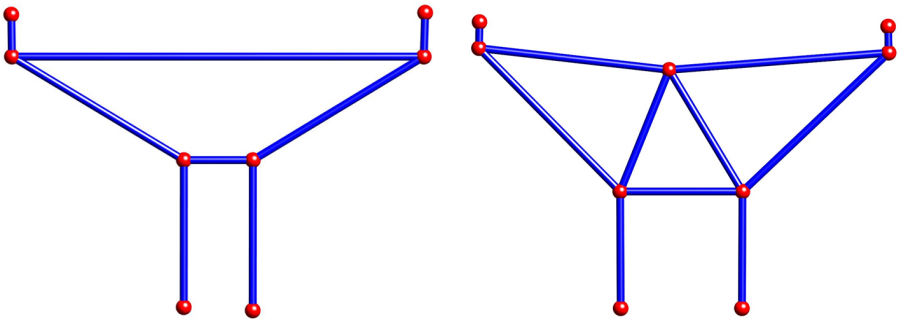

(a) Single-load result using the load combination where Load-1 and Load-2 act simultaneously

(b) Multi-load result using all three load combinations

Figure 5.8: Obtained truss-like structures after shape optimization for the tee joint structure

Table 5.2: STS indices of the obtained truss-like models of the tee joint case. The single-load model is based on the standard TO result with a load combination of Load-1 and Load-2.

Model	Single-load model			Multi-load model		
Load combination	Load-1	Load-2	Loads-1&2	Load-1	Load-2	Loads-1&2
Before optimization	0.58	0.61	0.84	0.81	0.81	0.85
After optimization (including inactive members)	0.76	0.76	0.99	0.90	0.89	0.99
After optimization (Excluding inactive members)	**0.76**	**0.76**	**0.99**	**0.99**	**0.99**	**0.99**

Table 5.3: STS indices of generated multi-load truss-like models of the column case.

load combination	Before optimization	After optimization
Load-1	0.78	0.99
Load-2	0.80	0.96
Load-3	0.80	0.99
Load-4	0.97	0.99
Load-1&2&3&4	0.87	0.99

The two cases demonstrate that a unified truss-analogy model considering multiple load combinations can be obtained through the proposed generation procedure. The generated ST models thus reduce difficulties in the steel design. However, at present, it is unclear whether the generated model provides the most economical design with respect to the considered load combinations. Further investigations in this direction need to be conducted. In addition, an approach where a condition is included to place all the steel in the same place as much as possible could also be an interesting alternative.

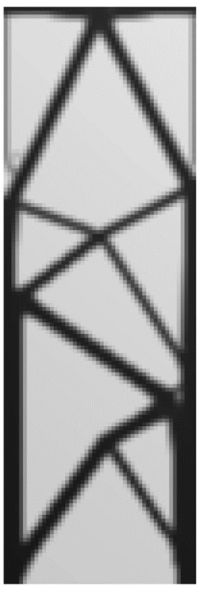

(a) Topology optimization result of the column case considering all five load combinations

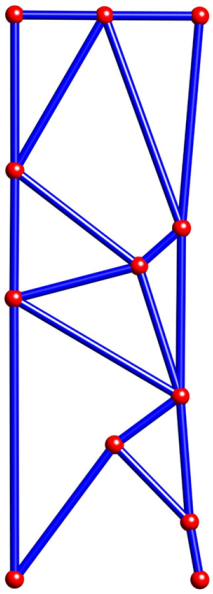

(b) Generated truss-like structure after shape optimization

Figure 5.9: Multi-load results for the column case

5.3. STRUT-AND-TIE DESIGNS CONSIDERING THE CONSTRUCTION COMPLEXITY

After obtaining the STM results, a procedure of steel design takes place to convert the ST models into the practical RC structure design. There are several requirements in designing practical structures. For example, a certain anchorage length is required to provide a sufficient bond between steel and concrete, and for reasons of constructability and cost the steel layouts are usually designed in a horizontal-and-vertical manner. These aspects are usually ignored in the TO method. The obtained ST models often have inclined ties and non-uniform tensile forces, which leads to inclined steel bars and various steel dimensions, thus increase the construction complexity. In this section, a preliminary case study is conducted in which the performance of different steel designs based on the variation of the generated ST model is compared and discussed.

5.3.1. INTRODUCTION OF THE TEST CASE AND THE GENERATED STRUT-AND-TIE MODEL

A deep beam with an opening is taken as an example. The geometry of the deep beam is shown in Figure 5.10. Brena and Morrison [29] conducted experiments to investigate this deep beam structure. The thickness of this beam is 112 mm and the design load is

133 kN. Following the proposed generation method described in Chapter 3, the OPT-STM model of this case is obtained. In the TO process, the volume fraction of the optimized result is set to 20 % of the original structure, and the density filter radius is set to 2.5 times the mesh size. The obtained TO result is shown in Figure 5.11a. The obtained OPT-STM model and equilibrium forces are shown in Figure 5.11b and Figure 5.11c respectively.

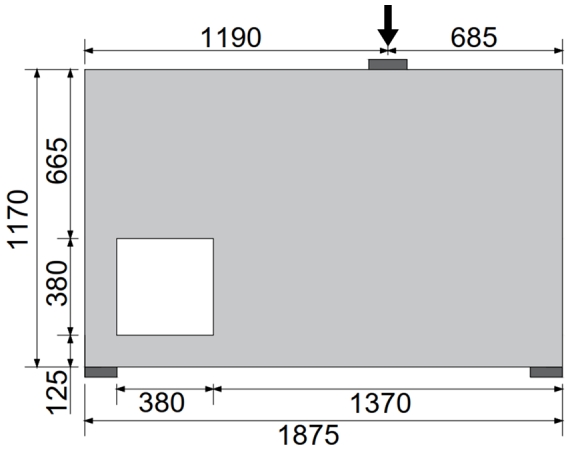

Figure 5.10: Geometry of the deep beam with an opening (mm)

5.3.2. STEEL DESIGNS BASED ON THE GENERATED STRUT-AND-TIE MODEL

Steel designs based on the OPT-STM model are investigated. Here, the steel layouts are created considering their construction complexity. There are two aspects concerning the construction complexity. The first aspect is that the use of inclined steel layouts increases the difficulty in practical construction, whereas the horizontal-and-vertical arrangement of steel reduces the construction complexity. The second aspect is the selection of the cross section of reinforcements. Adopting a uniform cross section for the steel design benefits the practical construction. Based on these two aspects, two steel designs are proposed.

The first one is the inclined steel design, as shown in Figure 5.12. It is directly created based on the obtained OPT-STM model, where the steel arrangement keeps an inclined reinforced bar. The cross sections of steel have been determined based on the calculated tensile forces, as in Eq.(5.4).

$$\frac{F}{A_s} \leq f_y \tag{5.4}$$

where F and f_y indicate the tensile forces of ties and steel yield strength, respectively. A_s is the required cross section of reinforcements. The capacity provided by the reinforcement should be larger than the force of the ties. In this section, the steel has a yield strength f_y equal to 420 MPa.

The second scheme is created by arranging the steel in a horizontal-and-vertical

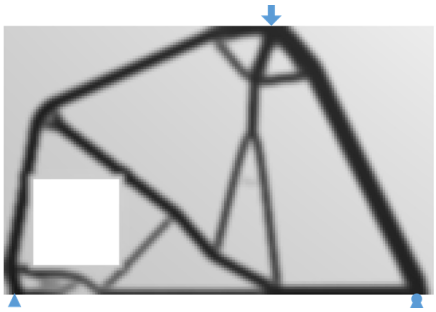

(a) Obtained TO result

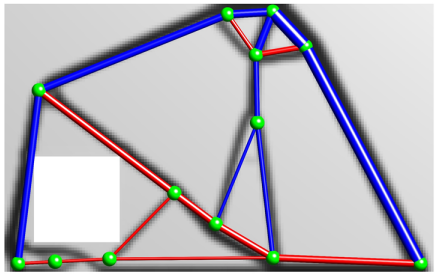

(b) Generated OPT-STM model. The red and blue bars indicate tensile and compressive members respectively. The line width indicates the magnitude of axial forces.

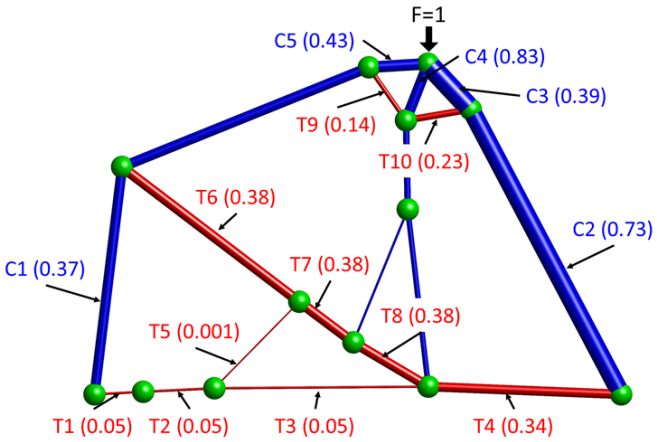

(c) Member forces of the topology based OPT-STM model (Normalized by 133 kN)

Figure 5.11: OPT-STM results of the deep beam structure

manner. In order to obtain a horizontal-and-vertical steel arrangement, we propose a procedure to transform the inclined ties to grid patches. In this case, the generated grid patch is shown in Figure 5.13. In the grid structure, the tensile force of the inclined ties is now transferred horizontally and vertically. Since concrete fills the entire structure, the inclined struts of the grid structure will not increase construction complexity. Based on the tensile force of the original inclined ties, we obtained the tensile forces in the created grid structure. The tensile forces of the created grid structure are shown in Figure 5.14. The resulting horizontal-and-vertical steel design considering sufficient capacity and adoption of uniform cross sections is shown in Figure 5.15.

5.3.3. PERFORMANCE COMPARISON OF TWO STEEL DESIGNS

Nonlinear finite element analysis (NLFEA) is used to gain further insight in the performance of the two proposed steel designs. The same solution strategy for NLFEA

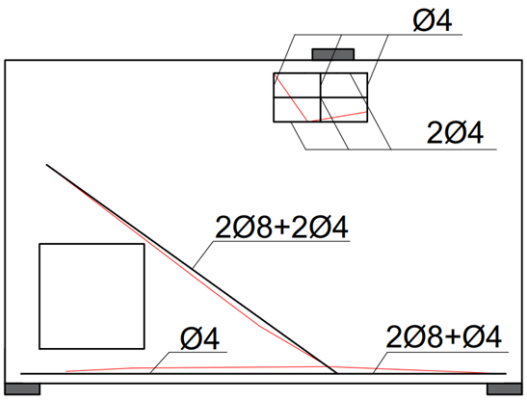

Figure 5.12: The inclined steel design (mm)

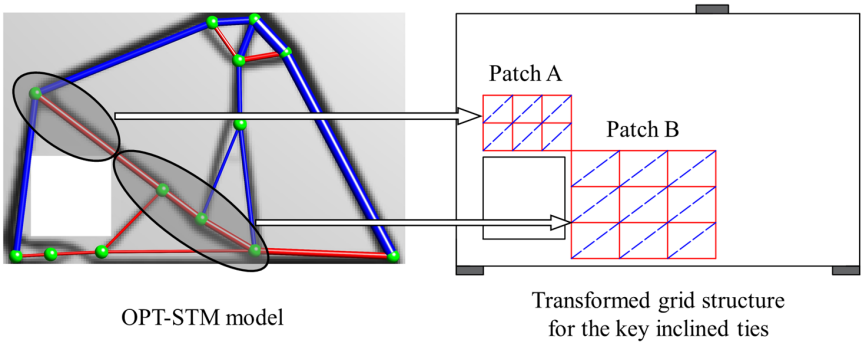

Figure 5.13: Transforming the inclined ties to horizontal and vertical grid structures. The grey regions indicate the key inclined ties. Two patches of grid structures are created due to the opening.

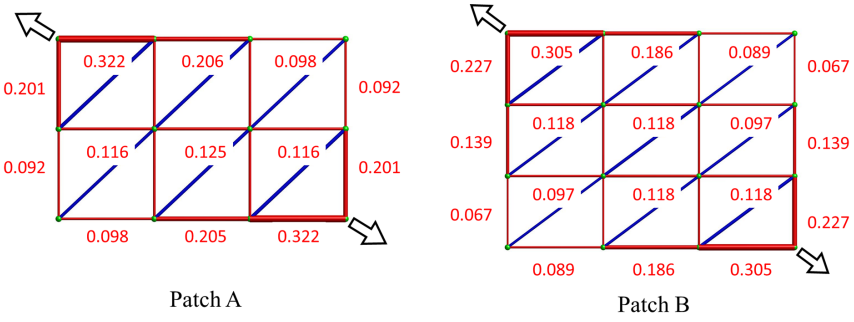

Figure 5.14: Tensile forces of the created grid structure (Normalized by 133 kN). Arrows indicates the force direction from the original inclined ties. The line width indicates the magnitude of axial forces.

as in Chapter 3 is used, as shown in Table 3.4, are used. Here, the concrete has a mean

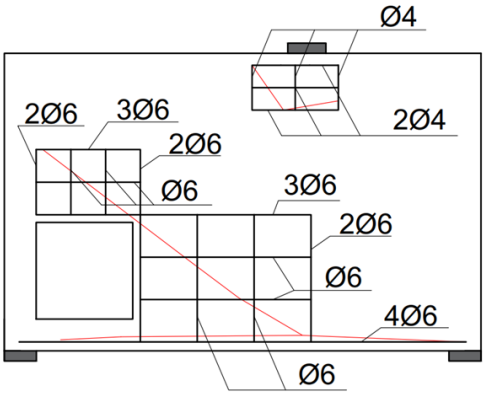

Figure 5.15: The horizontal-and-vertical steel design (mm)

compressive strength f_{cm} of 28 MPa. In this section, the steel does not show hardening behavior and ruptures at a strain equal to 10 %.

In order to obtain more insights, the design originating directly from the OPT-STM model is also evaluated for comparison. In the analysis of the OPT-STM design, reinforced steel bars are located along the ties of the ST model and their cross sections are based on the full use of the yield strength. Based on the simulation results, the load-displacement curves are presented in Figure 5.16. All steel designs have load capacities larger than the design load. This confirms the lower-bound result of the STM method. The steel strain and crack patterns in the ultimate state are shown in Figure 5.17 and Figure 5.18 respectively. The results of peak loads and steel usage are summarized in Table 5.4.

Table 5.4: Analysis results of different steel designs

	Peak load (N)	Steel usage (mm^3)	PS ratio (N/mm^3)
OPT-STM	158636	261773	0.606
Inclined scheme	163825	278702	0.588
Horizontal-vertical scheme	162612	535192	0.303

All designs fail due to steel rupturing and show a flexural failure mode. Compared to the design with the inclined scheme, the horizontal and vertical steel arrangement leads to a more ductile response. However, similar cracking patterns are obtained for all designs. In this case, although the three considered steel layouts originating from the same OPT-STM model are created under different considerations, they lead to a similar failure mode (similar crack patterns and rupturing points). A more economical design is obtained by the inclined scheme which has a similar PS ratio as the OPT-STM model. By considering the constructability, the horizontal and vertical scheme together with selecting uniform cross sections leads to a more ductile response at the expense of higher

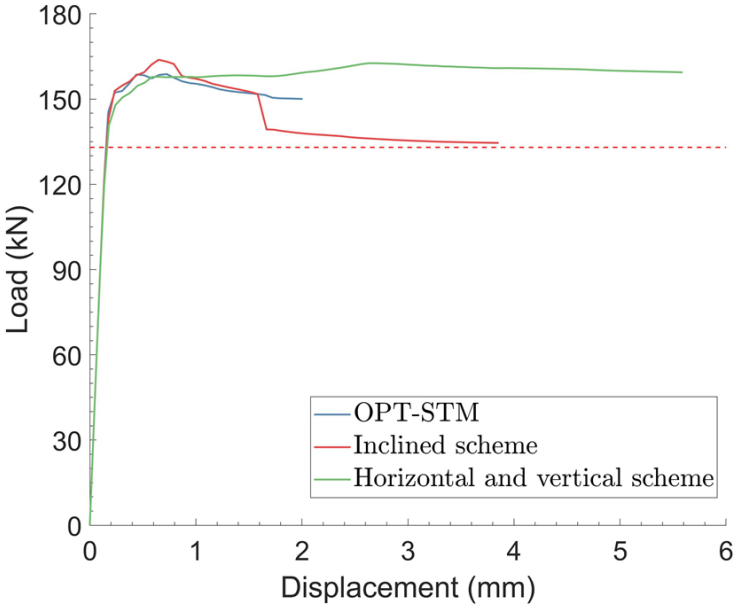

Figure 5.16: Load-displacement curves of three steel design schemes. The dashed line indicates the design load (133 kN)

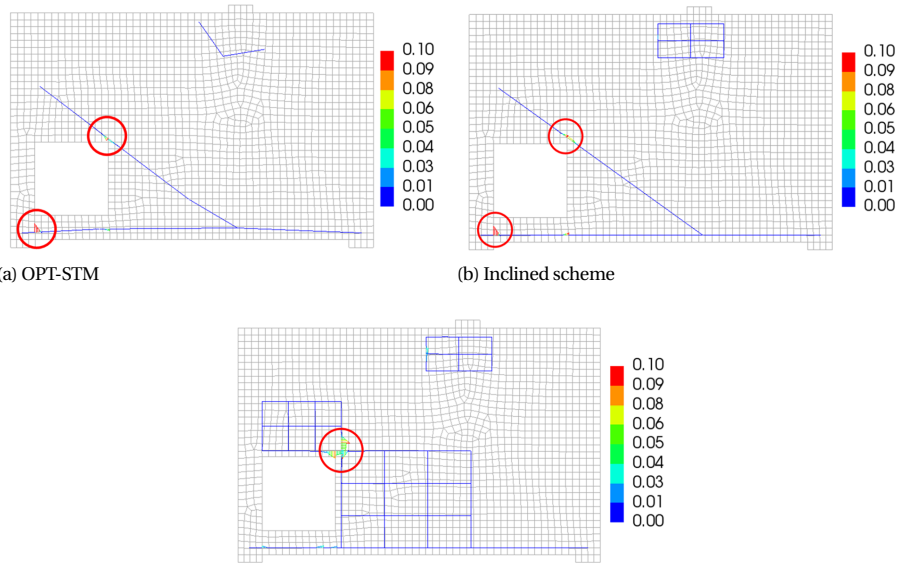

(a) OPT-STM

(b) Inclined scheme

(c) Horizontal and vertical scheme

Figure 5.17: The steel strain at the failure state of three designs. Steel rupturing is highlighted with red circles.

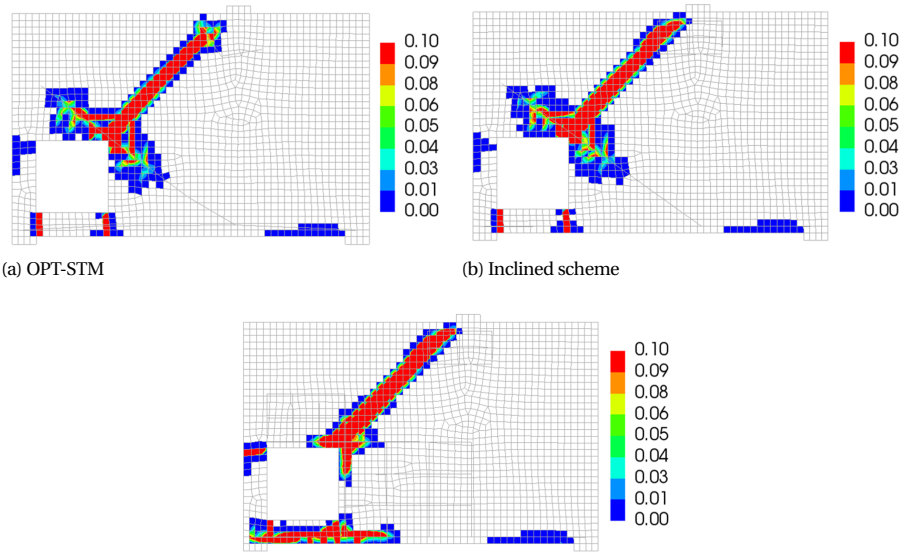

(a) OPT-STM

(b) Inclined scheme

(c) Horizontal and vertical scheme

Figure 5.18: The crack patterns at the failure state of three designs (mm)

steel usage. In fact, by the steel redesign concerning constructionability, the economical benefits that were realized by the OPT-STM model are sacrificed.

In the standard STM method, practical aspects are always left to engineers via a detailing process. And the resulting practical design could substantially deviate from the ST model. The difference between the practical design and the STM design affects the structural performance and the steel usage. It also increases additional work for engineers to apply the STM method. In order to develop a more applicable STM method, the main practical requirements need to be considered in an integrated way. In future investigations, the main practical requirements need to be identified and then considered in the STM-based design framework.

5.4. SUMMARY

Presently the standard STM method involves several subjective aspects. These subjective aspects are often determined based on the engineer's experience. They bring uncertainties in the STM design and hinder the wide application of the STM method. In this chapter, we identified important subjective aspects in the process of applying the STM method.

The developed ST model generation method in the thesis can be used to investigate these uncertainties. As a preliminary investigation, two identified uncertainties have been explored here. The first investigation investigated the ST model generation considering multiple load combinations. By incorporating the multi-load TO method into the framework of the developed ST model generation method, a suitable truss-like model is obtained. The generated truss-like model enables obtaining axial force equilibrium states for multiple load combinations. Through two case studies, the proposed multi-load ST model generation method is validated. It has not been demonstrated though that the resulting steel design is optimal.

The second investigation studied the influence of STM designs considering construction complexity. In practice, considering constructability, reinforcement is often placed vertically and horizontally and bars of the same cross section are used. The influence of considering construction complexity in STM designs is investigated through a case study. Two steel arrangements, an inclined scheme and a horizontal-and-vertical scheme, are created based on one generated ST model. Both designs have an ultimate capacity larger than the design load and lead to similar crack patterns. The inclined scheme leads to a more economical design, whereas the horizontal-and-vertical scheme results in a more ductile load-displacement response and higher steel usage. It is noted that the issue of limiting construction complexity was not an integrated part of the optimization process.

The STM method has been successfully used in designing D-regions for three decades. However, it is still a challenging task to apply the STM method for more complex D-regions. The existence of various choices not only affects the performance of the STM design, but also hinders the wide application of the STM method. Developing a systematic STM approach which avoids the subjective choices is an important research direction. Further systematic investigations are needed to reduce these subjective aspects. For example, practical requirements in an integrated (topology) optimization framework have not yet been devised. The proposed generation method is expected to form a fruitful basis for future refinements in this research direction.

6

CONCLUSIONS AND FUTURE WORK

6.1. CONCLUSIONS

Strut-and-Tie Modeling (STM) is a well-known method for designing D-regions of reinforced concrete (RC) structures. It uses a truss analogy model to simulate the load transfer mechanism. It is a powerful tool to provide insights to engineers for the steel placement and subsequent strength design in D-regions. The STM method is based on the lower-bound limit analysis of plasticity theory. With sufficient concrete and steel ductility, the RC design of the STM method underestimates the ultimate capacity. The safety of the resulting designs and the simple implementation of STM are favorable for engineers. In the past decades, researchers have conducted enormous efforts to extend and improve STM. However, there are still some uncertainties, and they hinder the development of STM towards a consistent approach for designing D-regions. This thesis aimed to pave the path towards a consistent STM design method. For this purpose, four main research questions have been defined in the Introduction. Here, we reflect on the main conclusions of each of these.

Among the various uncertainties of STM, finding an accurate truss-analogy model is the most prominent issue, and various TO methods have been proposed and adopted to solve this problem. However, which method yields the most suitable Strut-and-Tie (ST) model was still unknown. Very few investigations had been carried out regarding the systematic evaluation of TO results from the perspective of the STM method. Therefore, the first research question in this thesis has been to investigate the suitability of the proposed TO methods for STM and identify the best method.

In order to address this question, Chapter 2 of this thesis presents a comparative study of various TO approaches for STM. In order to investigate to what extent TO results benefit from STM and which method should be preferred, an evaluation method based on three measures has been proposed to quantitatively and objectively compare the optimized topologies from different TO methods for the STM method. These measures indicate whether an analyzable truss model could be extracted, to which extent tensile

stress regions are covered by tensile ties and how economical the design will be. Using the proposed evaluation method, 23 TO-based results for STM and 5 traditional ST models (manually generated without a TO process) for three design problems have been analyzed and compared. Based on the evaluated results we can conclude that using TO methods for STM has advantages. The influence of using various TO methods, parameter configurations and process settings has been studied, and the TO methods with good performance have been identified. Most standard TO methods, e.g., strain energy based SIMP (solid isotropic material with penalization) methods, ESO (Evolutionary structural optimization) methods using strain energy and Von Mises stress removal criteria and the homogenization method all showed similar performance. A remarkable finding is that approaches with the most sophisticated material models showed relatively weak performance. In addition, a main challenge not reported before of adopting TO methods to generate ST models was identified, which leads to the second research question of this thesis.

Currently, most TO methods only provide optimized material layouts as inspiration for creating ST models. The proposed TO results cannot be used directly as ST models. Manual and subjective adjustments are required to convert TO results into adequate ST models. These additional processes not only affect the performance of the desired design, but also hinder the application of TO methods for STM. The second research question is therefore how to perform this conversion in an automated and systematic manner. This question is answered in Chapter 3 of this thesis, which proposes a method to generate optimization-based Strut-and-Tie (OPT-STM) models. The proposed method successfully generates valid OPT-STM models for D-regions automatically and without manual adjustments. It performs well on a variety of 2D test problems according to the evaluation criteria introduced earlier and generally results in ST models with lower steel usage than alternative approaches. However, to determine the validity and safety of the generated layouts, more detailed evaluation is required, which forms part of the third research question. Therefore, also in Chapter 3, a procedure using nonlinear finite element analysis (NLFEA) has been proposed. Detailed NLFEA simulation of RC structures based on OPT-STM models show sufficient, yet not overly conservative, load capacity. Based on the findings it can be concluded that the proposed ST model generation method can be recommended for practical use; significant savings in design time and steel usage can be expected compared to manually created models.

Compared to investigations of 2D ST models, there are few studies on 3D ST models. As a result of the increased complexity of 3D D-regions, the difficulty and importance of determining suitable ST models increases. Chapter 4 addresses this problem by proposing an automatic generation method to generate suitable truss analogy models for 3D STM. This method has been developed by extending the previous 2D generation method. The proposed method enables the generation of three-dimensional optimization-based STM (3D-OPT-STM) models for various 3D D-regions in an automated manner, which simplifies the design process in engineering practice. The generated models again provide more economical design compared to manually created models. Moreover, based on the generation method, three important factors in STM have been discussed, including the parametric investigation of the four-pile cap, the influence of the complex load com-

bination and the load discretization. Based on these investigations it can be concluded that the generation method enables engineers to conveniently evaluate a large range of design options through parametric investigations. In addition, load conditions and discretization of distributed loads have significant impact on the resulting ST models. In order to conduct a more accurate STM analysis, using the generation method to compare several variants is recommended.

Finally, Chapter 5 addresses the last research question by identifying several additional important subjective aspects in the STM procedure. These aspects are often determined based on engineering experience and preference. They cause uncertainties in the STM design and hinder the development of a widely applicable STM method. Developing a systematic STM approach which reduces these subjective aspects is an important future research direction. A preliminary exploration of two identified subjective aspects have been conducted: 1) ST model generation considering multiple load combinations; 2) STM design considering construction complexity. The generation method proposed in this thesis could form a fruitful basis to investigate these aspects in the future.

6.2. FUTURE WORK

The generation method proposed in this thesis has shown to be effective and robust in generating suitable ST models. Nevertheless, this method can be further improved and refined to a systematic design approach as follows:

- Evaluating the applicability of the proposed method in practical engineering needs further investigation. Shortcomings of the proposed method may emerge and will contribute to future refinements of the method. Furthermore, it is of great interest to verify that the cost advantages predicted by this investigation indeed can be realized in practice.

- Developing a systematic STM approach by reducing the identified subjective aspects, such as load disretization, member dimensioning and steel design, is a challenge future research direction. A systematic approach will facilitate the STM application for engineers and contribute to a unified design practice of using STM method.

- In the current thesis we have demonstrated that TO forms a fruitful basis for finding truss analogies. Standard TO methods have been used for single and multi-load optimizations. The development of more advanced TO methods, tailored for STM applications, is recommended. For multi-load optimizations it has not yet been demonstrated that optimal solutions are obtained. The simple case of a two-sided constrained column, Figure 6.1, loaded by an axial load at its center, shows that standard TO methods might not always suffice as they do not distinguish tension from compression. Given the cost difference between concrete and steel, it is relevant to include this aspect in the formulation. Therefore, improving the proposed method is another future research direction. In addition, adopting suitable material models in the TO process may provide more effective layouts for STM.

Furthermore, considering the member orientation during the TO will contribute to obtain a practically orientated ST model.

- In addition to apply the proposed truss generation method for STM, the method could be extended to investigate suitable truss layouts for actual truss structures, such as bridges, grid shell structures and truss towers. The structural performance of these structure types is significantly affected by their geometry and topology. Economical designs with good structural performance could be automatically generated with future refinement of the proposed method.

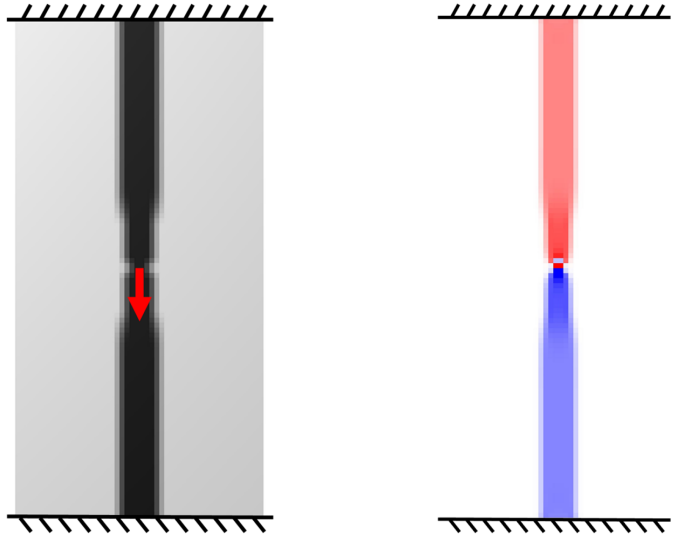

(a) TO result (b) Inclined scheme

Figure 6.1: Illustrative example of a column constrained at both sides with an axial load at its center. Red and blue parts indicate tensile and compressive stress. The intensity of the color indicates the stress magnitude. Standard TO leads to equal forces in the strut and tie, in absolute sense. A more economical solution would be obtained by only using a strut.

ACKNOWLEDGEMENTS

At the very end time of my PhD period, all kinds of things that happened in the past four years jumped into my mind. It is the right time to sort out my emotions and express my sincere thanks to those who helped and accompanied me during this unforgettable journey.

First of all, I would like to thank my promotors and supervisors, Max A.N. Hendriks and Matthijs Langelaar. It is my luck to meet you and conduct the PhD research under your supervision. During my research, you helped me to develop academic views and scientific thinking. When conducting research, I can always learn from your rigorous attitude and profound comments. I enjoyed our regular meetings, which are always inspiring and even brainstorming. Moreover, you are also supportive in my daily life. I can always gain advice and suggestions from you which are much more than I expected. I truly appreciate your careful guidance, immense patience and considerable supports which are the key elements in my PhD research.

I would like to thank my tutor Yue WU in Harbin Institute of Technology. I am grateful for your persistent supports and helps throughout the research and my personal life. I can always obtain suggestions and advice from you in every aspect of my life. You always provide me with a broad view of life and encourage me to make breakthroughs. It is my fortune to be your student and receive your care.

I would like to thank the doctoral committee members, Prof. Rots, Prof. van Keulen, Dr. Bruggi, Prof. Schevenels and Prof. Suiker, for the time and efforts in reviewing the thesis and attending the PhD defense. I would also like to thank my colleagues in the two different groups, Applied Mechanics and Precision and Microsystems Engineering. I truly appreciate all the help you offered me and the happy time we spent together. Special thanks to Manimaran Pari for providing me with suggestions and warm help.

I sincerely thank my friends for accompanying me during the four years. Thank you my roommates and friends, Xiao LIN, Kai WANG and Wenjing GUO. It is happy to spend time playing poker with you and learn some related skills. Besides, special thanks to Xiao LIN for bringing me various beers and introducing them to me, I am also grateful for our fun game time. I have a lot of happy memories in Room 95 together with Hao YU, Riming WANG and Ding DING. You always provided me with well-prepared food and a lot of interesting games. I can always learn a lot from you during the communication in our daily life. Many thanks to my friends in the faculty, Langzi CHANG, Hongzhi ZHANG, Chenjie YU, Fanxiang XU, Ze CHANG, Rui YAN, Yong ZHANG, Xiuli WANG, Lu CHENG, Fengqiao ZHANG, Jian ZHANG. I am grateful for all the help I received from you. It is always fun and relaxing to spend time with you on various activities, such as cycling, sports, table games and hotpots. I also want to thank Fengnian TIAN for the help and supports. I love the time we worked at the faculty of architecture and the time we went fishing together.

In addition, I want to particularly thank Weiming WANG. I really appreciate the valuable knowledge that I gained from you. It is indeed my fortune to meet you in TU Delft.

In the end, I want to thank my family for their unconditional supports and endless love. I do not think there is a language in the world that could express my deepest gratitude to you. I will bring all of the scientific knowledge, grateful joy and valuable memories with me to the next stage of my life, until the end of my life.

REFERENCES

[1] N. Aage, E. Andreassen, B. S. Lazarov, and O. Sigmund. Giga-voxel computational morphogenesis for structural design. *Nature*, 550:84, 2017.

[2] AASHTO. *LRFD bridge design specifications*. American Association of State Highway and Transportation Officials, Washington, DC., 7th edition edition, 2014.

[3] W. Abu-Ain, S. N. H. S. Abdullah, B. Bataineh, T. Abu-Ain, and K. Omar. Skeletonization algorithm for binary images. *Procedia Technology*, 11:704–709, 2013.

[4] ACI 318. *Building code requirements for structural concrete and commentary*. American Concrete Institute, ACI Committee 318-14, Farmington Hills, MI, 2008.

[5] H. Adeli and K. Balasubramanyam. Interactive layout optimization of trusses. *Journal of Computing in Civil Engineering*, 1(3):183–196, 1987.

[6] H. Adeli and K. Balasubramanyam. A synergic man-machine approach to shape optimization of structures. *Computers & Structures*, 30(3):553–561, 1988.

[7] M. Aldwaik and H. Adeli. Advances in optimization of highrise building structures. *Structural and Multidisciplinary Optimization*, 50(6):899–919, 2014.

[8] M. A. Ali and R. N. White. Formulation of optimal strut-and-tie models in design of reinforced concrete structures. *ACI Special Publication*, 193:979–998, 2000.

[9] M. A. Ali and R. N. White. Automatic generation of truss model for optimal design of reinforced concrete structures. *Structural Journal*, 98(4):431–442, 2001.

[10] V. S. Almeida, H. L. Simonetti, and L. O. Neto. Comparative analysis of strut-and-tie models using smooth evolutionary structural optimization. *Engineering Structures*, 56:1665–1675, 2013.

[11] A. Alshegeir and J. Ramirez. Computer graphics in detailing strut-tie models. *Journal of computing in civil engineering*, 6:220–232, 1992.

[12] O. Amir. A topology optimization procedure for reinforced concrete structures. *Computers & Structures*, 114–115:46–58, 2013.

[13] O. Amir and O. Sigmund. On reducing computational effort in topology optimization: how far can we go? *Structural and Multidisciplinary Optimization*, 44(1): 25–29, 2011.

[14] E. Andreassen, A. Clausen, M. Schevenels, B. S. Lazarov, and O. Sigmund. Efficient topology optimization in matlab using 88 lines of code. *Structural and Multidisciplinary Optimization*, 43(1):1–16, 2011.

[15] A. Arabzadeh, R. Aghayari, and A. Rahai. A new model for predicting the effective strength in reinforced concrete bottle-shaped struts. *International Journal of Civil Engineering*, 10(4):253–262, 2012.

[16] A. Ashour and K. H. Yang. Application of plasticity theory to reinforced concrete deep beams: a review. *Magazine of Concrete Research*, 60:657–664, 2008.

[17] M. Baandrup, O. Sigmund, H. Polk, and N. Aage. Closing the gap towards super-long suspension bridges using computational morphogenesis. *Nature Communications*, 11(1):1–7, 2020.

[18] Z. P. Bažant and M. Jirásek. Nonlocal integral formulations of plasticity and damage: survey of progress. *Journal of Engineering Mechanics*, 128(11):1119–1149, 2002.

[19] P. G. Bakir and H. M. Boduroglu. Mechanical behaviour and non-linear analysis of short beams using softened truss and direct strut & tie model. *Engineering Structures*, 27(4):639–651, 2005.

[20] B. Belletti, C. Damoni, and M. A. N. Hendriks. Development of guidelines for nonlinear finite element analyses of existing reinforced and pre-stressed beams. *European Journal of Environmental and Civil Engineering*, 15(9):1361–1384, 2011.

[21] M. P. Bendsøe and N. Kikuchi. Generating optimal topologies in structural design using a homogenization method. *Computer Methods in Applied Mechanics and Engineering*, 71:197–224, 1988.

[22] M. P. Bendsøe and O. Sigmund. *Topology optimization: theory, methods, and applications*. Springer Verlag, 2003.

[23] M. P. Bendsøe and N. Kikuchi. Generating optimal topologies in structural design using a homogenization method. *Computer Methods in Applied Mechanics and Engineering*, 71(2):197–224, 1988.

[24] K. Bergmeister, J. E. Breen, J. O. Jirsa, and M. E. Kreger. *Detailing for structural concrete*. Center for Transportation Research, University of Texas, Austin, Tex., 1993.

[25] F. Biondini, F. Bontempi, and P. G. Malerba. Optimal strut-and-tie models in reinforced concrete structures. *Computer Assisted Mechanics and Engineering Sciences*, 6(3-4):280–293, 1999.

[26] F. Biondini, F. Bontempi, and P. G. Malerba. Stress path adapting strut-and-tie models in cracked and uncracked RC elements. *Structural Engineering and Mechanics*, 12(6):685, 2001.

[27] J. L. Blévot and R. Frémy. Semelles sur pieux. *Institute Tech. du Bâtiment et des Travaux Publics*, 20(230):223–295, 1967.

[28] M. Bogomolny and O. Amir. Conceptual design of reinforced concrete structures using topology optimization with elastoplastic material modeling. *International Journal for Numerical Methods in Engineering*, 90:1578–1597, 2012.

[29] S. F. Brena and M. C. Morrison. Factors affecting strength of elements designed using strut-and-tie models. *ACI Structural Journal*, 104(3):267, 2007. ISSN 0889-3241.

[30] M. D. Brown and O. Bayrak. Investigation of deep beams with various load configurations. *ACI Structural Journal*, 104:611, 2007.

[31] M. Bruggi. Generating strut-and-tie patterns for reinforced concrete structures using topology optimization. *Computers & Structures*, 87:1483–1495, 2009. ISSN 978-0-81-551497-8.

[32] M. Bruggi. On the automatic generation of strut and tie patterns under multiple load cases with application to the aseismic design of concrete structures. *Advances in Structural Engineering*, 13:1167–1181, 2010. ISSN 3903829854.

[33] M. Bruggi. A numerical method to generate optimal load paths in plain and reinforced concrete structures. *Computers & Structures*, 170:26–36, 2016. ISSN 0045-7949.

[34] BS8110. *Structural use of concrete - Part 1: Code of practice for design and construction*. British Standard, London, 1997.

[35] C. S. Cai. Three-dimensional strut-and-tie analysis for footing rehabilitation. *Practice Periodical on Structural Design and Construction*, 7:14–25, 2002.

[36] CEN. *Eurocode 2: Design of concrete structures-Part 1-1: General rules and rules for buildings*. European Committee for Standardization, 2017.

[37] B. S. Chen, M. J. Hagenberger, and J. E. Breen. Evaluation of strut-and-tie modeling applied to dapped beam with opening. *Structural Journal*, 99:445–450, 2002.

[38] H. Chen, W.-J. Yi, and H.-J. Hwang. Cracking strut-and-tie model for shear strength evaluation of reinforced concrete deep beams. *Engineering Structures*, 163:396–408, 2018.

[39] Y.-H. Chou and C.-Y. Lin. Improved image interpreting and modeling technique for automated structural optimization system. *Structural and Multidisciplinary Optimization*, 40(1-6):215–226, 2010.

[40] J. L. Clarke. Behaviour and design of pile caps with four piles. *Technical Report of the Cement and Concrete Association*, 42:1–19, 1973.

[41] M. P. Collins and D. Mitchell. Rational approach to shear design–the 1984 canadian code provisions. *Journal Proceedings*, 83:925–933, 1986.

[42] Comite Euro-international du Beton. *Biulletin D'Information, No. 213/214*. CEB-FIP Model Code 1990, London, 1993.

[43] CSA. *Design of concrete structures*. Canadian Standards Association, Rexdale, Ontario, 2004.

[44] J.-C. Cuillière, V. François, and A. Nana. Automatic construction of structural cad models from 3d topology optimization. *Computer-Aided Design and Applications*, 15:107–121, 2018.

[45] S. Dey and M. M. Karthik. Modelling four-pile cap behaviour using three-dimensional compatibility strut-and-tie method. *Engineering Structures*, 198: 109499, 2019.

[46] Z. Du, W. Zhang, Y. Zhang, R. Xue, and X. Guo. Structural topology optimization involving bi-modulus materials with asymmetric properties in tension and compression. *Computational Mechanics*, 63(2):335–363, 2019.

[47] S. El-Metwally and W.-F. Chen. *Structural concrete: strut-and-tie models for unified design*. CRC Press, 2017. ISBN 1315155508.

[48] N. El-Mezaini and E. Çıtıpıtıog˘lu. Finite element analysis of prestressed and reinforced concrete structures. *Journal of Structural Engineering*, 117(10): 2851–2864, 1991.

[49] fib. *Practitioners guide to finite element modelling of reinforced concrete structures*. State-of-Art Report, CEB-FIB bulletin 45, Lausanne, Switzerland, 2008.

[50] fib. *Design examples for strut-and-tie models*. fib Bulletin No. 61, 2011.

[51] fib. *fib Model Code for Concrete Structures 2010*. International Federation for Structural Concrete, 2013.

[52] P. Foraboschi and A. Vanin. Non-linear static analysis of masonry buildings based on a strut-and-tie modeling. *Soil Dynamics and Earthquake Engineering*, 55:44–58, 2013.

[53] S. J. Foster and A. R. Malik. Evaluation of efficiency factor models used in strut-and-tie modeling of nonflexural members. *Journal of Structural Engineering*, 128:569–577, 2002.

[54] A. T. Gaynor, J. K. Guest, and C. D. Moen. Reinforced concrete force visualization and design using bilinear truss-continuum topology optimization. *Journal of Structural Engineering*, 139(4):607–618, 2013.

[55] I. Geevar and D. Menon. Strength of Reinforced Concrete Pier Caps-Experimental Validation of Strut-and-Tie Method. *ACI Structural Journal*, 116(1):261, 2019.

[56] H. Guan. Strut-and-tie model of deep beams with web openings-an optimization approach. *Structural Engineering and Mechanics*, 19(4):361–380, 2005.

[57] H. Guan and J.-H. Doh. Development of strut-and-tie models in deep beams with web openings. *Advances in Structural Engineering*, 10(6):697–711, 2007.

[58] J. K. Guest, J. H. Prévost, and T. Belytschko. Achieving minimum length scale in topology optimization using nodal design variables and projection functions. *International Journal for Numerical Methods in Engineering*, 61(2):238–254, 2004.

[59] X. Guo, W. Zhang, and W. Zhong. Doing topology optimization explicitly and geometrically—a new moving morphable components based framework. *Journal of Applied Mechanics*, 81(8):081009, 2014.

[60] A. N. Hanoon, M. S. Jaafar, F. Hejazi, and F. N. A. A. Aziz. Strut effectiveness factor for reinforced concrete deep beams under dynamic loading conditions. *Case Studies in Structural Engineering*, 6:84–102, 2016.

[61] A. N. Hanoon, S. R. Al Zaidee, Q. S. Banyhussan, and A. A. Abdulhameed. Modified strut effectiveness factor for frp-reinforced concrete deep beams. *International Journal of Engineering & Technology*, 7(4.20):485–490, 2018.

[62] Z.-Q. He and Z. Liu. Optimal three-dimensional strut-and-tie models for anchorage diaphragms in externally prestressed bridges. *Engineering Structures*, 32:2057–2064, 2010.

[63] U. P. Herranz, H. S. Maria, S. Gutiérrez, and R. Riddell. Optimal strut-and-tie models using full homogenization optimization method. *ACI Structural Journal*, 109:605–614, 2012.

[64] M.-H. Hsu and Y.-L. Hsu. Interpreting three-dimensional structural topology optimization results. *Computers & Structures*, 83(4-5):327–337, 2005.

[65] T. T. C. Hsu. Softened truss model theory for shear and torsion. *Structural Journal*, 85:624–635, 1988.

[66] T. T. C. Hsu, S. T. Mau, and B. Chen. Theory on shear transfer strength of reinforced concrete. *Structural Journal*, 84:149–160, 1987.

[67] H. Huang, S. Wu, D. Cohen-Or, M. Gong, H. Zhang, G. Li, and B. Chen. L1-medial skeleton of point cloud. *ACM Transactions on Graphics*, 32(4):61–65, 2013.

[68] X. Huang and Y. Xie. A further review of eso type methods for topology optimization. *Structural and Multidisciplinary Optimization*, 41(5):671–683, 2010.

[69] S.-J. Hwang and H.-J. Lee. Strength prediction for discontinuity regions by softened strut-and-tie model. *Journal of Structural Engineering*, 128(12):1519–1526, 2002.

[70] J. L. Jewett and J. V. Carstensen. Experimental investigation of strut-and-tie layouts in deep rc beams designed with hybrid bi-linear topology optimization. *Engineering Structures*, 197:109322, 2019.

[71] J. L. Jewett and J. V. Carstensen. Topology-optimized design, construction and experimental evaluation of concrete beams. *Automation in Construction*, 102: 59–67, 2019.

[72] W. Jiang, K. Xu, Z.-Q. Cheng, R. R. Martin, and G. Dang. Curve skeleton extraction by coupled graph contraction and surface clustering. *Graphical Models*, 75(3): 137–148, 2013.

[73] M. M. Karthik, J. B. Mander, and S. Hurlebaus. Displacement-based compatibility strut-and-tie method and application to monotonic and cyclic loading. *Journal of Structural Engineering*, 142:4016010, 2016.

[74] D.-J. Kim, J. Lee, and Y. H. Lee. Effectiveness factor of strut-and-tie model for concrete deep beams reinforced with frp rebars. *Composites Part B: Engineering*, 56:117–125, 2014. ISSN 1359-8368.

[75] M. Kociecki and H. Adeli. Two-phase genetic algorithm for topology optimization of free-form steel space-frame roof structures with complex curvatures. *Engineering Applications of Artificial Intelligence*, 32:218–227, 2014.

[76] M. Kociecki and H. Adeli. Shape optimization of free-form steel space-frame roof structures with complex geometries using evolutionary computing. *Engineering Applications of Artificial Intelligence*, 38:168–182, 2015.

[77] L. Krog, A. Tucker, M. Kemp, and R. Boyd. Topology optimisation of aircraft wing box ribs. In *10th AIAA/ISSMO multidisciplinary analysis and optimization conference*, page 4481, 2004.

[78] D. Kuchma, S. Yindeesuk, T. Nagle, J. Hart, and H. H. Lee. Experimental validation of strut-and-tie method for complex regions. *ACI Structural Journal*, 105:578–589, 2008. ISSN 0889-3241.

[79] H. G. Kwak and S. H. Noh. Determination of strut-and-tie models using evolutionary structural optimization. *Engineering Structures*, 28:1440–1449, 2006.

[80] P. Lampert and B. Thurlimann. Torsion tests of reinforced concrete beams. *Bericht Nr. 6506*, 2, 1968.

[81] T. C. Lee, R. L. Kashyap, and C.-N. Chu. Building skeleton models via 3-d medial surface axis thinning algorithms. *CVGIP: Graphical Models and Image Processing*, 56:462–478, 1994.

[82] F. Leondardt. Reducing the shear reinforcement in reinforced concrete beams and slabs. *Magazine of Concrete Research*, 17:187–198, 1965.

[83] L. J. Leu, C. W. Huang, C. S. Chen, and Y. P. Liao. Strut-and-tie design methodology for three-dimensional reinforced concrete structures. *Journal of Structural Engineering*, 132:929–938, 2006.

[84] M. T. Ley, K. A. Riding, S. Bae, and J. E. Breen. Experimental verification of strut-and-tie model design method. *ACI Structural Journal*, 104:749–755, 2007.

[85] C. Li and A. C. Bovik. Content-weighted video quality assessment using a three-component image model. *Journal of Electronic Imaging*, 19(1):11003, 2010.

[86] Q. Li, G. P. Steven, and Y. M. Xie. On equivalence between stress criterion and stiffness criterion in evolutionary structural optimization. *Engineering Structures*, 28(10):1440–1449, 2006.

[87] Q. Q. Liang, Y. M. Xie, and G. P. Steven. Topology optimization of strut-and-tie models in reinforced concrete structures using an evolutionary procedure. *ACI Structural Journal*, 97:322–332, 2000.

[88] Q. Q. Liang, Y. M. Xie, and G. P. Steven. Generating optimal strut-and-tie models in prestressed concrete beams by performance-based optimization. *ACI Structural Journal*, 98(2):226–232, 2001.

[89] C.-Y. Lin and L.-S. Chao. Automated image interpretation for integrated topology and shape optimization. *Structural and Multidisciplinary Optimization*, 20(2): 125–137, 2000.

[90] J. Liu and Y. Ma. A survey of manufacturing oriented topology optimization methods. *Advances in Engineering Software*, 100:161–175, 2016.

[91] S. Liu and H. Qiao. Topology optimization of continuum structures with different tensile and compressive properties in bridge layout design. *Structural and Multidisciplinary Optimization*, 43(3):369–380, 2011.

[92] J. G. MacGregor, J. K. Wight, S. Teng, and P. Irawan. *Reinforced concrete: Mechanics and design*, volume 3. Prentice Hall Upper Saddle River, NJ, 1997.

[93] P. Marti. Basic tools of reinforced concrete beam design. *Journal Proceedings*, 82: 46–56, 1985.

[94] B. S. Maxwell and J. E. Breen. Experimental evaluation of strut-and-tie model applied to deep beam with opening. *Structural Journal*, 97:142–148, 2000.

[95] C. Meléndez, J. Sagaseta, P. F. M. Sosa, and L. P. Rubio. Refined three-dimensional strut-and-tie model for analysis and design of four-pile caps. *ACI Structural Journal*, 116(4):15, 2019. ISSN 08893241.

[96] A. Mendoza-San-Agustin, F. Velázquez-Villegas, and A. Zepeda-Sánchez. Adaptation of topologic optimized structures based on skeletonization. *Ingeniería mecánica, tecnología y desarrollo*, 5(4):415–421, 2016.

[97] M. Mezzina, F. Palmisano, and D. Raffaele. Designing simply supported RC bridge decks subjected to in-plane actions: Strut-and-tie model approach. *Journal of Earthquake Engineering*, 16(4):496–514, 2012.

[98] D. Mitchell and M. P. Collins. Diagonal compression field theory-a rational model for structural concrete in pure torsion. *Journal Proceedings*, 71:396–408, 1974.

[99] M. Moradi and M. R. Esfahani. Application of the strut-and-tie method for steel fiber reinforced concrete deep beams. *Construction and Building Materials*, 131, 2017.

[100] E. Mörsch. *Concrete-Steel Construction (Der Eisenbetonbau)*. McGraw-Hill Book Co., New York, 1909.

[101] A. Muttoni, M. F. Ruiz, and F. Niketic. Design versus assessment of concrete structures using stress fields and strut-and-tie models. *ACI Structural Journal*, 112: 605–615, 2015.

[102] A. Nana, J.-C. Cuillière, and V. Francois. Automatic reconstruction of beam structures from 3d topology optimization results. *Computers & Structures*, 189: 62–82, 2017.

[103] M. Nehdi, Z. Omeman, and H. El-Chabib. Optimal efficiency factor in strut-and-tie model for frp-reinforced concrete short beams with (1.5< a/d< 2.5). *Materials and Structures*, 41(10):1713–1727, 2008. ISSN 1359-5997.

[104] M. P. Nielsen. *Limit analysis and concrete plasticity*. Prentice Hall, Inc, Englewood Cliffs, New Jersey, 1984.

[105] M. P. Nielsen and L. C. Hoang. *Limit analysis and concrete plasticity*. CRC Press, 2016. ISBN 0429075545.

[106] R. Oviedo, S. Gutiérrez, and H. Santa Maria. Experimental evaluation of optimized strut-and-tie models for a dapped beam. *Structural Concrete*, 17(3):469–480, 2016.

[107] F. Palmisano and A. Elia. Shape optimization of strut-and-tie models in masonry buildings subjected to landslide-induced settlements. *Engineering Structures*, 84: 223–232, 2015. ISSN 0141-0296.

[108] J. W. Park, S. Yindeesuk, T. Tjhin, and D. Kuchma. Automated finite-element-based validation of structures designed by the strut-and-tie method. *Journal of Structural Engineering*, 136:203–210, 2010.

[109] I. Paya, V. Yepes, F. González-Vidosa, and A. Hospitaler. Multiobjective optimization of concrete frames by simulated annealing. *Computer-Aided Civil and Infrastructure Engineering*, 23(8):596–610, 2008.

[110] R. Perera and J. Vique. Strut-and-tie modelling of reinforced concrete beams using genetic algorithms optimization. *Construction and Building Materials*, 23 (8):2914–2925, 2009.

[111] S. Qazi, L. Michel, E. Ferrier, and A. Limam. Strut-and-tie model for a reinforced concrete wall strengthened with carbon fibre-reinforced polymers. *Composite Structures*, 128:87–99, 2015.

[112] C. G. Quintero-Febres, G. Parra-Montesinos, and J. K. Wight. Strength of struts in deep concrete members designed using strut-and-tie method. *ACI Structural Journal*, 103:577, 2006.

[113] E. Rausch. Design of reinforced concrete in torsion (berechnung des eisenbetons gegen verdrehung). *Technische Hochschule, Berlin, Germany (in German)*, 1929.

[114] K.-H. Reineck. *Examples for the Design of Structural Concrete with Strut-and-Tie Mode*, volume 208. Farmington Hills (MI), 2002. ISBN 0-87031-086-0.

[115] W. Ritter. Die bauweise hennebique. *Schweizerische Bauzeitung*, 33(7):59–61, 1899.

[116] D. M. Rogowsky and J. G. MacGregor. Design of reinforced concrete deep beams. *Concrete International*, 8:49–58, 1986.

[117] J. Rombouts, G. Lombaert, L. De Laet, and M. Schevenels. A novel shape optimization approach for strained gridshells: Design and construction of a simply supported gridshell. *Engineering Structures*, 192:166–180, 2019.

[118] D. Sahoo, R. Gautam, B. Singh, and P. Bhargava. Strength and deformation characteristics of bottle-shaped struts. *Magazine of Concrete Research*, 60(2): 137–144, 2008. ISSN 0024-9831.

[119] D. Sahoo, B. Singh, and P. Bhargava. An appraisal of the aci strut efficiency factors. *Magazine of Concrete Research*, 61(6):445–456, 2009. ISSN 0024-9831.

[120] D. K. Sahoo and B. P. Varghese. Effect of confinement on the efficiency of bottle-shaped struts. *Magazine of Concrete Research*, 71(18):965–974, 2019. ISSN 1751-763X.

[121] J. Schlaich and K. Schafer. Design and detailing of structural concrete using strut-and-tie models. *Structural Engineer*, 69:113–125, 1991.

[122] J. Schlaich, K. Schafer, and M. Jennewein. Toward a consistent design of structural concrete. *PCI Journal*, 32:74–150, 1987. ISSN 9788578110796.

[123] G. Sharma and J. Martin. Matlab®: a language for parallel computing. *International Journal of Parallel Programming*, 37(1):3–36, 2009.

[124] V. Shobeiri and B. Ahmadi-Nedushan. Bi-directional evolutionary structural optimization for strut-and-tie modelling of three-dimensional structural concrete. *Engineering Optimization*, 49:2055–2078, 2017.

[125] O. Sigmund. On the design of compliant mechanisms using topology optimization. *Journal of Structural Mechanics*, 25(4):493–524, 1997.

[126] O. Sigmund and K. Maute. Topology optimization approaches: A comparative review. *Structural and Multidisciplinary Optimization*, 48:1031–1055, 2013.

[127] O. Sigmund and J. Petersson. Numerical instabilities in topology optimization: A survey on procedures dealing with checkerboards, mesh-dependencies and local minima. *Structural Optimization*, 16(1):68–75, 1998. doi: 10.1007/BF01214002.

[128] B. Singh, D. K. Sahoo, and N. M. Jacob. Efficiency factors of recycled aggregate concrete bottle-shaped struts. *Magazine of Concrete Research*, 65(14):878–887, 2013.

[129] R. Souza, D. Kuchma, J. Park, and T. Bittencourt. Adaptable strut-and-tie model for design and verification of four-pile caps. *ACI Structural Journal*, 106(2), 2009. ISSN 0889-3241.

[130] S. Sritharan. Strut-and-tie analysis of bridge tee joints subjected to seismic actions. *Journal of Structural Engineering*, 131(9):1321–1333, 2005.

[131] L. L. Stromberg, A. Beghini, W. F. Baker, and G. H. Paulino. Topology optimization for braced frames: combining continuum and beam/column elements. *Engineering Structures*, 37:106–124, 2012.

[132] R. K. L. Su and A. M. Chandler. Design criteria for unified strut and tie models. *Progress in Structural Engineering and Materials*, 3:288–298, 2001.

[133] R. K. L. Su and D. T. W. Looi. Revisiting unreinforced strut efficiency factor. *ACI Structural Journal*, 113(2):301–312, 2016.

[134] Y. Su, Y. Wu, W. Ji, and S. Shen. Shape generation of grid structures by inverse hanging method coupled with multiobjective optimization. *Computer-Aided Civil and Infrastructure Engineering*, 33(6):498–509, 2018.

[135] K. Svanberg. The method of moving asymptotes - a new method for structural optimization. *International Journal for Numerical Methods in Engineering*, 24: 359–373, 1987. ISSN 9781424438884.

[136] A. Takezawa, S. Nishiwaki, and M. Kitamura. Shape and topology optimization based on the phase field method and sensitivity analysis. *Journal of Computational Physics*, 229(7):2697–2718, 2010.

[137] C. Talischi, G. H. Paulino, A. Pereira, and I. F. Menezes. Polygonal finite elements for topology optimization: A unifying paradigm. *International journal for numerical methods in engineering*, 82(6):671–698, 2010.

[138] K. H. Tan, K. Tong, and C. Y. Tang. Direct strut-and-tie model for prestressed deep beams. *Journal of Structural Engineering*, 127(9):1076–1084, 2001.

[139] K. H. Tan, C. Y. Tang, and K. Tong. A direct method for deep beams with web reinforcement. *Magazine of Concrete Research*, 55:53–63, 2003.

[140] T. N. Tjhin and D. A. Kuchma. Computer-based tools for design by strut-and-tie method: Advances and challenges. *Structural Journal*, 99:586–594, 2002.

[141] T. N. Tjhin and D. A. Kuchma. Integrated analysis and design tool for the strut-and-tie method. *Engineering Structures*, 29:3042–3052, 2007.

[142] N. H. T. To, J. M. Ingham, and S. Sritharan. Strut-and-tie computer modelling of reinforced concrete bridge joint systems. *Journal of Earthquake Engineering*, 07 (03):463–493, 2003.

[143] N. P. van Dijk, K. Maute, M. Langelaar, and F. Van Keulen. Level-set methods for structural topology optimization: a review. *Structural and Multidisciplinary Optimization*, 48(3):437–472, 2013.

[144] G. Vantyghem, W. De Corte, E. Shakour, and O. Amir. 3d printing of a post-tensioned concrete girder designed by topology optimization. *Automation in Construction*, 112:103084, 2020. ISSN 0926-5805.

[145] F. J. Vecchio and M. P. Collins. The modified compression-field theory for reinforced concrete elements subjected to shear. *ACI Journal*, 83:219–231, 1986.

[146] F. J. Vecchio and M. P. Collins. Compression response of cracked reinforced concrete. *Journal of Structural Engineering*, 119(12):3590–3610, 1993. ISSN 0733-9445.

[147] M. Victoria, O. M. Querin, and P. Marti. Generation of strut-and-tie models by topology design using different material properties in tension and compression. *Structural and Multidisciplinary Optimization*, 44:247–258, 2011. ISSN 1615-147X.

[148] Z. Wang, A. C. Bovik, H. R. Sheikh, and E. P. Simoncelli. Image quality assessment: from error visibility to structural similarity. *IEEE Transactions on Image Processing*, 13(4):600–612, 2004.

[149] Y. Xia, Y. Wu, and M. A. N. Hendriks. Simultaneous optimization of shape and topology of free-form shells based on uniform parameterization model. *Automation in Construction*, 102:148–159, 2019. ISSN 0926-5805.

[150] Y. Xia, Y. Wu, and M. A. N. Hendriks. Simultaneous optimization of shape and topology of free-form shells based on uniform parameterization model. *Automation in Construction*, 102:148–159, 2019.

[151] Y. Xia, M. Langelaar, and M. A. N. Hendriks. Automated optimization-based generation and quantitative evaluation of strut-and-tie models. *Computers & Structures*, 238:106297, 2020. ISSN 0045-7949. doi: https://doi.org/10.1016/j.compstruc.2020.106297.

[152] Y. Xia, M. Langelaar, and M. A. N. Hendriks. A critical evaluation of topology optimization results for strut-and-tie modeling of reinforced concrete. *Computer-Aided Civil and Infrastructure Engineering*, 2020. ISSN 1093-9687.

[153] Y. Xia, M. Langelaar, and M. A. N. Hendriks. Optimization-based three-dimensional strut-and-tie model generation for reinforced concrete. *Computer-Aided Civil and Infrastructure Engineering (Accepted)*, 2020.

[154] Y. M. Xie and G. P. Steven. A simple evolutionary procedure for structural optimization. *Computers & Structures*, 49:885–896, 1993.

[155] V. Yepes, J. V. Marti, and T. Garcia-Segura. Cost and co2 emission optimization of precast–prestressed concrete u-beam road bridges by a hybrid glowworm swarm algorithm. *Automation in Construction*, 49:123–134, 2015.

[156] G. Yi and N. H. Kim. Identifying boundaries of topology optimization results using basic parametric features. *Structural and Multidisciplinary Optimization*, 55:1641–1654, 2017.

[157] G. Yi, B. D. Youn, and N. H. Kim. Geometric feature identification from topology optimization results. In *11th World Congress on Structural and Multidisciplinary Optimisation*, Sydney Australia, June 2015.

[158] G. Yin, X. Xiao, and F. Cirak. Topologically robust cad model generation for structural optimisation. *Computer Methods in Applied Mechanics and Engineering*, 369:113102, 2020.

[159] M. Yu, J. Li, and G. Ma. *Theorems of Limit Analysis*. Springer, New York, 2009.

[160] Y. M. Yun. Computer graphics for nonlinear strut-tie model approach. *Journal of Computing in Civil Engineering*, 14:127–133, 2000.

[161] Y. M. Yun and B. H. Kim. Two-dimensional grid strut-tie model approach for structural concrete. *Journal of structural engineering*, 134:1199–1214, 2008.

[162] Y. M. Yun and J. A. Ramirez. Strength of struts and nodes in strut-tie model. *Journal of Structural Engineering*, 122:20–29, 1996.

[163] Y. M. Yun, H. S. Chae, B. Kim, and J. A. Ramirez. Verification of three-dimensional grid strut-and-tie model approach in structural concrete. *ACI Structural Journal*, 115(1):27–40, 2018.

[164] Y. M. Yun, B. Kim, and J. A. Ramirez. Three-dimensional grid strut-and-tie model approach in structural concrete design. *ACI Structural Journal*, 115(1):15–26, 2018. ISSN 0889-3241.

[165] Y. M. Yun, H. S. Chae, and J. A. Ramirez. A three-dimensional strut-and-tie model for a four-pile reinforced concrete cap. *Journal of Advanced Concrete Technology*, 17(7):365–380, 2019. ISSN 1346-8014.

[166] T. Y. Zhang and C. Y. Suen. A fast parallel algorithm for thinning digital patterns. *Communications of the ACM*, 27(3):236–239, 1984.

[167] Y. Zhang and S. Liu. Design of conducting paths based on topology optimization. *Heat and Mass Transfer*, 44(10):1217–1227, 2008.

[168] J. Zhong, L. Wang, M. Zhou, and Y. Li. New method for generating strut-and-tie models of three-dimensional concrete anchorage zones and box girders. *Journal of Bridge Engineering*, 22(8):04017047, 2017.

[169] J. T. Zhong, L. Wang, P. Deng, and M. Zhou. A new evaluation procedure for the strut-and-tie models of the disturbed regions of reinforced concrete structures. *Engineering Structures*, 148:660–672, 2017. ISSN 18737323. doi: 10.1016/j.engstruct.2017.07.012.

[170] L. Zhou, Z. Liu, and Z. He. Elastic-to-plastic strut-and-tie model for deep beams. *Journal of Bridge Engineering*, 23(4):4018007, 2018.

[171] L.-Y. Zhou, Z.-Q. He, and Z. Liu. Investigation of optimal layout of ties in stm developed by topology optimization. *Structural Concrete*, 17(2):175–182, 2016.

[172] J.-H. Zhu, W.-H. Zhang, and L. Xia. Topology optimization in aircraft and aerospace structures design. *Archives of Computational Methods in Engineering*, 23(4): 595–622, 2016.

[173] C. Zhuang, Z. Xiong, and H. Ding. A level set method for topology optimization of heat conduction problem under multiple load cases. *Computer Methods in Applied Mechanics and Engineering*, 196(4-6):1074–1084, 2007.

CURRICULUM VITÆ

夏毅 (Yi XIA)

03-06-1991 Born in Zunyi, China.

EDUCATION

2009–2013	BSc student Tongji University, China
2013–2015	MSc student Harbin Institute of Technology, China
2016–2020	Ph.D. Candidate Delft University of Technology, The Netherlands

LIST OF PUBLICATIONS

1. **Y. Xia**, Y. Wu, M. A. N. Hendriks, *Simultaneous optimization of shape and topology of free-form shells based on uniform parameterization model*, Automation in Construction **102**, 148–159 (2019).

2. **Y. Xia**, M. Langelaar, M. A. N. Hendriks, *A critical evaluation of topology optimization results for strut-and-tie modeling of reinforced concrete*, Computer-Aided Civil and Infrastructure Engineering **35**, 850–869 (2020).

3. **Y. Xia**, M. Langelaar, M. A. N. Hendriks, *Automated optimization-based generation and quantitative evaluation of Strut-and-Tie models*, Computers & Structures **238**, 106297 (2020).

4. **Y. Xia**, M. Langelaar, M. A. N. Hendriks, *Optimization-Based Three-Dimensional Strut-and-Tie Model Generation for Reinforced Concrete*, Computer-Aided Civil and Infrastructure Engineering (2020) . (in press)

5. **Y. Xia**, Y. Wu, M. A. N. Hendriks, *Does Strut-and-Tie Modelling benefit from topology optimization?*, fib Symposium Proceedings, Shanghai, China (2020). (in progress)